

**DOT/FAA/AR-00/11**

Office of Aviation Research  
Washington, D.C. 20591

# **Statistical Loads Data for BE-1900D Aircraft in Commuter Operations**

April 2000

Final Report

This document is available to the U.S. public  
through the National Technical Information  
Service (NTIS), Springfield, Virginia 22161.



U.S. Department of Transportation  
**Federal Aviation Administration**

## **NOTICE**

This document is disseminated under the sponsorship of the U.S. Department of Transportation in the interest of information exchange. The United States Government assumes no liability for the contents or use thereof. The United States Government does not endorse products or manufacturers. Trade or manufacturer's names appear herein solely because they are considered essential to the objective of this report. This document does not constitute FAA certification policy. Consult your local FAA aircraft certification office as to its use.

This report is available at the Federal Aviation Administration William J. Hughes Technical Center's Full-Text Technical Reports page: [www.actlibrary.tc.faa.gov](http://www.actlibrary.tc.faa.gov) in Adobe Acrobat portable document format (PDF).

1. Report No. DOT/FAA/AR-00/11		2. Government Accession No.		3. Recipient's Catalog No.	
4. Title and Subtitle STATISTICAL LOADS DATA FOR BE-1900D AIRCRAFT IN COMMUTER OPERATIONS				5. Report Date April 2000	
				6. Performing Organization Code AAR-430	
7. Author(s) Daniel O. Tipps, Donald A. Skinn, and John W. Rustenburg University of Dayton Thomas A. Zeiler University of Alabama				8. Performing Organization Report No. UDR-TR-1999-00061	
9. Performing Organization Name and Address University of Dayton Research Institute University of Alabama Structural Integrity Division Dept of Aerospace Engineering & Mechanics 300 College Park Box 870280 Dayton, OH 45469-0120 Tuscaloosa, AL 355487-0280				10. Work Unit No. (TRAIS) RPD-510	
				11. Contract or Grant No. 98-G-018	
12. Sponsoring Agency Name and Address U.S. Department of Transportation Federal Aviation Administration Office of Aviation Research Washington, DC 20591				13. Type of Report and Period Covered Final Report	
				14. Sponsoring Agency Code ACE-110	
15. Supplementary Notes The Federal Aviation Administration William J. Hughes Technical Center COTR is Thomas DeFiore					
16. Abstract  The University of Alabama is supporting Federal Aviation Administration (FAA) research on the structural integrity requirements for the US commuter airplane fleet. The primary objective of this research is to support the FAA Airborne Data Monitoring Systems Research Program by developing new and improved methods and criteria for processing and presenting commuter airplane flight and ground loads usage data. The scope of activities performed involves defining the service related factors that affect the operational life of commuter aircraft and providing processed data in statistical formats that will enable the FAA to reassess existing certification criteria. Equally important, these new data will enable the FAA, the aircraft manufacturers, and the airlines to better understand and control those factors that influence the structural integrity of commuter aircraft.  The University of Dayton under contract with the University of Alabama processed digital flight recorder data collected from 903 flights representing approximately 585 flight hours recorded on 28 typical BE-1900D aircraft during typical operational usage by a single commuter airline. This report presents statistical summaries of aircraft usage data, ground loads data, flight loads data, and systems operational data collected from these aircraft. Statistical data are presented for parameters such as gust and maneuver acceleration, airspeed, altitude, flight duration and distance, engine RPM and torque, time at propeller reversal, derived gust velocity, V-n diagrams, and vertical and longitudinal accelerations during ground operations. This report presents the results from this effort.					
17. Key Words Digital flight data recorder, Flight profiles, Gust accelerations, Maneuver accelerations, Statistical summaries			18. Distribution Statement This document is available to the public through the National Technical Information Service (NTIS), Springfield, Virginia 22161.		
19. Security Classif. (of this report) Unclassified		20. Security Classif. (of this page) Unclassified		21. No. of Pages 71	22. Price N/A

## PREFACE

The Flight Systems Integrity Group of the Structural Integrity Division of the University of Dayton Research Institute (UDRI) performed this work jointly with the University of Alabama (UA) for the Federal Aviation Administration (FAA) under Purchase Order Number P007131. The Program Manager for the University of Alabama was Dr. Thomas A. Zeiler of the Department of Aerospace Engineering and Mechanics. For the University of Dayton, Mr. Daniel O. Tipps was the Principal Investigator and provided overall technical direction; Mr. Donald A. Skinn developed the data reduction algorithms and software, established the data reduction criteria, and performed the data processing; and Mr. John W. Rustenburg created the statistical data presentation formats, performed the data analysis, and plotted the data. The Program Manager for the FAA was Mr. Thomas DeFiore of the FAA William J. Hughes Technical Center, Atlantic City International Airport, New Jersey, and the Program Technical Advisor was Mr. Terence Barnes of the FAA Aircraft Certification Office, Renton, Washington.

UDRI would like to extend its appreciation to Mr. Bob Houghton who supported the program for the airline and approved the release of the final processed data and to Mr. Jack Downey who collected the flight loads data, pre-processed the data, and provided other supporting information about the aircraft.

## TABLE OF CONTENTS

	Page
EXECUTIVE SUMMARY	xi
1. INTRODUCTION	1
2. AIRCRAFT DESCRIPTION	1
3. AIRLINE DATA COLLECTION AND EDITING SYSTEM	2
3.1 Data Collection System	2
3.2 Data Editing System	2
4. UNIVERSITY OF DAYTON RESEARCH INSTITUTE DATA PROCESSING	3
4.1 Recorded Parameters	3
4.2 Derived and Extracted Parameters	3
4.2.1 Identification of Liftoff and Touchdown	4
4.2.2 Flight Distance	4
4.2.3 Flight Duration	4
4.2.4 Design Load Factor Definition	4
4.2.5 Derived Gust Velocity	5
4.3 Data Reduction	7
4.3.1 Initial Quality Screening	7
4.3.2 Aircraft Identification	8
4.3.3 Time History Files	8
4.3.4 Relational Database	8
4.3.5 Permanent Data Files	9
4.4 Data Reduction Criteria	9
4.4.1 Phases of Flight	9
4.4.2 Sign Convention	10
4.4.3 Peak-Valley Selection	10
4.4.4 Separation of Maneuver and Gust Load Factors	12
4.4.5 Flap Detents	13
4.4.6 Altitude Bands	13
4.4.7 Vertical Acceleration Bias Correction	14

5.	DATA PRESENTATION	14
5.1	Aircraft Usage Data	17
5.1.1	Altitude and Flight Distance Data	17
5.1.2	Coincident Airspeed and Altitude Data	17
5.1.3	Maximum Operating Airspeed Data	18
5.1.4	Flight Duration	18
5.2	Ground Loads Data	18
5.2.1	Airspeed at Liftoff and Touchdown	18
5.2.2	Pitch Angle at Liftoff	18
5.2.3	Load Factor Data During Ground Operations	19
5.3	Flight Loads Data	19
5.3.1	Gust Loads Data	19
5.3.1.1	Gust Load Factor Data	19
5.3.1.2	Comparison of BE-1900D Gust Load Factor Data With Other Aircraft	19
5.3.1.3	Comparison of BE-1900D Gust Load Factor Data With Other Technical Data	20
5.3.1.4	Gust Velocity Data	20
5.3.1.5	V-n Diagrams	20
5.3.2	Maneuver Loads Data	21
5.3.2.1	Maneuver Load Factor Data	21
5.3.2.2	Comparison of BE-1900D Maneuver Load Factor Data With Other Technical Data	21
5.3.2.3	Bank Angle Data	21
5.3.3	Combined Maneuver and Gust Loads Data	21
5.3.3.1	Combined Maneuver and Gust Load Factor Data	22
5.3.3.2	Comparison of Individual Aircraft Usage	22
5.3.3.3	Comparison of BE-1900D Flight Loads Data With Other Commuter Aircraft and Other Technical Data	23

5.4	Systems Operational Data	23
5.4.1	Flap System Data	23
5.4.1.1	Airspeed During Flap Usage	23
5.4.1.2	Time by Flap Detent Setting	23
5.4.2	Propulsion System Data	24
5.4.2.1	Propeller Data	24
5.4.2.2	Engine RPM and Torque Level Data	24
6.	CONCLUSIONS AND RECOMMENDATIONS	25
7.	REFERENCES	27
	APPENDIX A—Statistical Formats, Aircraft Usage Data	

## LIST OF ILLUSTRATIONS

Figure		Page
1	BE-1900D Three-View Drawing	2
2	Description of Phases of Flight	9
3	Sign Convention for Airplane Accelerations	10
4	The Peak-Between-Means Classification Criteria	11
5A	Current Acceleration Value Passes Into Deadband	11
5B	Current Acceleration Value Passes Through Deadband	11
6	Time History Plot of Engine RPM and Torque	25

## LIST OF TABLES

Table		Page
1	BE-1900D Aircraft Characteristics	1
2	Recorded Flight and Ground Loads Parameters	3
3	Parameter Editing Values	8
4	Phase of Flight Starting Criteria	10
5	Peak Classification Criteria	12
6	BE-1900D Flap Detents	13
7	Altitude Above Airport Bands	13
8	Absolute Pressure Altitudes	14
9	Statistical Formats	15
10	Individual Aircraft Statistical Data	22

## LIST OF SYMBOLS AND ABBREVIATIONS

$\bar{A}$	aircraft PSD gust response factor
$A_N$	incremental load factor at operating weight ( $n_z-1$ )
$A_{NLLF}$	incremental gust or maneuver design load factor at maximum gross weight ( $n_z-1$ )
$A_r$	aspect ratio $b^2/S$
$a$	speed of sound (ft/sec)
$a_0$	speed of sound at sea level (ft/sec)
$\bar{c}$	wing mean geometric chord (ft)
$\bar{C}$	aircraft discrete gust response factor
$C_{L_\alpha}$	wing lift curve slope per radian
$C_{L_{\max}}$	maximum lift coefficient
c.g.	center of gravity
$D$	distance
$F(PSD)$	continuous gust alleviation factor
$g$	gravity constant, 32.17 ft/sec <sup>2</sup>
$H_p$	pressure altitude (ft)
$K$	gust alleviation constant
$K_g$	discrete gust alleviation factor, $0.88 \mu / (5.3 + \mu)$
$L$	turbulence scale length (ft)
$m$	lift curve slope per radian
$M$	Mach number
$n$	load factor (g)
$N$	number of occurrences for $U_\sigma$ (PSD gust procedure)
$nm$	nautical mile
$n_x$	longitudinal load factor (g)
$n_z$	normal load factor (g)
$N_0$	number of zero crossings per nautical mile (PSD gust procedure)
$q$	dynamic pressure (lbs/ft <sup>2</sup> )
$\rho$	air density, slugs/ft <sup>3</sup> (at altitude)
$\rho_0$	standard sea level air density 0.0023769 slugs/ft <sup>3</sup>

$S$	wing area (ft <sup>2</sup> )
$U_{de}$	derived gust velocity (ft/sec)
$U_{\sigma}$	continuous turbulence gust intensity (ft/sec)
$V_B$	design speed for maximum gust
$V_C$	calibrated or design cruise speed
$V_D$	design dive speed
$V_e$	equivalent airspeed
$V_T$	true airspeed

## EXECUTIVE SUMMARY

The Federal Aviation Administration (FAA) William J. Hughes Technical Center funded the University of Alabama (UA) to conduct a Commuter Operational Loads Survey Program. Phase I of the UA program involved the collection and analysis of actual operational flight and ground loads data collected from Digital Flight Data Recorders (DFDR) installed on a fleet of 30 BE-1900D aircraft operated by a single commuter airline. For the Flight Loads Program, the UA subcontracted the processing and analysis of the flight loads data and preparation of the final report to the University of Dayton Research Institute (UDRI). The operator collected the data on site from the BE-1900D aircraft and provided UDRI with disks containing data on 14 parameters. UDRI processed and analyzed the data and developed the statistical data formats for this report.

Presented herein are analyses and statistical summaries of data collected from 903 flights representing approximately 585 flight hours recorded on 28 BE-1900D aircraft during typical operations (data from two aircraft were determined to be unreliable). Basic statistical information on parameters such as airspeeds, altitude, flight duration and distance, and maneuver and gust accelerations are shown in formats that can be easily compared to an aircraft manufacturer's existing design criteria. Additional aircraft data are also presented for items such as bank and pitch angles, flap usage, engine RPM and torque, reversed propeller usage, and vertical and longitudinal load factor during ground operations. UDRI also derived some unique BE-1900D data parameters that were used to develop gust velocities, V-n diagrams, and various coincident flight events and compared these data with published operational limits and data from other aircraft types.

The statistical data formats that were developed for this program should be useful to the FAA, the aircraft manufacturers, and the airlines for assessing existing certification criteria contained in the FAA's Federal Aviation Regulation (FAR) and by the airlines and the aircraft manufacturer to better understand and control those factors that influence the structural integrity of commuter aircraft.

## 1. INTRODUCTION.

The Federal Aviation Administration (FAA) funded the University of Alabama (UA) to conduct a Commuter Operational Loads Survey Program to collect, process, and evaluate statistical flight loads data from commuter aircraft used in normal commuter airline operations. The objectives of this program were to a) acquire, evaluate, and utilize typical operational in-service data for comparison with the prior data used in the design and qualification testing of civil transport aircraft and b) provide a basis to improve the structural criteria and methods of design, evaluation, and substantiation of future airplanes.

The first phase of the program involved the collection and analysis of operational flight and ground loads data collected from Digital Flight Data Recorders (DFDR) installed on a fleet of BE-1900D aircraft. The University of Dayton Research Institute (UDRI) under contract with the UA performed the editing, reduction, processing, and analysis of the data collected and prepared the final report.

The resulting aircraft usage and statistical loads data are presented in formats that fulfill the requests of the University of Alabama, aircraft manufacturers, and the FAA. The report includes aircraft usage and statistical loads derived from recorded data obtained from 28 airplanes consisting of 903 flights and approximately 585 hours of commuter operations from a single operator.

## 2. AIRCRAFT DESCRIPTION.

Table 1 [1] presents certain operational characteristics of the BE-1900D aircraft equipped with digital flight data recorders.

TABLE 1. BE-1900D AIRCRAFT CHARACTERISTICS

Maximum Taxi Weight	17,060 lb
Maximum Takeoff Weight	16,950 lb
Maximum Landing Weight	16,600 lb
Zero-Fuel Weight	15,000 lb
Operating Empty Weight*	10,350 lb*
Fuel Capacity	668 U.S. gallons
Two P&W PT6A-67D Turboprops	@ 1,279 shp each
Wing Span	57 ft 11.25 in
Wing Reference Area	310 ft <sup>2</sup>
Wing MAC	5.32 ft
Length	57 ft 10 in
Height	15 ft 6 in
Tread	17 ft 2 in
Wheel Base	23 ft 9.5 in

\*Note: Operating Empty Weight is not a [1] value but was provided by the airline.

Figure 1 shows front, top, and side views of the aircraft.

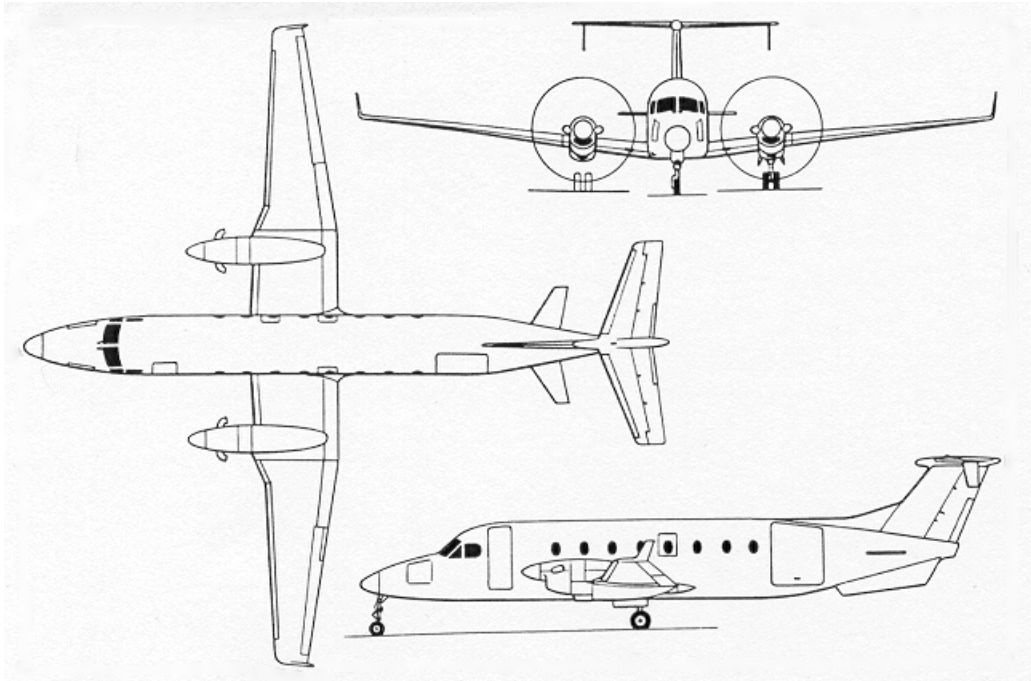


FIGURE 1. BE-1900D THREE-VIEW DRAWING [2]

### 3. AIRLINE DATA COLLECTION AND EDITING SYSTEM.

The airline data collection and editing system consists of two major components: (1) the data collection system installed on board the aircraft and (2) the ground data editing station. The airline performed the collection and pre-processing of the BE-1900D recorded data and then provided it to UDRI on disks.

#### 3.1 DATA COLLECTION SYSTEM.

The airline onboard data collection system consists of a Loral Digital Flight Data Recorder (DFDR), Part Number S703-1000-00.

#### 3.2 DATA EDITING SYSTEM.

The airline ground data editing station performed a number of functions during the process of transferring the raw flight data into DOS file formats and onto hard disks. The Download/Transcription Software used by the airline was AACO Inc. Part Number FSW-0002-017 and the download process was performed in accordance with AACO Inc. Document Number GGA-0011-001 Rev C1. The two most important functions of this software were an integrity check of the data and removal of flight sensitive information. The airline removed all sensitive information and forwarded the desensitized data to UDRI and the UA for flight loads processing and analysis. Table 2 lists the recorded data parameters, which were provided to UDRI.

TABLE 2. RECORDED FLIGHT AND GROUND LOADS PARAMETERS

Parameter	Units	Sample Rate
Normal Acceleration	g	8 per second
Longitudinal Acceleration	g	4 per second
Flap Position (L&R)	Discrete	1 per second
Pitch Control	Degrees	2 per second
RPM L	RPM	1 per second
RPM R	RPM	1 per second
Prop. Reverse (L&R)	Discrete	1 per second
Indicated Airspeed	Knots	1 per second
Pressure Altitude	Feet	1 per second
Bank Angle	Degrees	2 per second
Pitch Angle	Degrees	2 per second
Magnetic Heading	Degrees	1 per second
Torque L	Ft-lb	1 per second
Torque R	Ft-lb	1 per second

#### 4. UNIVERSITY OF DAYTON RESEARCH INSTITUTE DATA PROCESSING.

The parameters listed in table 2 were provided to UDRI in engineering units on 100-MB jaz disks containing compressed (zipped) text files for multiple flights from different aircraft. These files were processed by UDRI to extract the parameters required for statistical flight loads presentation. This section describes the reduction of these data and the derivation of all other required supporting parameters.

##### 4.1 RECORDED PARAMETERS.

All of the parameters listed in table 2 except pitch control were used for statistical analysis and data presentation. Pitch control is the measure of the control yoke in the fore and aft direction and indicates the amount of elevator deflection being input by the pilot. Previously, UDRI discovered that measurements of pilot input to cable driven systems do not accurately relate to the actual position of the elevator during flight because the cable can stretch. Thus, because of the questionable accuracy and lack of any useful purpose for the pitch control data, they were not processed.

##### 4.2 DERIVED AND EXTRACTED PARAMETERS.

Certain information and parameters needed in the data reduction are not recorded and need to be either extracted or derived from the available time history data. In some cases UDRI had to calculate some of these parameters. For example, since the derivation of the lift curve slopes (discussed in 4.2.5) and the quarter chord wing sweep angle (estimated from figure 1 to be 6 degrees) were not available from the aircraft manufacturer, UDRI estimates of these values may not reflect those used by the aircraft manufacturer. In addition, since gross weight was not a

recorded parameter, either a 45-day average takeoff weight of 14,500 lbs or the maximum design takeoff gross weight of 16,950 lbs was used for those calculations where weight was a required parameter. Each of these calculations and the derivation of other required parameters is discussed in the following paragraphs.

#### 4.2.1 Identification of Liftoff and Touchdown.

In the absence of a squat switch the approximate time of liftoff and touchdown was determined by an algorithm that used time history information of pitch angle, vertical and longitudinal accelerations, and changes in altitude and indicated airspeed. The actual time at liftoff is determined by calculating the average pitch angle while the aircraft is on the ground. Then, the point in time when the pitch angle changes by more than 2 degrees from this average is defined as the time of liftoff. The time of touchdown was selected by using the best combination of when the pitch angle, vertical and longitudinal accelerations, airspeed, and altitude indicated that contact with the runway had occurred.

#### 4.2.2 Flight Distance.

The flight distance  $D$  is obtained by numerically integrating true velocity  $V_T$  from the time of liftoff ( $t_0$ ) to the time of touchdown ( $t_n$ ).  $V_T$  is the true average velocity during the time increment  $\Delta t$ .

$$D = \sum_{t_0}^{t_n} \Delta t \cdot V_T \quad (1)$$

For a perfect speed indicator, the indicated airspeed equals the calibrated airspeed. In this report the indicated air speed is assumed to equal the calibrated airspeed. Assuming incompressible flow and neglecting the small effects at low Mach numbers, the true airspeed ( $V_T$ ) can be described as a function of calibrated air speed ( $V_C$ ) and the square root of the ratio of air density at sea level ( $\rho_0$ ) to air density at altitude ( $\rho$ ).

Thus,

$$V_T \approx V_C \sqrt{\frac{\rho_0}{\rho}} \quad (2)$$

For altitudes below 36,089 feet, the density  $\rho$  is expressed as a function of altitude based on the International Standard Atmosphere by

$$\rho = \rho_0 (1 - 6.876 \times 10^{-6} \times H_p)^{4.256} \quad (3)$$

where  $\rho_0$  is air density at sea level (0.0023769 slugs/ft<sup>3</sup>) and  $H_p$  is pressure altitude (ft). Pressure altitude is a recorded parameter.

#### 4.2.3 Flight Duration.

The flight duration is defined as the time from aircraft liftoff to touchdown.

#### 4.2.4 Design Load Factor Definition.

The gust and maneuver load spectra specified in AFS-120-73-2 [3] are expressed in terms of a load factor ratio  $A_N/A_{NLLF}$ . AFS-120-73-2 defines this ratio as the incremental load factor at

operating weight divided by the incremental design limit load factor at maximum gross weight. Therefore, in order to compare the BE-1900D gust and maneuver flight load factor spectra with the AFS-120-73-2 flight load spectra, UDRI had to estimate the aircraft design limit load factor for both gust and maneuver. These limit load factors do not necessarily reflect the true design values.

For the gust spectra comparison the incremental gust design limit load factor is specified in AFS-120-73-2 as follow:

$$A_{NLLF} = \frac{30KVm}{498\frac{W}{S}} \quad (4)$$

$$K = \frac{1}{2}\left(\frac{W}{S}\right)^{\frac{1}{4}} \quad \text{for } W/S < 16 \text{ psf} \quad (5)$$

$$K = 1.33 - \frac{2.67}{(W/S)^{\frac{3}{4}}} \quad \text{for } W/S > 16 \text{ psf} \quad (6)$$

$V$  = Airplane design cruising speed  $V_c$ , knots

$m$  = Lift curve slope,  $C_L$  per radian

$W/S$  = Wing loading at maximum gross weight, psf

AFS-120-73-2 does not specify the method for determining the incremental maneuver design limit load factor. Therefore, this load factor was calculated in accordance with the approach specified in FAR 23.337 using the maximum takeoff gross weight of 16,950 lbs.

For the positive incremental load factor:  $A_{NLLF} = 2.1 + [24,000 / (W + 10,000)] - 1$  (7)

For the negative incremental load factor:  $A_{NLLF} = -0.4\{2.1 + [24,000 / (W + 10,000)]\} - 1$

#### 4.2.5 Derived Gust Velocity.

Derived gust velocity is an important statistical load parameter, which can be derived from measured normal accelerations. The calculation of derived gust velocity from measured normal accelerations requires knowledge of atmospheric density, equivalent airspeed, dynamic pressure, and the lift curve slope. The derived gust velocity,  $U_{de}$ , is computed from the peak values of gust incremental normal acceleration as

$$U_{de} = \frac{\Delta n_z}{C} \quad (8)$$

where  $\Delta n_z$  is gust peak incremental normal acceleration and  $\bar{C}$  is the aircraft response factor considering the plunge-only degree of freedom and is calculated from

$$\bar{C} = \frac{\rho_0 V_e C_{L_\alpha} S}{2W} K_g \quad (9)$$

where

$$\begin{aligned} \rho_0 &= 0.002377 \text{ slugs/ft}^3, \text{ standard sea level air density} \\ V_e &= \text{equivalent airspeed (ft/sec)} \\ C_{L_\alpha} &= \text{aircraft lift curve slope per radian} \\ S &= \text{wing reference area (ft}^2\text{)} \\ W &= \text{gross weight (lbs)} \\ K_g &= \frac{0.88\mu}{5.3 + \mu} = \text{gust alleviation factor} \\ \mu &= \frac{2W}{\rho g \bar{c} C_{L_\alpha} S} \\ \rho &= \text{air density, slug/ft}^3, \text{ at pressure altitude (Hp), from equation 3} \\ g &= 32.17 \text{ ft/sec}^2 \\ \bar{c} &= \text{wing mean geometric chord (ft)} \end{aligned}$$

Equivalent air speed ( $V_e$ ) is a function of true air speed ( $V_T$ ) and the square root of the ratio of air density at altitude ( $\rho$ ) to air density at sea level ( $\rho_0$ )

$$V_e = V_T \sqrt{\frac{\rho}{\rho_0}} \quad (10)$$

For altitudes below 36,089 feet, the density  $\rho$  is expressed as a function of altitude based on the International Standard Atmosphere by

$$\rho = \rho_0 (1 - 6.876 \times 10^{-6} \times H_p)^{4.256}$$

where  $\rho_0$  is air density at sea level (0.0023769 slugs/ft<sup>3</sup>) and  $H_p$  is pressure altitude (ft). Pressure altitude is a recorded parameter.

The dynamic pressure ( $q$ ) is calculated from the air density and velocity

$$q = \frac{1}{2} \rho V^2 \quad (11)$$

where

$$\begin{aligned} \rho &= \text{air density at altitude (slugs/ft}^3\text{)} \\ V &= \text{true air speed (ft/sec)} \end{aligned}$$

For this study the wing lift curve slope ( $C_{l_\alpha}$ ) was obtained from the UDRI approximation [4]

$$C_{l_\alpha} = \frac{2\pi A_r}{2 + \left( 4 + A_r^2 \beta^2 \left( 1 + \frac{\tan^2 \Lambda}{\beta^2} \right) \right)^{1/2}} \quad (12)$$

$$A_r = \frac{b^2}{S} = \text{Wing Aspect Ratio}$$

$b$  = Wing Span

$$\beta = \sqrt{1 - M^2}$$

$C_{l_\alpha}$  = Wing Lift Curve Slope per Radian

$\Lambda$  = Quarter Chord Sweep Angle

$M$  = Mach number

Mach number is derived from true airspeed and speed of sound ( $a$ ):

$$M = \frac{V_T}{a} \quad (13)$$

The speed of sound ( $a$ ) is a function of pressure altitude ( $H_p$ ) and the speed of sound at sea level and is

$$a = a_0 \sqrt{(1 - 6.876 \times 10^{-6} \times H_p)} \quad (14)$$

thus

$$M = \frac{V_T}{a_0 \sqrt{(1 - 6.86 \times 10^{-6} \times H_p)}}$$

where the speed of sound at sea level  $a_0$  is 1116.4 fps or 661.5 knots.

Equation 12 provides an estimate of the wing lift curve slope. Airplane gust response calculations are based on the use of the airplane lift curve slope. Reference 5 suggests using an average factor of 1.15 to represent the ratio between the airplane lift curve slope and the wing lift curve slope. Therefore, the wing lift curve slope values were multiplied by 1.15. In this case, the wing lift curve slope,  $C_{l_\alpha}$ , is the untrimmed rigid lift curve slope for the entire aircraft.

### 4.3 DATA REDUCTION.

The following paragraphs describe the procedures UDRI used to process the recorded parameters.

#### 4.3.1 Initial Quality Screening.

All incoming data files are initially screened for missing or incomplete data before being accepted into the final database. Individual flights are edited to remove erroneous or meaningless data such as discontinuous elapsed time data, evidence of nonfunctional channels or sensors,

multiple flights on one file, and incomplete flight phases. Flight files with missing or incomplete data are identified and rejected from the final database.

#### 4.3.2 Aircraft Identification.

The 30 aircraft were identified by using the numerical tail number. However, during data editing the flap data from two aircraft were determined to be unreliable because the flap signal switched rapidly between detent settings during flight. UDRI treated all the data from these two aircraft as suspect and eliminated all data from these aircraft from the database. Thus, the final database sample size consisted of 903 flights, representing 585 flight hours recorded on 28 aircraft, and contained over 90% of the recorded flights. This is considered a very good recovery rate.

#### 4.3.3 Time History Files.

Each file provided by the airline contains multiple flights for each airplane. At UDRI these files were first separated into individual flight files. For each flight load parameter time history files were generated and compressed in a zip file. All time history files for a given aircraft were stored on a common 230-MB magneto-optical (MO) disk for later recall by the flight loads processing software. Data editing and verification were performed on the data as the time histories were prepared. Messages alerted the user that obviously erroneous data had been removed and/or that questionable data had been retained but needed to be manually reviewed prior to their acceptance. Table 3 lists the limits against which each parameter was compared. Parameters that are not included in the list were accepted as received.

TABLE 3. PARAMETER EDITING VALUES

	Item	Min	Max
1.	Pressure Altitude (Hp)	-2,000 ft	45,000 ft
2.	Indicated Airspeed	0 kts	420 kts
3.	Normal Acceleration	-2 g	+4 g
4.	Longitudinal Acceleration	±1.0 g	±1.0 g
5.	Propeller Reverse	0	1
6.	Pitch Attitude	-20°	+30°
7.	Flap Position	0	2
8.	Bank Angle	-60	+60
9.	Magnetic Heading	0°	360°

#### 4.3.4 Relational Database.

Important characteristics about each set of flights received from the airline are recorded in a relational database. Airline identifier, aircraft tail number, and disk identifier of the disk received from the airline are in the data. Each flight was assigned a unique flight sequence number. The flight sequence number assigned to the first flight of the set and the number of flights in the set were also entered. Also recorded was the disk identifier of the MO disk that contained the compressed time history files of all flights in the set.

#### 4.3.5 Permanent Data Files.

In addition to the time history file, five other files were created and permanently stored for each flight. The first file contains a chronologically sorted list of the phases of flight and their corresponding starting times for the flight. This file provides the means of separating the flight into flight phases in subsequent data analysis processing. This file is compressed and stored in the time history zip file for the flight. The second file contains the accumulated time and distance for various combinations of phase of flight and pressure altitude bands. The third file contains the accumulated time and distance for various ranges of altitude above the airport during departure and approach. These two files provide the capability to present data results in terms of normalized unit time and/or distance. The fourth file contains vertical acceleration peaks and coincident phase of flight, pressure altitude, indicated airspeed, and flap setting. The fifth file contains longitudinal acceleration peaks and coincident phase of flight.

### 4.4 DATA REDUCTION CRITERIA.

To process the measured data into statistical flight loads format, specific data reduction criteria were established for each parameter. These criteria are discussed in this section.

#### 4.4.1 Phases of Flight.

Each flight was divided into nine phases—four ground phases (taxi out, takeoff roll, landing roll, and taxi in) and five airborne phases (departure, climb, cruise, descent, and approach). Figure 2 shows these nine phases of a typical flight.

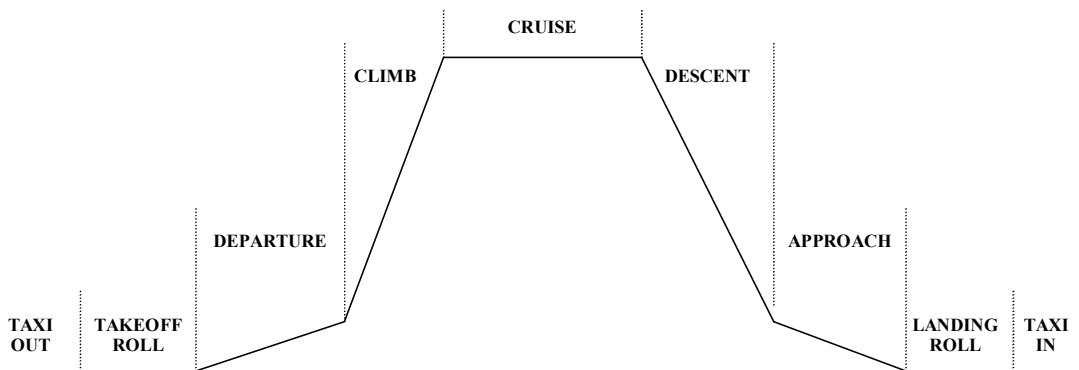


FIGURE 2. DESCRIPTION OF PHASES OF FLIGHT

Table 4 lists the conditions for determining the starting times for each phase. It should be noted that an airborne phase can occur several times per flight because it is determined by the rate of climb and the position of the flaps. When this occurs, the flight loads data are combined and presented in a single flight phase. The UDRI software creates a file that chronologically lists the phases of flight and their corresponding starting times.

TABLE 4. PHASE OF FLIGHT STARTING CRITERIA

Phase of Flight	Conditions at Start of Phase
Taxi Out	Initial condition
Takeoff Roll	Computed airspeed $> 45$ knots or $n_x > 0.15$ g
Departure	Time at liftoff; flaps extended
Climb	Flaps retracted; rate of climb $\geq 750$ ft/min. for at least 20 seconds
Cruise	Flaps retracted; rate of climb $\leq 750$ ft/min. for at least 20 seconds
Descent	Flaps retracted; rate of descent $\geq 750$ ft/min. for at least 20 seconds
Approach	Flaps extended
Landing Roll	Touchdown
Taxi In	Magnetic heading change greater than 13.5 degrees after touchdown

The criterion for defining the start of the takeoff roll is the earlier of 1) the time that the indicated speed exceeds 45 knots or 2) the time that the longitudinal acceleration exceeds 0.15 g prior to liftoff. The criterion for defining the start of taxi in is the time when the aircraft turns off the active runway. The method for detecting turn off is to monitor magnetic heading for a change greater than 13.5 degrees from the landing magnetic heading. The time when the heading starts to change in the turn off direction is then identified as the start of the turn or the beginning of the taxi in phase. This method can, however, fail to detect a shallow turn off onto a parallel taxiway. In this case an average landing roll of 32 seconds duration is assumed and the turn off is marked as 32 seconds after touchdown.

#### 4.4.2 Sign Convention.

Acceleration data are recorded in two directions: normal ( $z$ ) and longitudinal ( $x$ ). As shown in figure 3, the positive  $z$  direction is up and the positive  $x$  direction is forward.

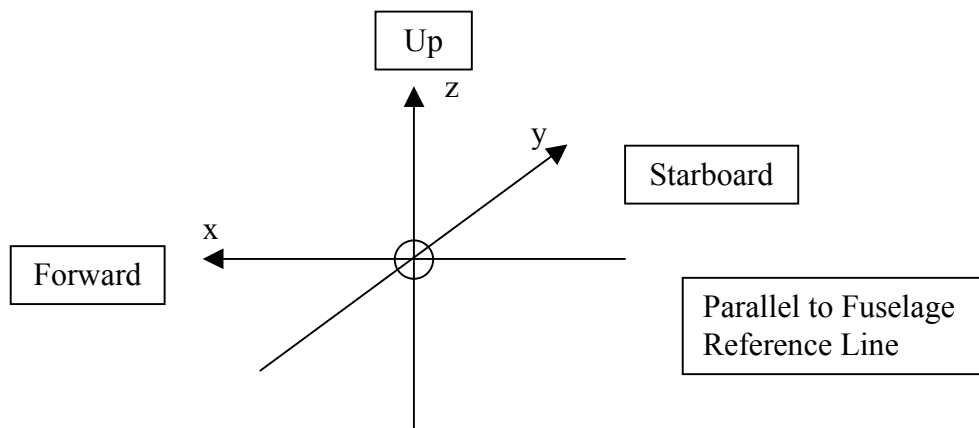


FIGURE 3. SIGN CONVENTION FOR AIRPLANE ACCELERATIONS

#### 4.4.3 Peak-Valley Selection.

The peak-between-means method presented in reference 6 was used to select the peaks and valleys in the acceleration data. This method is consistent with past practices and pertains to all

accelerations ( $n_x, \Delta n_z, \Delta n_{z_{man}}, \Delta n_{z_{gust}}$ ). Figure 4 depicts an example of the peak-between-mean criteria. This method counts upward events as positive and downward events as negative. Only one peak or one valley is counted between two successive crossings of the mean. A threshold zone (dead band) is used in the data reduction to ignore irrelevant loads variations around the mean. For the normal accelerations  $\Delta n_z$ , the threshold zone is  $\pm 0.05$  g; for longitudinal accelerations  $n_x$ , the threshold zone is  $\pm 0.005$  g.

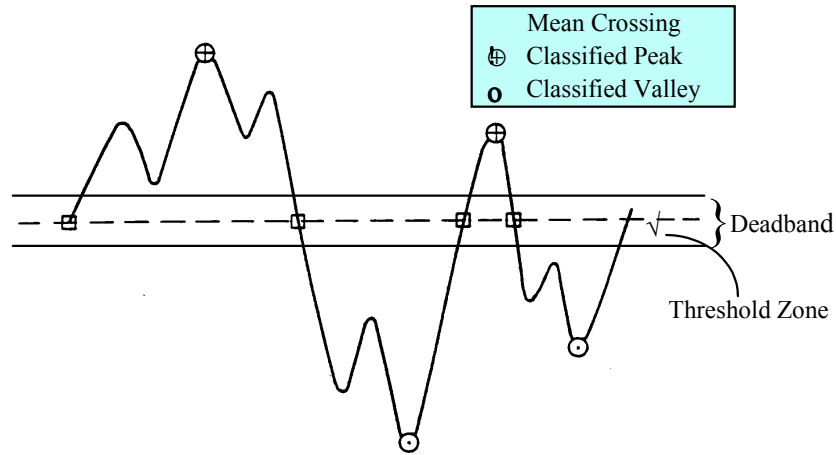


FIGURE 4. THE PEAK-BETWEEN-MEANS CLASSIFICATION CRITERIA

A peak is generated only when the acceleration data cross into or through the deadband. Two situations must be considered: the position of the current acceleration value relative to the deadband and the position of the previous acceleration value relative to the deadband. In the peak-between-means counting algorithm, the previous acceleration value is that value in a consecutive set of values, all of which lie either above the deadband or below the deadband. The previous value is established as a peak when the current value has crossed into or through the deadband. Figures 5A and 5B demonstrate the concept of current and previous acceleration values. In figure 5A the current acceleration value passes into the deadband whereas in figure 5B the current value passes through the deadband.

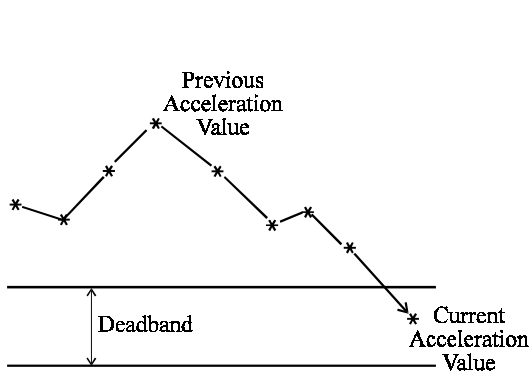


FIGURE 5A. CURRENT ACCELERATION VALUE PASSES INTO DEADBAND

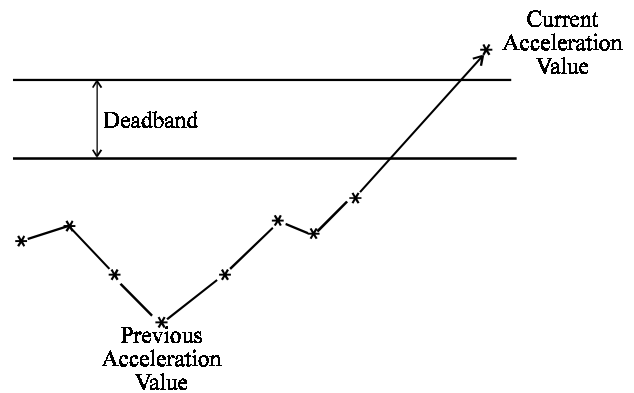


FIGURE 5B. CURRENT ACCELERATION VALUE PASSES THROUGH DEADBAND

Italicized text in table 5 summarizes the action(s) taken when the various possibilities occur. Note that when a previous acceleration value is retained as a potential peak, its coincident time is also retained.

TABLE 5. PEAK CLASSIFICATION CRITERIA

Previous Acceleration Value Relative to Deadband	Current Acceleration Value Relative to Deadband		
	Below	Within	Above
Above Previous value is potential positive peak	Current acceleration passes through deadband. <i>Previous value classified as a positive peak. Current value retained as a potential negative peak.</i>	Current acceleration passes into deadband. <i>Previous value classified as a positive peak. Acceleration value flagged as being in deadband.</i>	Current acceleration is on same side of deadband as previous. <i>If current &gt; previous value, retain current value as potential positive peak and release previous.</i>
Within At start of processing, or a peak was established but current acceleration value has not since gone outside of deadband	Current acceleration passes downward out of deadband. <i>Current value is retained as a potential negative peak.</i>	<i>No Action Required</i>	Current acceleration passes upward out of deadband. <i>Current value retained as potential positive peak.</i>
Below Previous value is potential negative peak	Current acceleration is on same side of deadband as previous. <i>If current value &lt; previous value, retain current value as potential negative peak and release previous value.</i>	Current acceleration passes into deadband. <i>Previous value is established as a negative peak. Acceleration value flagged as being in deadband.</i>	Current acceleration passes through deadband. <i>Previous value is classified as a negative peak. Current value retained as potential positive peak.</i>

#### 4.4.4 Separation of Maneuver and Gust Load Factors.

The incremental acceleration measured at the center of gravity (c.g.) of the aircraft may be the result of either maneuvers or gusts. In order to derive gust and maneuver statistics, the maneuver induced acceleration and gust response accelerations must be separated from the total acceleration history. Reference 7 reports the results of a UDRI study to evaluate methods of separating maneuver and gust load factors from measured acceleration time histories. As a result of this study it was recommended and accepted by the FAA that a cycle duration rule be used to separate gusts and maneuvers. A cycle duration of 2.0 seconds was recommended for use with B-737 and MD-82/83 aircraft. Review of the BE-1900D response characteristics has shown that this cycle duration can also be used with the BE-1900D data. In order to avoid the inclusion of peaks and valleys associated with very small load variations that are insignificant to the aircraft structure, a threshold zone of  $\Delta n_z = \pm 0.05$  g was established. An algorithm was then developed to extract the acceleration peaks and valleys.

For each flight the maximum and minimum total accelerations were determined from just after liftoff to just before touchdown. For the inflight phases, the  $\Delta n_z$  cumulative occurrences were determined as cumulative counts per nautical mile and cumulative counts per 1000 hours using the peak-between-means counting method of reference 6 as explained in section 4.4.3. The

measurements of  $\Delta n_z$ ,  $\Delta n_{z_{gust}}$ , and  $\Delta n_{z_{man}}$  are maintained as three unique data streams. The  $\Delta n_z$ ,  $\Delta n_{z_{gust}}$ , and  $\Delta n_{z_{man}}$  data are plotted as cumulative occurrences of a given acceleration increment per nautical mile and per 1000 flight hours. The incremental normal load factor  $\Delta n_z$  is the airplane limit load factor minus 1.0 g. As a result of the threshold zone, only accelerations greater than  $\pm 0.05$  g (measured from a 1.0-g base) are counted for data presentation.

#### 4.4.5 Flap Detents.

When flaps are extended, the effective deflection is considered to be that of the applicable detent, as indicated in table 6. The flap deflection ranges and placard speeds reflect the flap design placards [1].

TABLE 6. BE-1900D FLAP DETENTS

Flap Detent	Flap Setting	Operational Placard Speed (KIAS)
0	Retracted	248
1	Half	188
2	Full	154

#### 4.4.6 Altitude Bands.

For the departure and approach phases of flight, the altitudes are maintained as the altitude above the departure airport and arrival airport, respectively. The altitude bands used are as shown in table 7.

TABLE 7. ALTITUDE ABOVE AIRPORT BANDS

Band 1	0 – 250 feet
Band 2	251 – 500 feet
Band 3	501 – 750 feet
Band 4	751 – 1,000 feet
Band 5	1,001 – 1,500 feet
Band 6	1,501 – 2,000 feet
Band 7	2,001 – 3,000 feet
Band 8	3,001 – 4,000 feet
Band 9	4,001 – 5,000 feet
Band 10	> 5,000 feet

For all other flight phases the altitude bands reflect the absolute pressure altitude as shown in table 8.

TABLE 8. ABSOLUTE PRESSURE ALTITUDES

Band 1	< 500 feet
Band 2	501 – 1,500 feet
Band 3	1,501 – 4,500 feet
Band 4	4,501 – 9,500 feet
Band 5	9,501 – 14,500 feet
Band 6	14,501 – 19,500 feet
Band 7	19,501 – 24,500 feet

#### 4.4.7 Vertical Acceleration Bias Correction.

For a flight any bias occurring in the vertical (i.e., normal) acceleration measurement is removed by adjusting the difference between a known 1-g level and the actual acceleration recorded value. This difference is the correction/bias that will be added/subtracted from all measured load factor values for the flight.

## 5. DATA PRESENTATION.

This section presents statistical summaries of aircraft usage data, ground loads data, flight loads data, and systems operational data collected from BE-1900D aircraft during typical operational usage by a single commuter airline. Statistical data are presented for parameters such as gust and maneuver acceleration, airspeed, altitude, flight duration and distance, engine RPM and torque, time at propeller reversal, derived gust velocity, V-n diagrams, and vertical and longitudinal accelerations during ground operations. These data were reduced and processed into statistical formats that are typically used in presenting this type of data. These data can then be used by the FAA, the aircraft manufacturers, and the airlines to assess existing certification criteria contained in the FAA's Federal Aviation Regulation (FAR) or by the airlines and the aircraft manufacturer to better understand and control those factors that influence the structural integrity of commuter aircraft.

During data editing, it was found that the recorded data for certain flights/aircraft exhibited random errors and were unreliable. When this occurred, statistical data for any parameters associated, directly or indirectly, with the unreliable measurements from those flights and in some cases all data from that aircraft were eliminated from the database. The data presented herein are based on a total of 903 flights out of 1012 from 28 of the 30 aircraft representing approximately 585 flight hours of data.

Table 9 contains a list of the statistical data formats and identifies the corresponding figure where the processed data plot or table can be found in appendix A. The figures have been grouped into categories identified as aircraft usage, ground loads, flight loads, gust loads, maneuver loads, combined maneuver and gust loads, and operational data for the flap and propulsion systems. Each figure is discussed in the following paragraphs.

TABLE 9. STATISTICAL FORMATS

<b>AIRCRAFT USAGE DATA</b>		Figure
Correlation of Maximum Altitude and Flight Distance, Percent of Flights		A-1
Percent of Total Distance in Altitude Bands		A-2
Coincident Flight Distance and Maximum Flight Altitude		A-3
Coincident Altitude at Maximum Indicated Airspeed, All Flight Phases		A-4
Maximum Speed and Coincident Altitude During Climb		A-5
Maximum Speed and Coincident Altitude During Cruise		A-6
Maximum Speed and Coincident Altitude During Descent		A-7
Maximum Speed and Coincident Altitude During all Flight Phases		A-8
Number of Flights vs Flight Duration		A-9
Cumulative Probability of Flight Duration		A-10
<b>GROUND LOADS DATA</b>		
Cumulative Probability of Airspeed at Liftoff and Touchdown		A-11
Cumulative Probability of Pitch Angle at Liftoff		A-12
Cumulative Frequency of Longitudinal Load Factor During Taxi Operations		A-13
Cumulative Frequency of Incremental Vertical Load Factor During Taxi Operations		A-14
Cumulative Occurrences per 1000 Flights of Longitudinal Load Factor During Takeoff Roll		A-15
Cumulative Occurrences of Incremental Vertical Load Factor During Takeoff Roll		A-16
Cumulative Occurrences per 1000 Flights of Longitudinal Load Factor During Landing Roll		A-17
Cumulative Occurrences of Incremental Vertical Load Factor During Landing Roll		A-18
<b>FLIGHT LOADS DATA</b>		
<b>GUST LOADS DATA</b>		
Cumulative Occurrences of Incremental Gust Load Factor per 1000 Hours by Pressure Altitude for Combined Climb, Cruise, and Descent Phases		A-19
Cumulative Occurrences of Incremental Gust Load Factor per Nautical Mile by Pressure Altitude for Combined Climb, Cruise, and Descent Phases		A-20
Cumulative Occurrences of Incremental Gust Load Factor per 1000 Hours by Altitude Above Airport for Departure Phase		A-21
Cumulative Occurrences of Incremental Gust Load Factor per Nautical Mile by Altitude Above Airport for Departure Phase		A-22
Cumulative Occurrences of Incremental Gust Load Factor per 1000 Hours by Altitude Above Airport for Approach Phase		A-23
Cumulative Occurrences of Incremental Gust Load Factor per Nautical Mile by Altitude Above Airport for Approach Phase		A-24
Comparison of Cumulative Occurrences of Incremental Gust Load Factor per 1000 Hours for BE-1900D, B-737-400, and MD-82/83, Combined Flight Phases		A-25
Comparison of BE-1900D and B-737-400 Gust Response Factors		A-26
Comparison of Cumulative Occurrences of Incremental Gust Load Factor per Nautical Mile, BE-1900D vs AFS-120-73-2		A-27
Cumulative Occurrences of Derived Gust Velocity per Nautical Mile for Flap Extended		A-28
Cumulative Occurrences of Derived Gust Velocity per Nautical Mile for < 500 Feet		A-29
Cumulative Occurrences of Derived Gust Velocity per Nautical Mile for 500-1500 Feet		A-30
Cumulative Occurrences of Derived Gust Velocity per Nautical Mile for 1500-4500 Feet		A-31
Cumulative Occurrences of Derived Gust Velocity per Nautical Mile for 4500-9500 Feet		A-32

Table 9. STATISTICAL FORMATS (Continued)

GUST LOADS DATA (Continued)	Figure
Cumulative Occurrences of Derived Gust Velocity per Nautical Mile for 9500-19,500 Feet	A-33
Cumulative Occurrences of Derived Gust Velocity per Nautical Mile for 19,500-29,500 Feet	A-34
Coincident Gust Load Factor and Speed vs V-n Diagram for Half Flaps During Departure	A-35
Coincident Gust Load Factor and Speed vs V-n Diagram for Full Flaps During Departure	A-36
Coincident Gust Load Factor and Speed vs V-n Diagram for Half Flaps During Approach	A-37
Coincident Gust Load Factor and Speed vs V-n Diagram for Full Flaps During Approach	A-38
<b>MANEUVER LOADS DATA</b>	
Cumulative Occurrences of Incremental Maneuver Load Factor per 1000 Hours by Pressure Altitude for Combined Climb, Cruise, and Descent Phases	A-39
Cumulative Occurrences of Incremental Maneuver Load Factor per Nautical Mile by Pressure Altitude for Combined Climb, Cruise, and Descent Phases	A-40
Cumulative Occurrences of Incremental Maneuver Load Factor per 1000 Hours by Altitude Above Airport for Departure Phase	A-41
Cumulative Occurrences of Incremental Maneuver Load Factor per Nautical Mile by Altitude Above Airport for Departure Phase	A-42
Cumulative Occurrences of Incremental Maneuver Load Factor per 1000 Hours by Altitude Above Airport for Approach Phase	A-43
Cumulative Occurrences of Incremental Maneuver Load Factor per Nautical Mile by Altitude Above Airport for Approach Phase	A-44
Comparison of Cumulative Occurrences of Incremental Maneuver Load Factor per Nautical Mile, BE-1900D vs AFS-120-73-2	A-45
Cumulative Occurrences per Flight of Peak Bank Angle	A-46
<b>COMBINED MANEUVER AND GUST LOADS DATA</b>	
Cumulative Occurrences of Incremental Load Factor per 1000 Hours by Pressure Altitude for Combined Climb, Cruise, and Descent Phases	A-47
Cumulative Occurrences of Incremental Load Factor per Nautical Mile by Pressure Altitude for Combined Climb, Cruise, and Descent Phases	A-48
Cumulative Occurrences of Incremental Load Factor per 1000 Hours by Altitude Above Airport for Departure Phase	A-49
Cumulative Occurrences of Incremental Load Factor per Nautical Mile by Altitude Above Airport for Departure Phase	A-50
Cumulative Occurrences of Incremental Load Factor per 1000 Hours by Altitude Above Airport for Approach Phase	A-51
Cumulative Occurrences of Incremental Load Factor per Nautical Mile by Altitude Above Airport for Approach Phase	A-52
Cumulative Occurrences of Incremental Load Factor per 1000 Hours for Combined Flight Phases	A-53
Cumulative Occurrences of Incremental Load Factor per 1000 Hours for Individual aircraft, Combined Flight Phases	A-54
Comparison of Cumulative Occurrences of Incremental Load Factor per 1000 Hours for BE-1900D, B-737-400, and MD-82/83, Combined Flight Phases	A-55
Comparison of Cumulative Occurrences of Incremental Load Factor per 1000 Hours for BE-1900D and SAE 931257, Combined Flight Phases	A-56

TABLE 9. STATISTICAL FORMATS (Continued)

SYSTEMS OPERATIONAL DATA	Figure
<b>FLAP SYSTEM</b>	
Cumulative Probability of Maximum Airspeed During Flap Extension	A-57
Percent of Time in Flap Detent During Departure and Approach	A-58
<b>PROPULSION SYSTEM</b>	
Cumulative Probability of Time in Reversed Propeller	A-59
Cumulative Probability of Speed at Time of Propeller Reversal, Left Propeller	A-60
Cumulative Probability of Time with Propeller in Reverse, Left Propeller	A-61
Cumulative Probability of RPM at Liftoff	A-62
Cumulative Time at RPM Levels	A-63
Cumulative Probability of Maximum RPM During Reverse Cycle, Left Propeller	A-64
Cumulative Probability of Maximum Torque During Takeoff Roll	A-65
Cumulative Time at Torque Levels	A-66

## 5.1 AIRCRAFT USAGE DATA.

The aircraft usage data include flight profile statistics such as altitudes, speeds, and flight distance information. This information is useful for deriving typical flight profiles; for defining loading spectra for structural fatigue, durability, and damage tolerance analyses; and for developing future design criteria. Aircraft usage data are presented in figures A-1 through A-10.

### 5.1.1 Altitude and Flight Distance Data.

Measured operational altitudes and their correlation to flight distance are presented. The table in figure A-1 shows the correlation between the maximum altitude attained in flight and the flight distance flown in percent of flights. The data show that the maximum altitude attained during almost 80% of all flights does not exceed 15,000 feet with approximately half of these between 10,000 and 15,000 feet. Also, over 90 percent of the flights are of 250 nautical miles length or less. Figure A-2 presents the percent of total flight distance spent in various altitude bands as a percent of flight distance. The flight distances in figure A-2 do not reflect the actual stage lengths or great circle distances between departure and arrival location but do reflect the actual distances flown based on the numerical integration approach mentioned in paragraph 4.2.3. Deviation from direct flight between departure and arrival points resulting from traffic control requirements will increase the actual distance flown by some unknown amount. To a much lesser extent, the climb and descent distances are slightly larger than the level flight distance. Head or tail winds also are unknown contributors. The integrated distance accounts for such variables. The combined information in figures A-1 and A-2 provides a useful picture of the flight profile distribution.

### 5.1.2 Coincident Airspeed and Altitude Data.

Flight distance and altitude statistics are useful in the generation of flight profiles. Figure A-3 shows the maximum altitude reached for each flight and the corresponding distance flown for that flight. The plot seems to confirm that the maximum altitude reached per flight is a function

of the flight distance. Figure A-4 contains a line intersecting the x-axis at 248 knots which represents the maximum allowable operating speed for each altitude. The data points were generated by locating the airspeed and corresponding altitude during each flight where the aircraft came the closest to this limit condition or the highest airspeed was used when the limit was exceeded. The data show that this speed limit was exceeded for some of the flights.

### 5.1.3 Maximum Operating Airspeed Data.

The maximum speed attained by coincident altitude and by phase of flight is very useful in obtaining a picture of the flight speed profile. Figures A-5, A-6, and A-7 present the maximum airspeed attained for the climb, cruise, and descent phases of flight by altitude. Figure A-8 shows the data for all the flight phases combined. Each data point represents the maximum airspeed attained within each 1000 foot band of altitude; therefore, the actual point is plotted for the maximum speed and the corresponding altitude where the maximum speed occurred. For each plot, UDRI has drawn in the aircraft design operational speed line obtained from reference 1. The plots show that this limit is occasionally being slightly exceeded during the cruise and descent phases of flight.

### 5.1.4 Flight Duration.

Flight duration is also important in the generation of flight profiles. The bar chart in figure A-9 contains a breakdown of the number of flights flown versus the time duration of each flight from takeoff to landing. The mean flight length was determined to be 36.4 minutes. Figure A-10 presents the same flight duration data in a cumulative probability format.

## 5.2 GROUND LOADS DATA.

The ground loads data include frequency and probability information on vertical and longitudinal accelerations, speeds, and pitch angle associated with takeoff, landing, and ground operations. These data are of primary importance to landing gear and landing gear backup structure and to a lesser extent to the wing, fuselage, and empennage. Ground load data are presented in figures A-11 through A-18.

### 5.2.1 Airspeed at Liftoff and Touchdown.

Figure A-11 shows the cumulative probabilities of airspeed at liftoff and at touchdown. The variation in the probability of airspeed is very similar for the two conditions, except that for identical probabilities the liftoff speeds are approximately 30 knots higher than the touchdown speeds.

### 5.2.2 Pitch Angle at Liftoff.

Information about pitch angle is useful as a performance parameter to show the attitude of the aircraft. The cumulative probability of pitch angle at the instant of liftoff is shown in figure A-12. A majority of the data shows the pitch angle at liftoff to be between 3-5 degrees.

### 5.2.3 Load Factor Data During Ground Operations.

The cumulative frequencies of longitudinal and vertical load factors are presented for the ground phases of operations. These data are useful for calculating loads on the landing gear and the backup structure. Figures A-13 and A-14 present longitudinal and vertical load factors, respectively during taxi operations broken out by taxi in and out. Figures A-15 and A-16 show these data during the takeoff roll. Figures A-17 and A-18 present these data during the landing roll phase of flight broken out with and without the use of propeller reversal.

## 5.3 FLIGHT LOADS DATA.

The flight loads data presented in this section include statistical formats that describe the gust, maneuver, and combined maneuver and gust loads environment. For these loading conditions, the normal acceleration data have been plotted in two ways: 1) as cumulative occurrences per 1000 hours and 2) as cumulative occurrences per nautical mile.

### 5.3.1 Gust Loads Data.

The gust loads data are presented as cumulative occurrences of vertical gust load factor and as cumulative occurrences of derived gust velocity per nautical mile. Gust load factor data are also compared with recorded data from other aircraft types and with other published data. Coincident gust load factor and speed data are presented on representative V-n diagrams by flap position for the approach and departure phases of flight. The gust loads data are presented in figures A-19 through A-38.

#### 5.3.1.1 Gust Load Factor Data.

Figure A-19 presents the cumulative occurrences of incremental vertical gust load factor per 1000 hours by pressure altitude for the combined climb, cruise, and descent phases of flight; figure A-20 presents these same data per nautical mile. Figures A-21 through A-24 show the cumulative occurrences of incremental vertical gust load factor for the departure and approach phases of flight by altitude above the airport. The combined phase acceleration data do not show a reduction of gust encounters with increasing altitude as would normally be expected. However, the data samples are quite small for both the combined phases and the departure and approach phases. Experience has shown that increased sample sizes will change the statistical data results. In addition, the departure and approach acceleration data are plotted by altitude above the airport and can not be directly compared to other data samples plotted as a function of pressure altitude. Data presented in this format will be more influenced by turbulence resulting from ground effects.

#### 5.3.1.2 Comparison of BE-1900D Gust Load Factor Data With Other Aircraft.

Figure A-25 shows the difference in severity of vertical load factor for gust between a commuter aircraft, the BE-1900D, and two large transport aircraft, the B-737 and the MD82/83 during routine commercial operations. UDRI previously processed the large transport aircraft data for the FAA, which published it in Department of Transportation reports references 8, 9 and 10. The BE-1900D aircraft load factor response to gust is more than twice the severity of the B-737. To

explain this difference, UDRI calculated the aircraft discrete gust response factor (using equation 9) using the maximum takeoff weight and the operational speed limit for the BE-1900D and the B-737-400 aircraft. The comparison of the calculated BE-1900D gust response factor to that of the B-737-400 as shown in figure A-26 explains why the difference in severity of load factor occurs.

#### 5.3.1.3 Comparison of BE-1900D Gust Load Factor Data With Other Technical Data.

Comparisons of the BE-1900D gust load factor data per nautical mile were made between the BE-1900D and the twin engine general usage spectra contained in FAA report number AFS-120-73-2 [3]. Figure A-27 shows that the twin engine general spectra for gust is more severe than the BE-1900D spectra.

#### 5.3.1.4 Gust Velocity Data.

The derived gust velocity,  $U_{de}$ , was computed from the measured gust acceleration data using the equations described in section 4.2.5. Figure A-28 shows the cumulative occurrences of derived gust velocity per nautical mile with the flaps extended. Even with only 903 flight hours of data, the plot shows there are a few occurrences of derived gust velocity that exceed the FAR 23.345 requirement of 25 ft/sec.

Figures A-29 through A-34 show the cumulative occurrences of derived gust velocity per nautical mile for selected altitude levels. Derived gust velocity data, previously developed for the B-737-400 aircraft [9], have also been plotted on these same figures for comparison purposes.

Although the comparison of gust velocities encountered per nautical mile for each aircraft shows fairly close agreement, the derivation of gust velocity from measured accelerations (as seen in equation 9 in section 4.2.5) requires the coincident parameters of gross weight, speed, and altitude. Unfortunately, gross weight was not a measured parameter for the BE-1900D. Therefore, for purposes of this report a constant gross weight equal to the 45-day average takeoff gross weight of 14,500 lbs as determined by the airline was assumed in the determination of derived gust velocity. Thus the resulting derived gust velocity spectra are based on a constant gross weight of 14,500 lbs, but these spectra would change if the actual gross weights were known.

#### 5.3.1.5 V-n Diagrams.

The V-n diagrams in figures A-35 through A-38 are shown for illustration only and represent a gross weight of 14,500 lbs. and a sea level altitude. The V-n diagrams are drawn using an airspeed limit of 188 KIAS for flap detent position 1 (half) and an airspeed limit of 154 KIAS for flap detent position 2 (full). These figures show the coincident gust load factor and airspeed plotted with respect to the illustrated gust V-n diagram for each flap setting. Figure A-35 shows that all the gust load factor data for half flaps during departure fall within the V-n envelope. Unfortunately, the data for full flap operations, figure A-36, proved to be unreliable so this figure was left intentionally blank. Figures A-37 and A-38 show that a few of the gust load factors occur at airspeeds that slightly exceed the speed limits with either half or full flap deployed during the approach phase of flight. UDRI looked at each of these incidents and found that the

overspeeds occurred during a few seconds coincident with the flaps being lowered and while the aircraft was slowing for its approach.

### 5.3.2 Maneuver Loads Data.

The maneuver loads data are presented as cumulative occurrences of incremental vertical load factor per 1000 hours and per nautical mile by altitude for various phases of flight. Maneuver load factor data are also compared with recorded data from other aircraft types and with other published data. Cumulative occurrences of the maximum bank angle attained during each turning maneuver are also presented in this section. The maneuver loads data are presented in figures A-39 through A-46.

#### 5.3.2.1 Maneuver Load Factor Data.

Figures A-39 and A-40 present the cumulative occurrences of maneuver load factor per 1000 hours and per nautical mile by pressure altitude for the combined climb, cruise, and descent flight phases. Figures A-41 and A-42 present the total cumulative occurrences of incremental maneuver load factor per 1000 hours and per nautical mile for the departure phase of flight by altitude above the airport. Figures A-43 and A-44 show the same information for the approach phase of flight. Considering the extremely small data samples in the altitude bands, no clear conclusions can be drawn from the data presented.

#### 5.3.2.2 Comparison of BE-1900D Maneuver Load Factor Data With Other Technical Data.

While the comparisons of spectra between the BE-1900D and those contained in FAA report number AFS-120-73-2 [3] show the twin engine general spectra for gust to be more severe (figure A-27), the same comparison using only the maneuver load factor data as seen in figure A-45 shows very little difference in usage.

#### 5.3.2.3 Bank Angle Data.

Information about the bank angle can be used for determining the number of asymmetrical maneuvers and the aircraft attitude during these maneuvers. The cumulative occurrences of peak bank angle occurring per bank are shown per flight in figure A-46. The data show that the maximum bank angle recorded was 50 degrees.

### 5.3.3 Combined Maneuver and Gust Loads Data.

For the statistical data presented in this section, the maneuver and gust load factors were not separated, but the total load factor occurrences regardless of the cause were used in the derivation of the figures. The combined maneuver and gust loads data are presented as cumulative occurrences of incremental vertical load factor per 1000 hours and per nautical mile by altitude for various phases of flight. Also, comparisons of usage were made between individual aircraft within the airline's fleet of instrumented aircraft, data recorded on other commuter aircraft, and other published small aircraft data.

### 5.3.3.1 Combined Maneuver and Gust Load Factor Data.

Figures A-47 and A-48 show the cumulative occurrences of total combined maneuver and gust normal load factor per 1000 hours and per nautical mile for the combined climb, cruise, and descent phases of flight by pressure altitude. Figures A-49 and A-50 show the combined cumulative acceleration occurrences for the departure phase by altitude above airport while figures A-51 and A-52 show similar data for the approach phase.

The combined cumulative occurrences of incremental load factor for maneuver and gust are presented for all the flight phases combined in figure A-53. The plot shows the maximum incremental positive and negative load factor recorded to be about +1.2 g's. The BE-1900D data contained in figure A-53 are also used in other sections of this report when load factor comparisons are made with other aircraft and other published data.

### 5.3.3.2 Comparison of Individual Aircraft Usage.

Figure A-54 contains a comparison of usage between individual aircraft within the airline's fleet of instrumented aircraft. The identification of each plot by aircraft tail number was omitted to avoid cluttering the plot. The individual aircraft data, presented as cumulative occurrences of incremental vertical load factor per 1000, are typically used to compare the severity of usage and/or to calculate the damage (i.e., fatigue) between individual aircraft. The data show a considerable amount of scatter in usage between individual aircraft. However, this could be the result of the small amount of data available for each aircraft. Table 10 shows the amount of data available for each aircraft by tail number.

TABLE 10. INDIVIDUAL AIRCRAFT STATISTICAL DATA

Aircraft Tail Number	Number of Flights	Flight Time (hrs)	Aircraft Tail Number	Number of Flights	Flight Time (hrs)
830	29	22.1	845	38	22.4
831	44	22.9	846	29	21.9
832	26	19.9	847	40	19.9
833	30	21.8	848	34	18.7
834	34	20.2	852	28	25.4
835	6	5.0	853	33	22.8
836	31	20.0	854	23	22.0
837	32	19.9	855	34	23.2
838	33	21.0	856	30	17.7
839	42	23.5	857	22	21.3
840	30	25.0	858	32	17.8
841	33	22.0	859	42	19.4
842	37	21.6	860	39	25.1
844	41	22.1	862	31	21.0

### 5.3.3.3 Comparison of BE-1900D Flight Loads Data With Other Commuter Aircraft and Other Technical Data.

Comparisons of usage were made between data recorded on other commuter aircraft and other published small aircraft data. Figure A-55 provides a comparison of the relative severity of vertical load factor for gust and maneuver combined between five commuter type aircraft, the BE-1900D, the Canadair Challenger CL-601, the DeHavilland Dash-8 aircraft [11], the Fairchild/Dornier 328 [12], and the Fokker F-27 [13].

The BE-1900D spectra were also compared with Beech Aircraft Company developed data plotted in SAE Technical Paper number 931257 [14]. The SAE paper shows load spectra data developed based on AFS-120-73-2 data and LR-516 data and a spectra consisting of combined ESDU Item No.69023 and NASA SP-279 spectra data. These data are compared in figures A-56 with the BE-1900D combined maneuver and gust load spectra data and show the BE-1900D recorded spectra to be less severe than for the two Beech developed spectra.

## 5.4 SYSTEMS OPERATIONAL DATA.

This section contains operational usage data recorded on the BE 1900D flap and propulsions systems.

### 5.4.1 Flap System Data.

Flap usage statistics are of value in the design of flap structure, backup structure, and other flap components. There are three flap positions for this aircraft: retracted, half, and full. A sensor located in the flap track of the aircraft recorded the actual flap detent positions as either 0, 1, or 2. Data showing the maximum aircraft airspeed while the flaps were deployed and the time the flaps were in use are presented in this section.

#### 5.4.1.1 Airspeed During Flap Usage.

Figure A-57 presents the cumulative probability of maximum airspeed encountered with the flaps in use during the approach and departure phases of flight. Since the actual position of the flap was measured by a sensor on the flap track as either stowed, half, or full, all data occurring while the flaps were in transition are plotted against the sensor indication at the time of the measurement.

#### 5.4.1.2 Time by Flap Detent Setting.

Figure A-58 presents the percent of time spent in each flap position for both the departure and approach phases of flight. During departure the flaps were almost always set in the half down position. For the approach phase the ratio was about 60 to 40 for half versus the full down position.

## 5.4.2 Propulsion System Data.

Statistical formats describing propeller usage and engine RPM and torque operation data are included in this section.

### 5.4.2.1 Propeller Data.

Data showing whether the right and left propellers were reversed or not and the corresponding time were recorded. However, only data from the left propeller were processed because a sampling of the data taken from both propellers showed that thrust reversal was always used on both engines simultaneously. Figure A-59 presents the cumulative probability of total time that left propeller thrust reversal was employed. As can be seen from the plot, propeller reversal was used on about 56 percent of all flights. Also, UDRI investigated why the lower portion of the curve showed an unusually large amount of time recorded with the propeller reversed. UDRI found that on several occasions the reversed propeller parameter indicated that the propeller was in the reversed position for long periods of time while the aircraft was not in the landing roll phase of flight.

Figure A-60 shows the cumulative probability of the indicated airspeed at the time the propeller reversal action was taken. The plot shows about a 30% probability of occurrences for speeds between 10-20 and 20-40 knots with a lesser probability for the propellers to be reversed at all other speed ranges up to 100 knots. Figure A-61 shows the cumulative probability of time with the propeller in the reversed position. This plot shows that 90 percent of the time the propeller stays in the reversed position from 0-30 seconds.

### 5.4.2.2 Engine RPM and Torque Level Data.

RPM and torque data were recorded for both the left and right engines. Engine RPM data are presented in figure A-62 for each engine as the cumulative probability of RPM at liftoff. The plot shows the left side engine to have a slightly higher value of RPM. Figure A-63 presents the cumulative time spent per flight as a function of the RPM setting. This plot shows a majority of the time was spent at an RPM level around 1500, which can be associated with the cruise portion of the flight. Another level around 1000-1200 RPM can be associated with the ground portion of the flight.

Figure A-64 shows the cumulative probability of maximum RPM at the instant of propeller reversal and during the time the propeller is reversed. The data shows very little change in RPM between the two events. The engine RPM level while the propeller is reversed that is used most often to slow the aircraft ranges between 1000-1200 RPM.

The cumulative probability of maximum engine torque during takeoff roll is shown for both the left and right engines in figure A-65. This plot also indicates that both engines generated the same amount of torque. Figure A-66 shows the cumulative time spent per flight at each torque level. The data tend to show significant time at torque levels between 0-900 ft-lbs. and also at torque levels between 2500 and 3500 ft-lbs., which could indicate ground and airborne operations, respectively.

A time history plot of engine RPM and torque for a typical flight is shown in figure 6 and indicates how the RPM and torque levels vary throughout the flight.

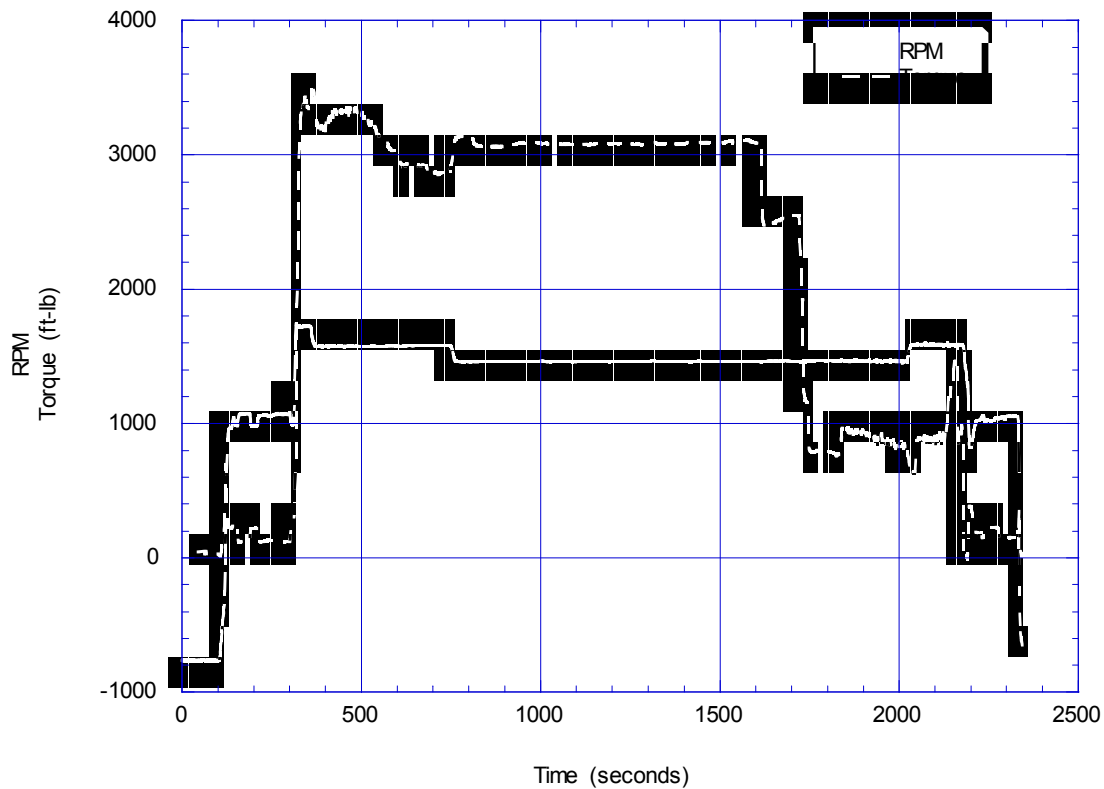


FIGURE 6. TIME HISTORY PLOT OF ENGINE RPM AND TORQUE

## 6. CONCLUSIONS AND RECOMMENDATIONS.

The objectives of this program were achieved. All of the participants worked well together to complete the project ahead of schedule. The overall quality of the recorded data was very good. The statistical data formats that were developed provide a very in-depth look at the various parameters that influence the structural integrity of commuter aircraft. These formats present data that should be useful to the FAA, the aircraft manufacturers, and the airlines. The following paragraphs discuss the most noteworthy findings.

The derived and processed data presented in the many statistical formats seemed to match, with some exceptions, what one would expect for an aircraft of this type. For instance, the altitude, airspeed, and flight distance data revealed flight profiles that were consistent with a commuter type aircraft. The spectra of left and right banked turns were essentially symmetrical, which indicated the aircraft experiences an equal number of left and right turns. The use of half flaps occurred during takeoff, while both half and full flaps were used during the approach phase. Some flights, however, indicated only the use of full flaps during approach.

Comparisons of the BE-1900D statistical data with their operational limits and with data from other aircraft and published data revealed some interesting anomalies that require further study.

- The operational speed limits associated with flap deployment during some of the flight phases were exceeded. The V-n diagram data seem to indicate that in a few instances the flaps were being lowered at speeds in excess of the flap operational limit speed. If this is true, the flaps were being subjected to loads in excess of design. This situation appeared on only a few flights and it was not clear whether these data were correct or if an instrumentation problem existed. It is recommended that the instrumentation be reviewed for these aircraft to ascertain their proper operation.
- Large differences in measured gust load factors between the commuter type aircraft and the large transport aircraft were found but were accounted for by the differences in the load factor response of each aircraft.
- The gust load factor spectra prescribed in AFS-120-73-2 for use in the fatigue design of “general usage, twin engine” aircraft were considerably more severe than those encountered by this commuter airline in normal operations. The maneuver spectra specified in the same document were also more severe than actually encountered but not quite to the extent of the gust spectra requirements. This may be an indication of why light aircraft designed under the FAR-23 requirements exhibit useful lives in excess of those predicted using the AFS-120-73-2 design requirements. It also emphasizes the need for revision and update of the AFS-120 documents.
- Comparison of the derived gust velocities for the commuter aircraft and the larger commercial aircraft shows no major differences, which indicated operation in the same turbulence environment. Since derivation of derived gust velocity requires knowledge of the aircraft’s gross weight and this information was not available for the BE-1900D, an average takeoff gross weight was assumed in order to do the calculations. It is recommended that future data include at least the aircraft takeoff and landing weight for improved accuracy of the derived gust velocities.

The statistical information presented in this report is based on only 585 flight hours of collected data. For military aircraft a rule of thumb has been that a minimum number of recorded flight hours equal to one design life is necessary to provide a reliable database. However, military aircraft generally fly a variety of different mission profiles. In contrast, except for duration, the commercial aircraft is used in a fairly well defined mission. While the number of recorded flight hours equal to one design life may not be necessary, what this number should be is not quite clear at this time. At the same time, the 817.7 hours on which the data in reference 7 are based were found to be insufficient to provide meaningful results. The data for the reference 8 aircraft when based on over 19,000 flight hours show important differences. Comparison of results presented in references 7 and 8 seems to indicate that, at least for a large commercial aircraft, a minimum of 10,000 flight hours is necessary to obtain reasonable statistical stability in the data. Therefore, it would seem prudent to continue gathering commuter type data until a stable database is obtained.

Several of the basic data formats presented in this report for the commuter type aircraft are different from those used for larger commercial aircraft, such as presented in references 8 and 9. For example, the basic load factor data for climb, cruise, and descent were combined instead of showing the data separately by phase. Also, the departure and approach load factor data were presented by altitude above the airport instead of by pressure altitude. A consistent set of formats for all types of aircraft would be highly desirable. It would allow comparisons of the loading environments between different types of commercial aircraft. This will translate into a more realistic comparison between the design requirements of FAR-25 and FAR-23. This comparison becomes more important as the commuter type aircraft increase in size, passenger carrying capacity, and range performance.

Load factor spectra compared between individual aircraft showed large variations. This most likely occurred because of such a small sample size. Therefore, the use of such data in assessing relative fatigue damage when based on limited sample sizes will not provide reliable results.

Some of the flights received contained bad data that appeared to have resulted from the onboard instrumentation system. For example, the flap position indicator signal on two aircraft switched rapidly back and forth between half and full positions during the flight, the signal that indicated the direction of propeller rotation was reversed on several of the aircraft. Also, negative RPM values were measured on some flights. While these problems can usually be found during editing, they cause disruptions to the normal processing activity and take a considerable amount of time to determine the cause of the problem and what course of action needed to be taken. Therefore, it is important that all onboard instrumentation be checked for proper installation, calibration, and sign convention prior to data recording during operational flights. This will assure a maximum of useable data and will help to expedite the data editing and processing effort.

Additional instrumentation to record related parameters such as gross weight, fuel weight, lateral acceleration, and Mach number should be installed to provide more in-depth and accurate information to the user of these data. Also, the lack of a squat switch on the landing gear made establishing the exact moment of liftoff and touchdown difficult. This can lead to inaccuracies in the determination of the start of departure and landing phases and possibly the misplacement of load factor occurrences associated with these phases. Installation of a squat switch and these additional parameters are highly recommended.

## 7. REFERENCES.

1. FAA Type Certificate Data Sheet Number A-24CE, Revision 68.
2. Anonymous, "Jane's All the Worlds Aircraft 1997-1998," page 710.
3. "Fatigue Evaluation of Wing and Associated Structures on Small Aircraft," Department of Transportation Report No. AFS-120-73-2, May 1973.
4. Nicolai, Leland M., "Fundamentals of Aircraft Design," University of Dayton, 1975.

5. Hoblit, Frederic M. et al., "Development of a Power Spectral Gust Design Procedure for Civil Aircraft," Technical Report FAA-ADS-53, 1966.
6. de Jonge, B., "Reduction of Incremental Load Factor Acceleration Data to Gust Statistics," DOT/FAA/CT-94/57, August 1994.
7. Rustenburg, John W., Donald Skinn, and Daniel O. Tipps, "An Evaluation of Methods to Separate Maneuver and Gust Load Factors from Measured Acceleration Time Histories," DOT/FAA/AR-99/14, April 1999.
8. Skinn, D., P. Miedlar, and L. Kelly, "Flight Loads Data for a Boeing 737-400 in Commercial Operation," Department of Transportation Report DOT/FAA/AR-95/21, April 1996.
9. Rustenburg, John W., Donald Skinn, and Daniel O. Tipps, "Statistical Loads Data for Boeing 737-400 Aircraft in Commercial Operations," Department of Transportation Report DOT/FAA/AR-98/28, August 1998.
10. Skinn, Donald, Daniel O. Tipps, and John Rustenburg, "Statistical Loads Data for MD-82/83 Aircraft in Commercial Operations," Department of Transportation Report DOT/FAA/AR-98/65, February 1999.
11. David, G. M. M., "Analysis of Fatigue Loads Data Obtained From Transport Canada Challenger & Dash-8 Aircraft Engaged in Low-Level Flying Operations," Transport Canada Report TP 11574, November 1992.
12. Brunbauer, Robert, Bernd Herbing, Holger Hickethier, and Reiner Teske, "Results of the Dornier 328 Operational Loads Recording Campaign," 20<sup>th</sup> ICAF Symposium, 12-16 July 1999, Bellevue, Washington.
13. de Jonge, J. B. and P. A. Hol, "Variation in Load Factor Experience of Fokker F-27 and F-28 Operational Acceleration Exceedance Data," Department of Transportation Report DOT/FAA/AR-96/114, December 1996.
14. Smith, Johnny, "Structural Airworthiness of New and Aging Aircraft: Load Spectra Derivation and Measurement," SAE Technical Paper Series No. 931257, presented at 1993 SAE General, Corporate, and Regional Aviation Meeting and Exposition, May 18-20, 1993, Wichita, Kansas.

APPENDIX A – STATISTICAL FORMATS, AIRCRAFT USAGE DATA

Maximum Altitude (1000 feet)

		Maximum Altitude (1000 feet)					
BE-1900D 903 flts, 585 hrs, 136440 nm		0-5	5-10	10-15	15-20	20-25	Total
Flight Distance (nm)	0-50	11.960	0.775	0.000	0.000	0.000	12.735
	50-100	2.215	7.420	0.221	0.000	0.000	9.856
	100-150	0.000	10.631	17.165	1.218	0.000	29.014
	150-200	0.000	5.648	14.286	4.873	0.000	24.806
	200-250	0.000	0.332	6.091	4.651	4.319	15.393
	250-300	0.000	0.554	1.772	2.769	0.997	6.091
	300-350	0.000	0.000	0.443	0.664	0.554	1.661
	350-400	0.000	0.000	0.111	0.111	0.000	0.221
	400-450	0.000	0.000	0.111	0.111	0.000	0.221
	Total	14.175	25.360	40.199	14.396	5.869	100.000

FIGURE A-1. CORRELATION OF MAXIMUM ALTITUDE AND FLIGHT DISTANCE, PERCENT OF FLIGHTS

Total Flight Distance (nm)

		Total Flight Distance (nm)								
903 flts, 585 hrs, 136440 nm		0-50	50-100	100-150	150-200	200-250	250-300	300-350	350-400	400-450
Altitude Band (feet)	19,500-24,500	0	0	0	0	12.13	4.9	17.51	0	0
	14,500-19,500	0	0	2.4	11.76	21.63	25.97	28.12	18.26	6.55
	9,500-14,500	0	1.35	36.5						
	4,500-9,500	5.86	56.63	40.09	31.49	20.55	22.22	13.98	16.49	9.23
	1,500-4,500	73.77	33.51	16.49	14.49	9.2	12.15	10.35	15.14	5.81
	500-1,500	16.08	5.84	3.33						
	<500	4.29	2.67	1.19	1.12	0.81	0.77	0.72	0.86	0.56
	Total Percent	100	100	100	100	100	100	100	100	100
Number of Flights	115	89	262							

FIGURE A-2. PERCENT OF TOTAL DISTANCE IN ALTITUDE BANDS

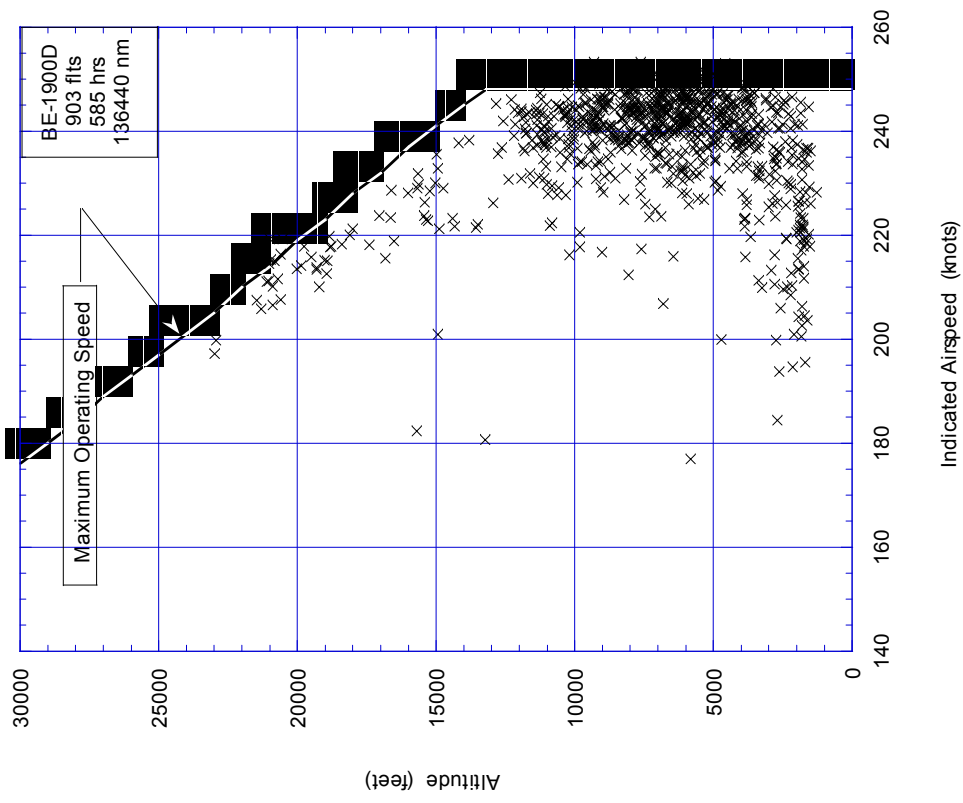


FIGURE A-4. COINCIDENT ALTITUDE AT MAXIMUM INDICATED AIRSPEED, ALL FLIGHT PHASES

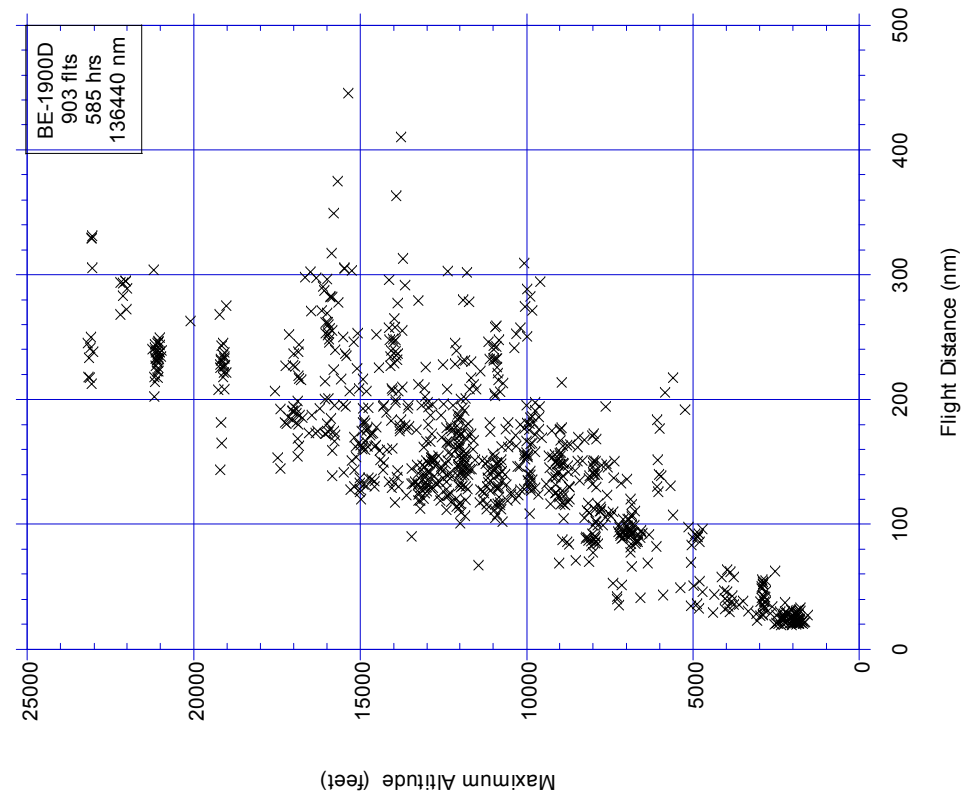


FIGURE A-3. COINCIDENT FLIGHT DISTANCE AND MAXIMUM FLIGHT ALTITUDE

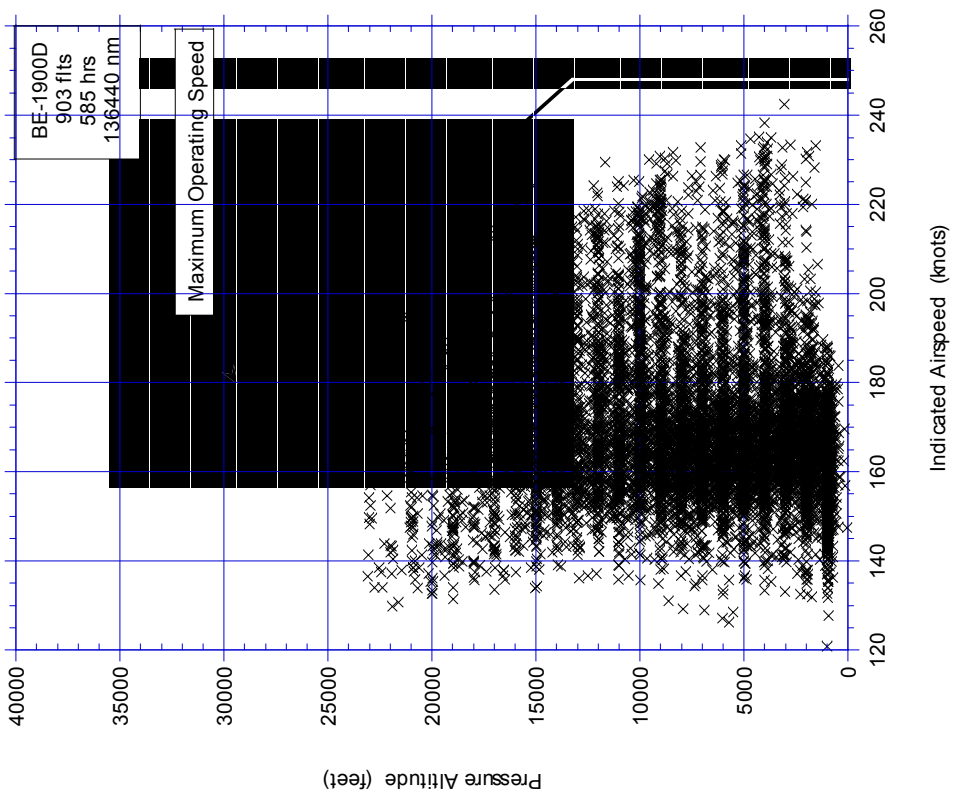


FIGURE A-5. MAXIMUM SPEED AND COINCIDENT ALTITUDE DURING CLIMB

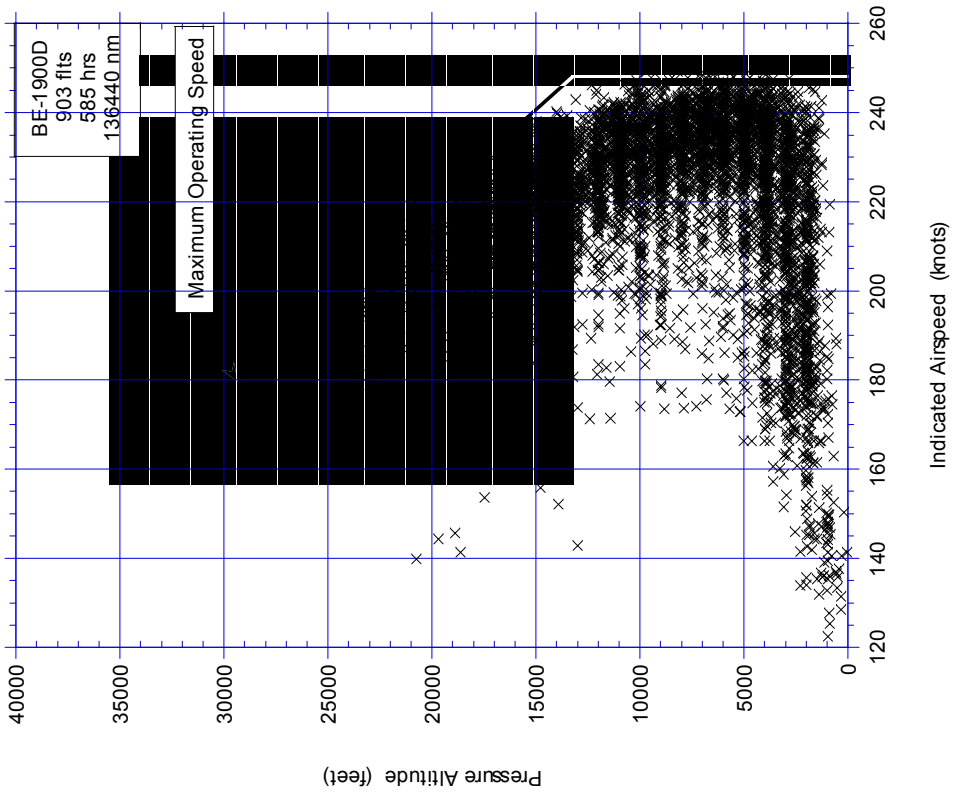


FIGURE A-6. MAXIMUM SPEED AND COINCIDENT ALTITUDE DURING CRUISE

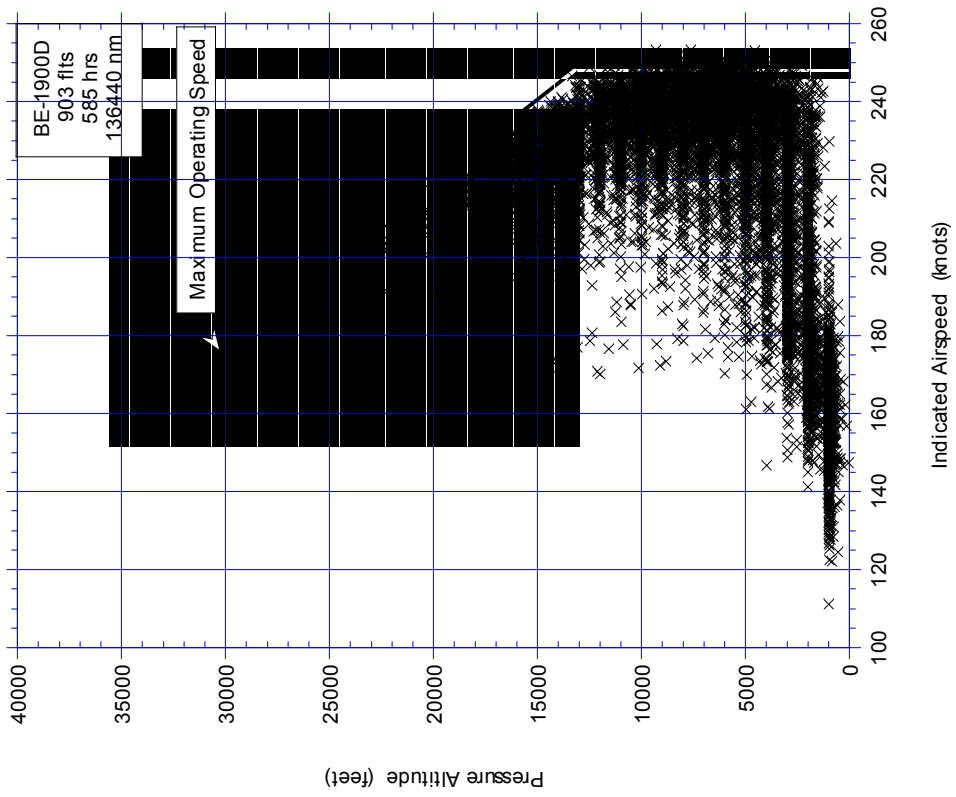


FIGURE A-8. MAXIMUM SPEED AND COINCIDENT ALTITUDE DURING ALL FLIGHT PHASES

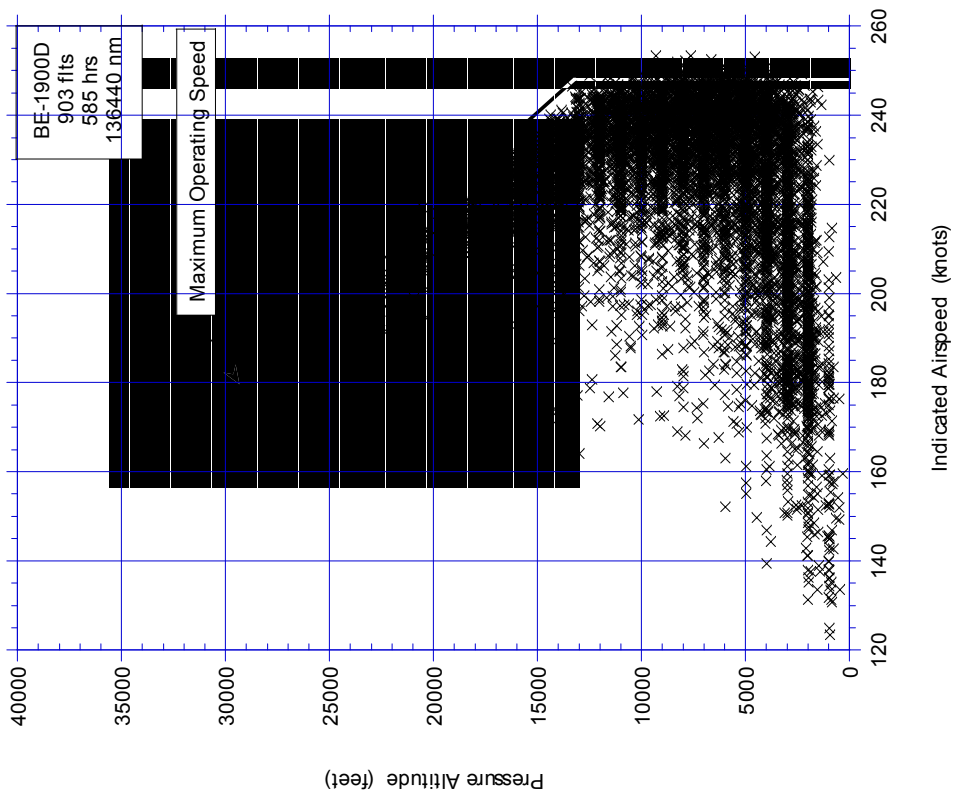


FIGURE A-7. MAXIMUM SPEED AND COINCIDENT ALTITUDE DURING DESCENT

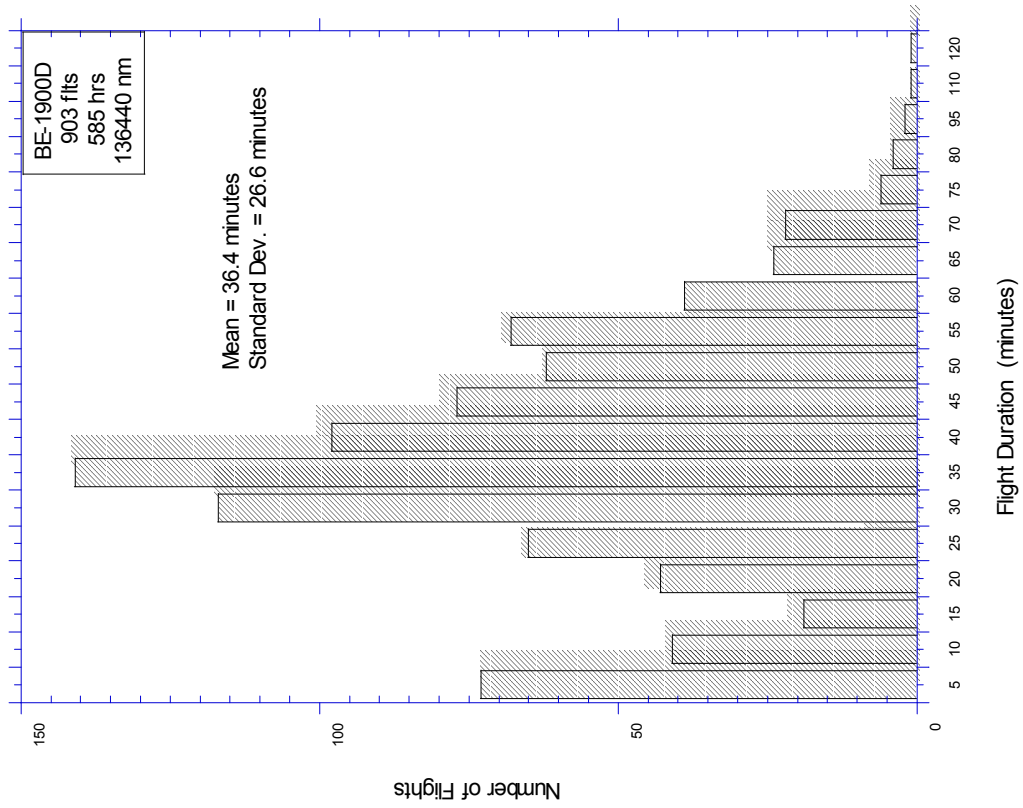


FIGURE A-9. NUMBER OF FLIGHTS VS FLIGHT DURATION

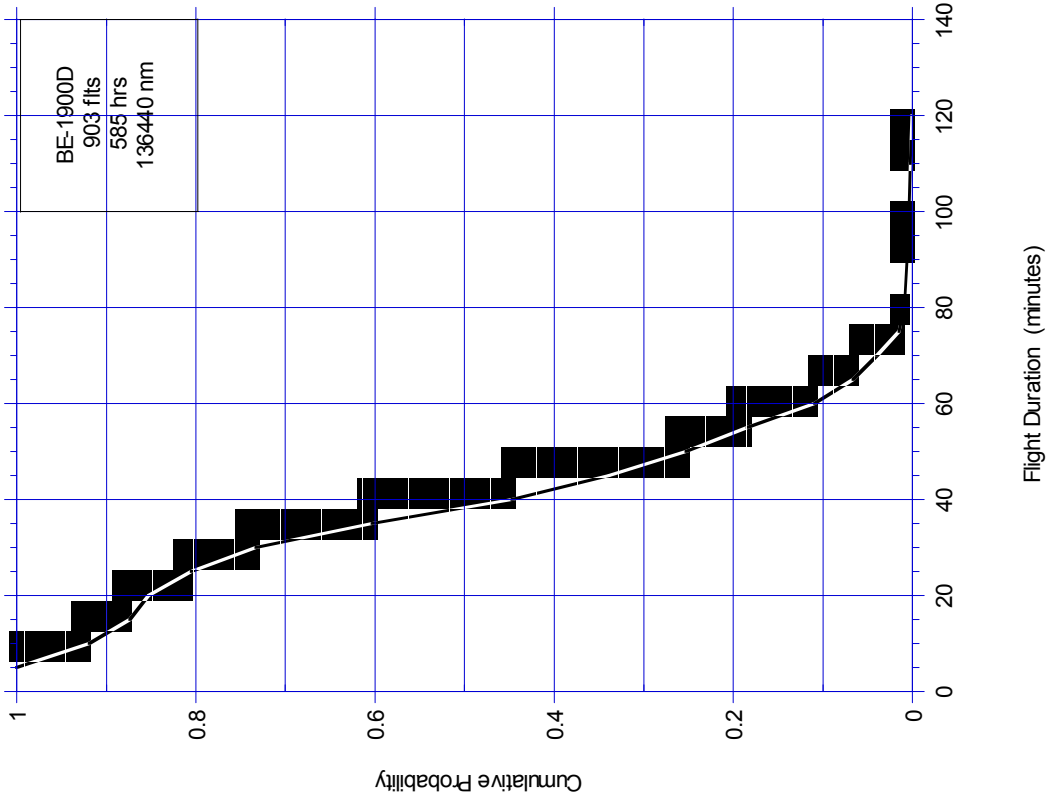


FIGURE A-10. CUMULATIVE PROBABILITY OF FLIGHT DURATION

APPENDIX A - STATISTICAL FORMATS,  
GROUND LOADS DATA

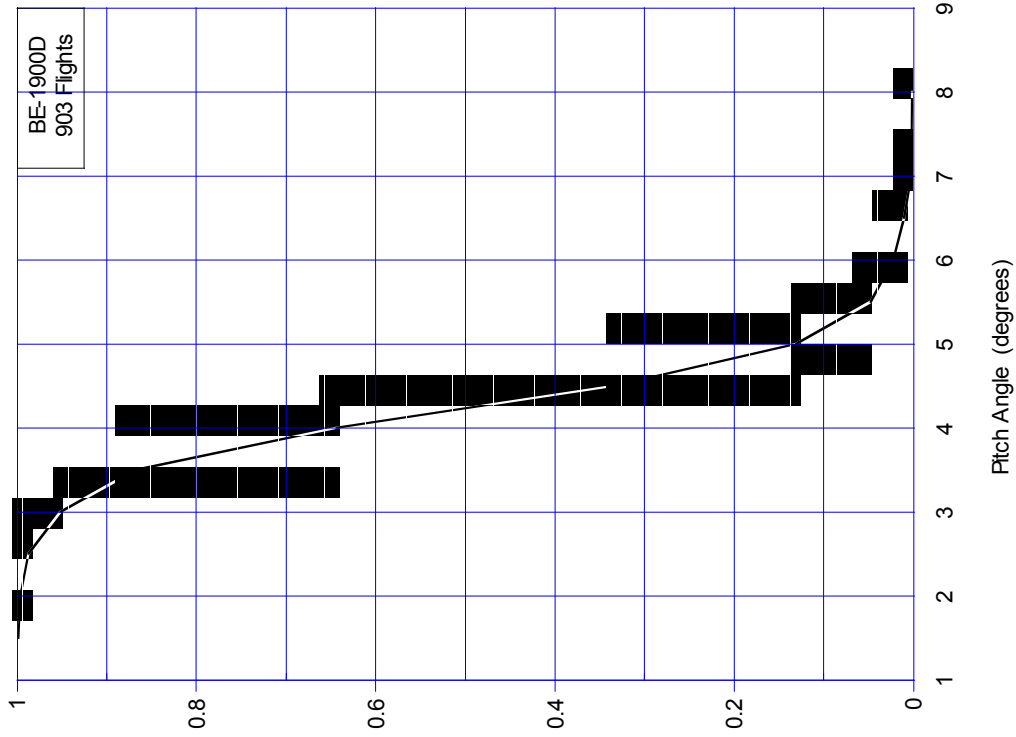


FIGURE A-11. CUMULATIVE PROBABILITY OF AIRSPEED AT LIFTOFF AND TOUCHDOWN

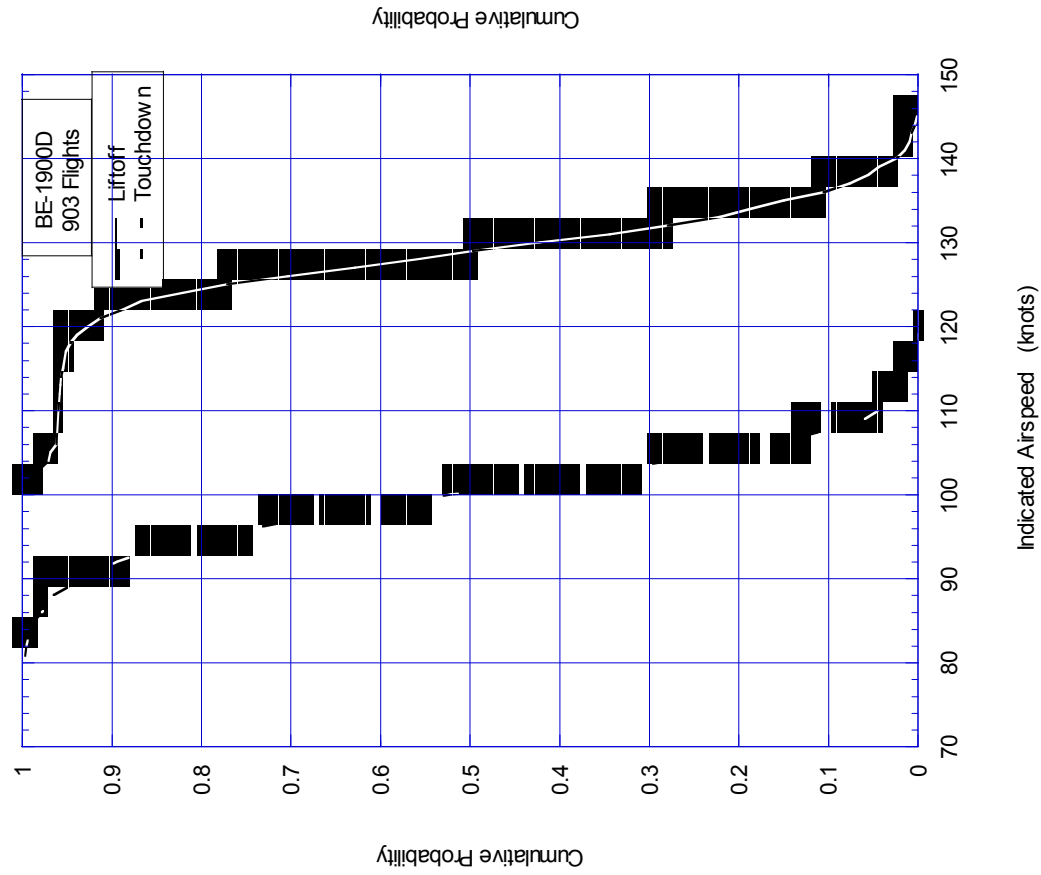


FIGURE A-12. CUMULATIVE PROBABILITY OF PITCH ANGLE AT LIFTOFF

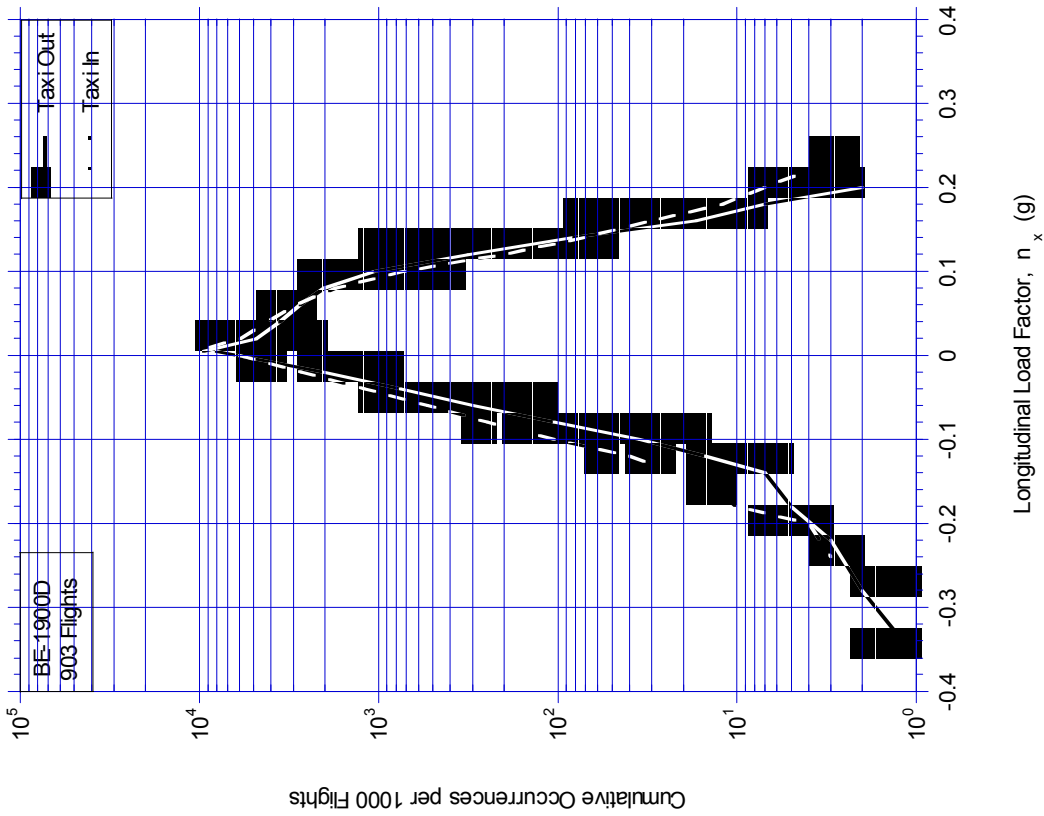


FIGURE A-13. CUMULATIVE FREQUENCY OF LONGITUDINAL LOAD FACTOR DURING TAXI OPERATIONS

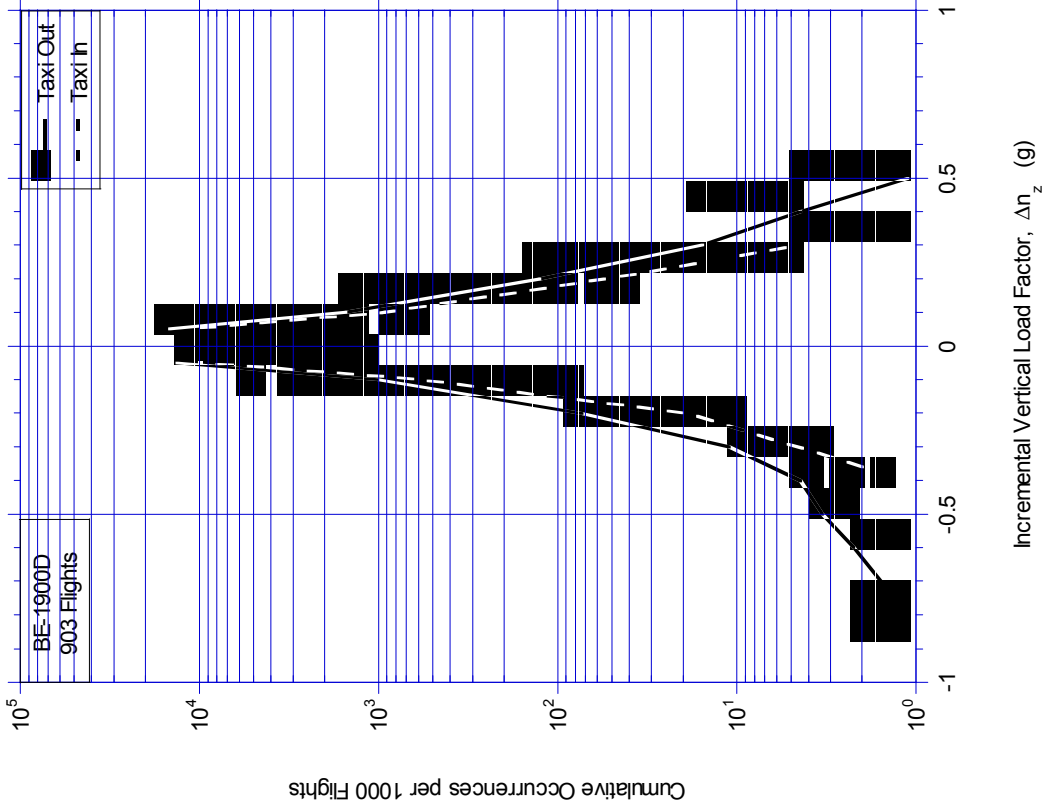


FIGURE A-14. CUMULATIVE FREQUENCY OF INCREMENTAL VERTICAL LOAD FACTOR DURING TAXI OPERATIONS

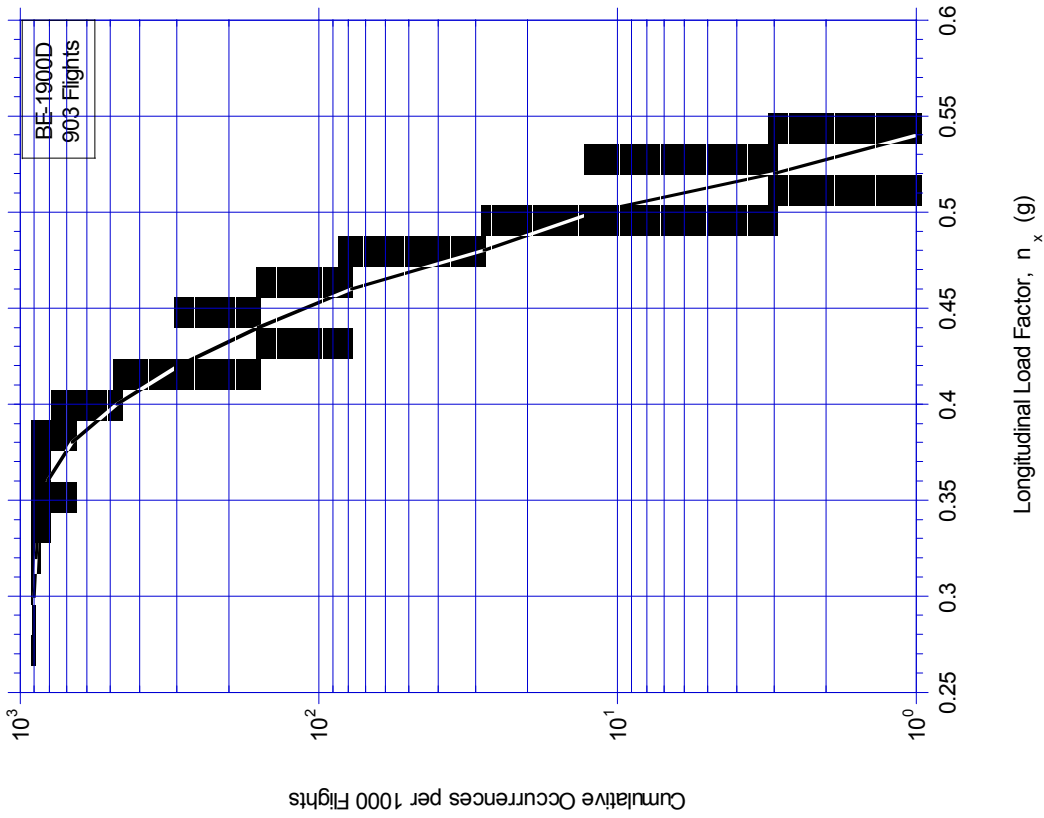


FIGURE A-15. CUMULATIVE OCCURRENCES PER 1000 FLIGHTS OF LONGITUDINAL LOAD FACTOR DURING TAKEOFF ROLL

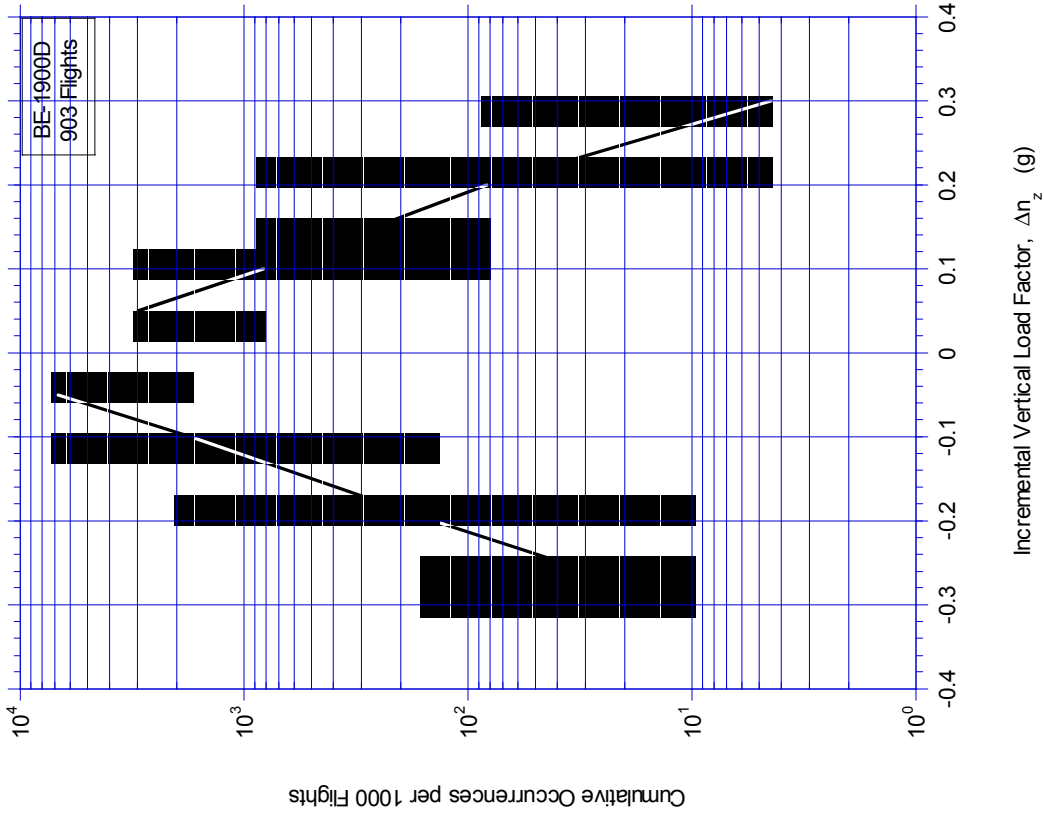


FIGURE A-16. CUMULATIVE OCCURRENCES OF INCREMENTAL VERTICAL LOAD FACTOR DURING TAKEOFF ROLL

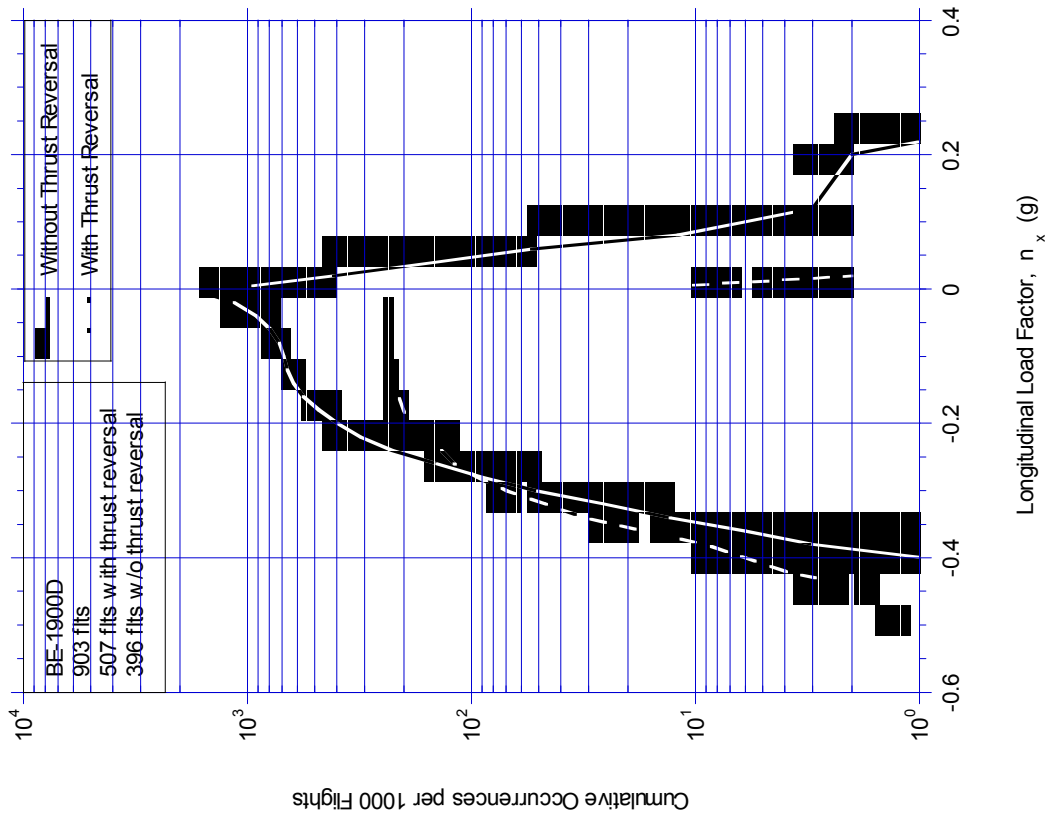


FIGURE A-17. CUMULATIVE OCCURRENCES PER 1000 FLIGHTS OF LONGITUDINAL LOAD FACTOR DURING LANDINGS

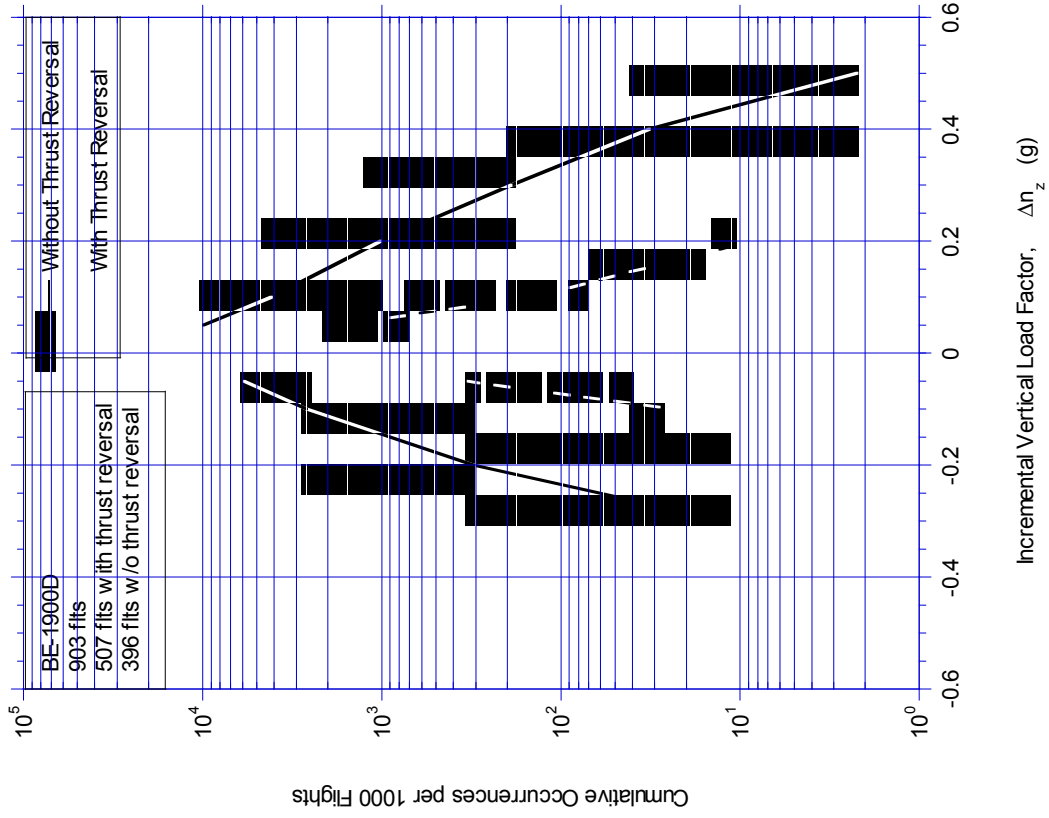


FIGURE A-18. CUMULATIVE OCCURRENCES OF INCREMENTAL VERTICAL LOAD FACTOR DURING LANDINGS

APPENDIX A - STATISTICAL FORMATS,  
FLIGHT LOADS DATA, GUST LOADS DATA

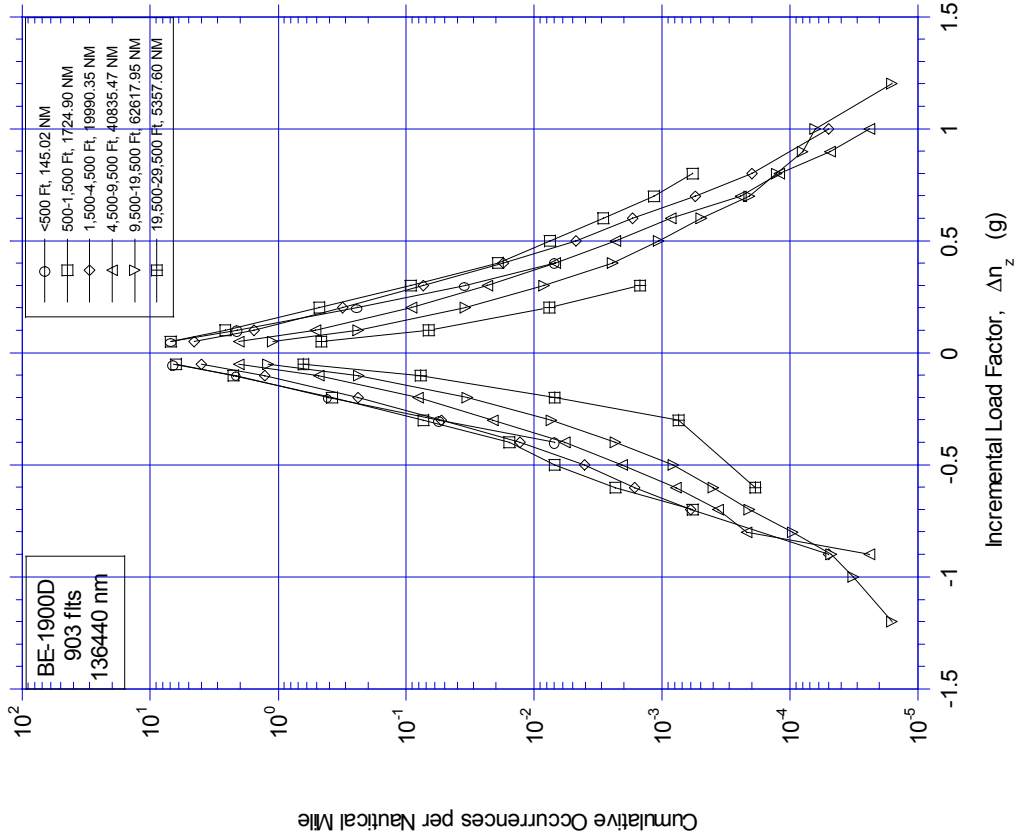


FIGURE A-19. CUMULATIVE OCCURRENCES OF  
INCREMENTAL GUST LOAD FACTOR PER 1000 HOURS  
BY PRESSURE ALTITUDE FOR COMBINED CLIMB,  
CRUISE, AND DESCENT PHASES

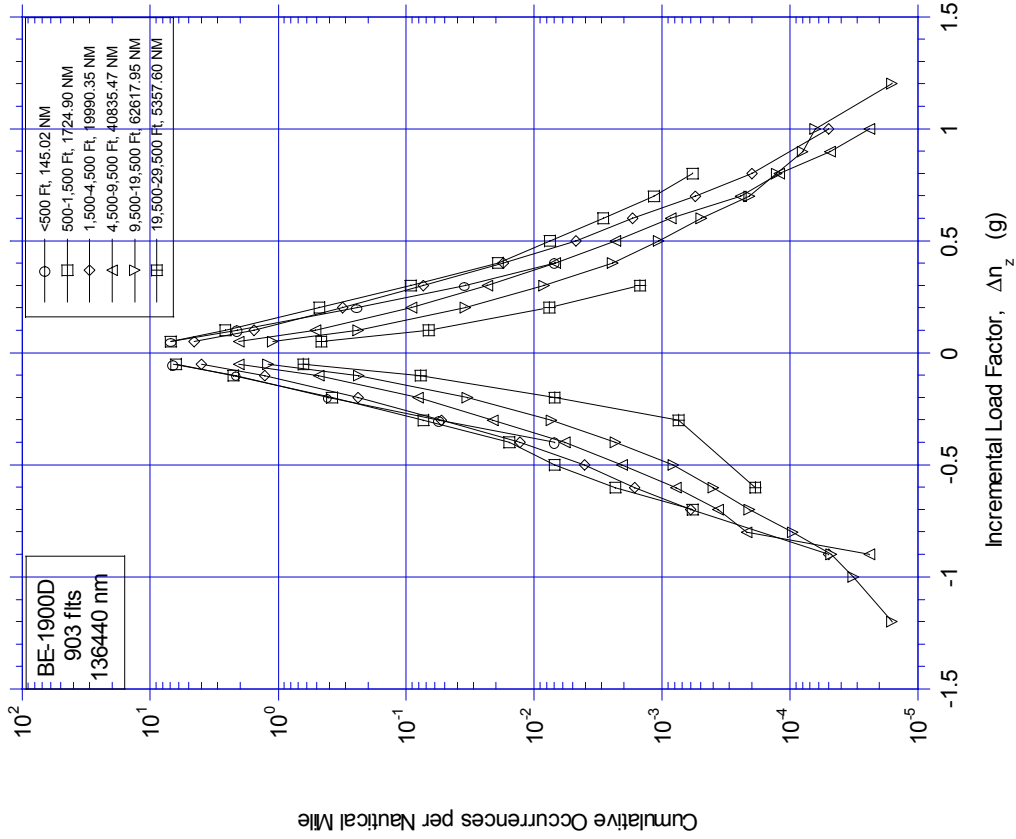


FIGURE A-20. CUMULATIVE OCCURRENCES OF  
INCREMENTAL GUST LOAD FACTOR PER NAUTICAL  
MILE BY PRESSURE ALTITUDE FOR COMBINED CLIMB,  
CRUISE, AND DESCENT PHASES

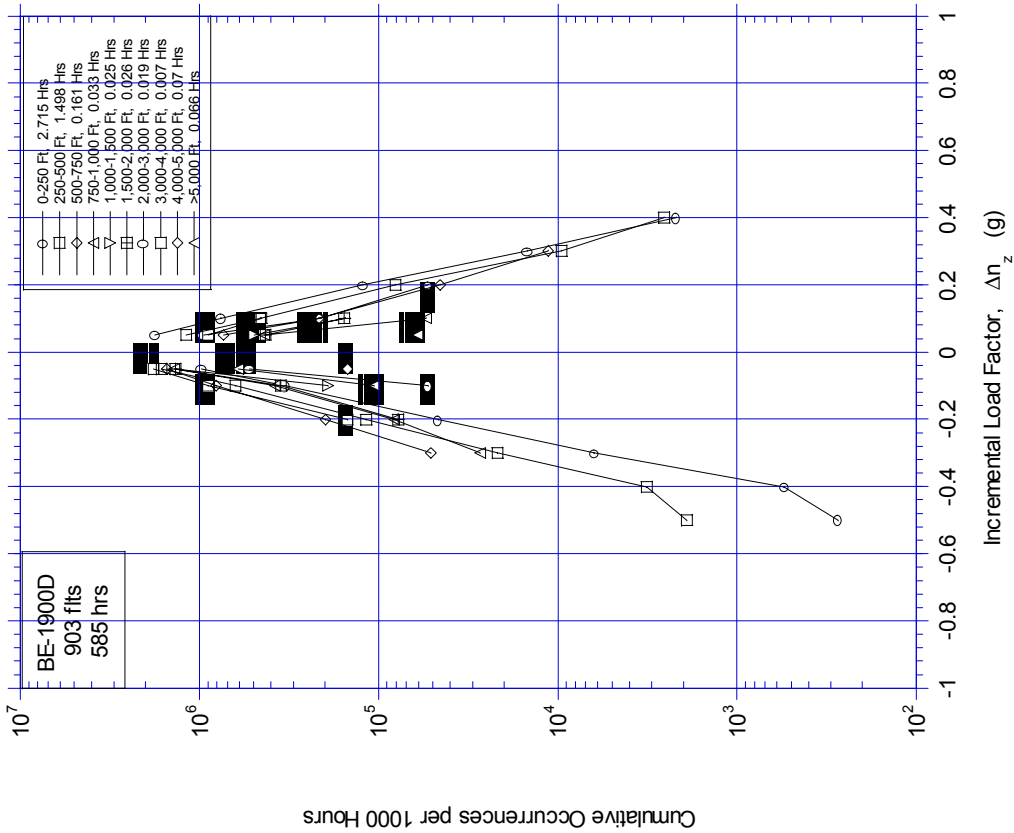


FIGURE A-21. CUMULATIVE OCCURRENCES OF INCREMENTAL GUST LOAD FACTOR PER 1000 HOURS BY ALTITUDE ABOVE AIRPORT FOR DEPARTURE PHASE

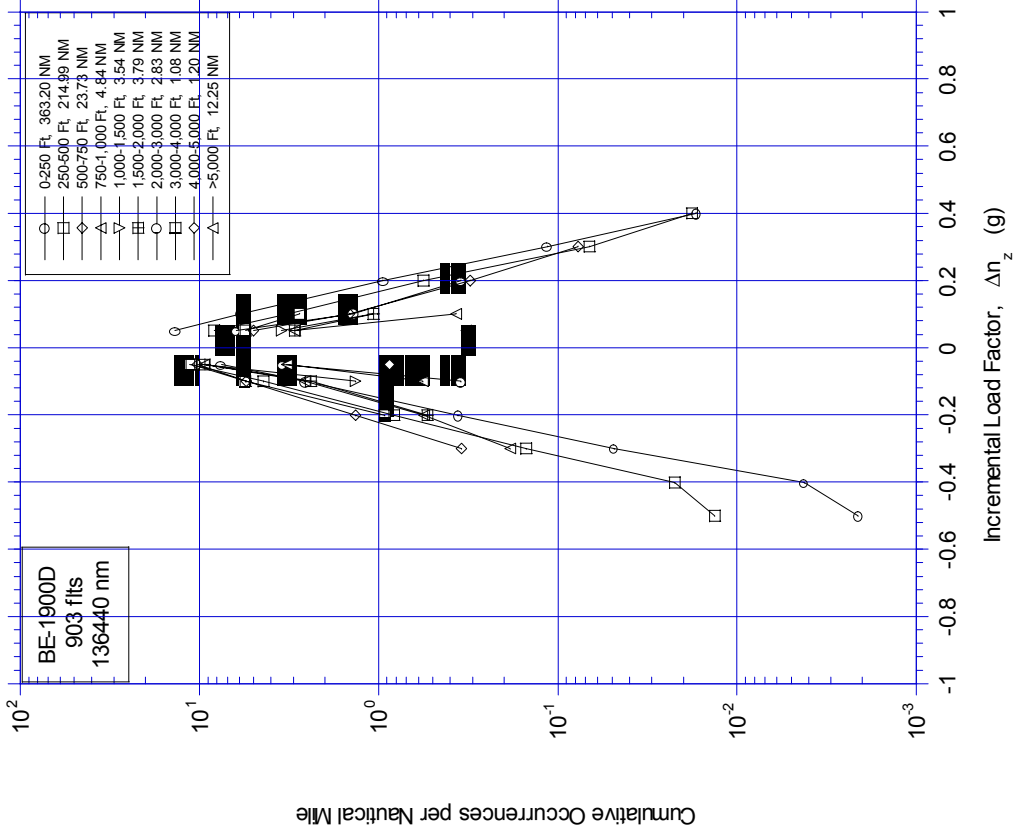


FIGURE A-22. CUMULATIVE OCCURRENCES OF INCREMENTAL GUST LOAD FACTOR PER NAUTICAL MILE BY ALTITUDE ABOVE AIRPORT FOR DEPARTURE PHASE

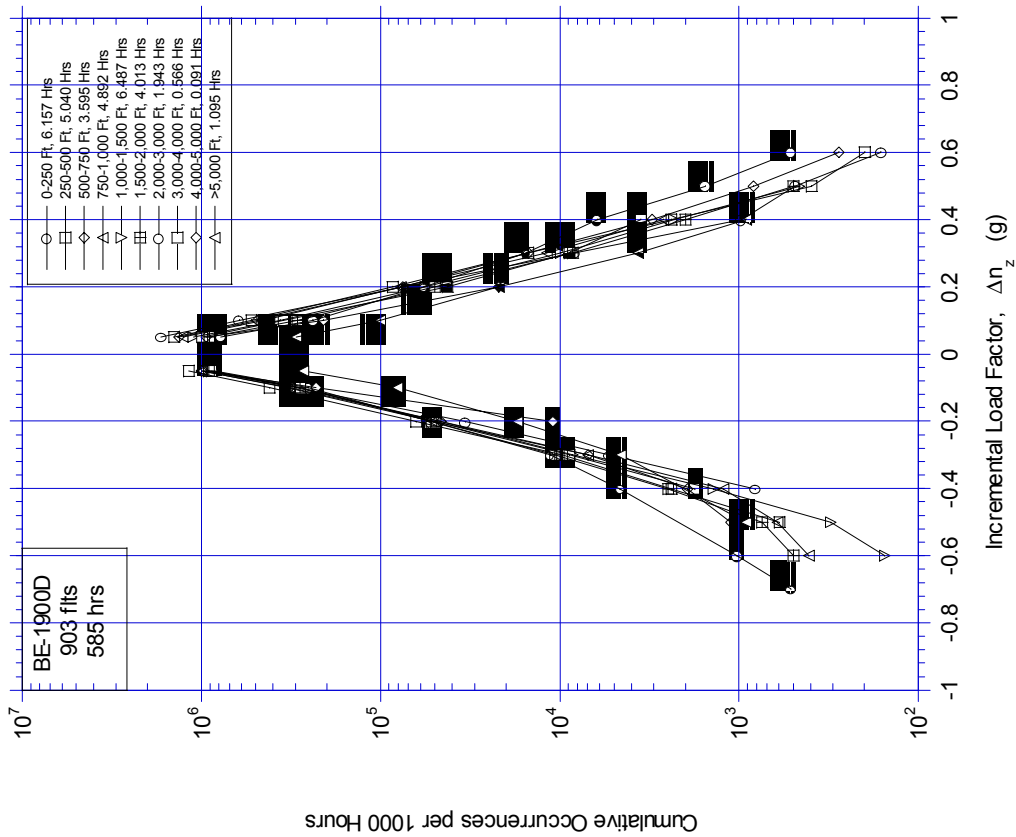


FIGURE A-23. CUMULATIVE OCCURRENCES OF INCREMENTAL GUST LOAD FACTOR PER 1000 HOURS BY ALTITUDE ABOVE AIRPORT FOR APPROACH PHASE

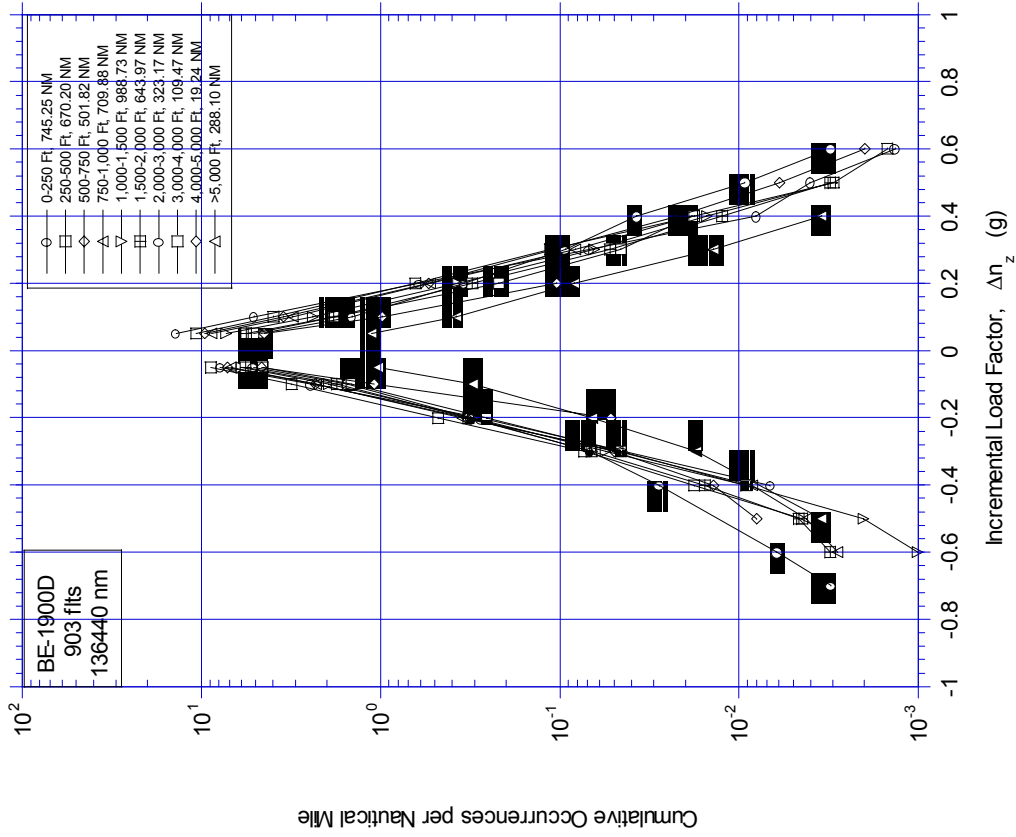


FIGURE A-24. CUMULATIVE OCCURRENCES OF INCREMENTAL GUST LOAD FACTOR PER NAUTICAL MILE BY ALTITUDE ABOVE AIRPORT FOR APPROACH PHASE

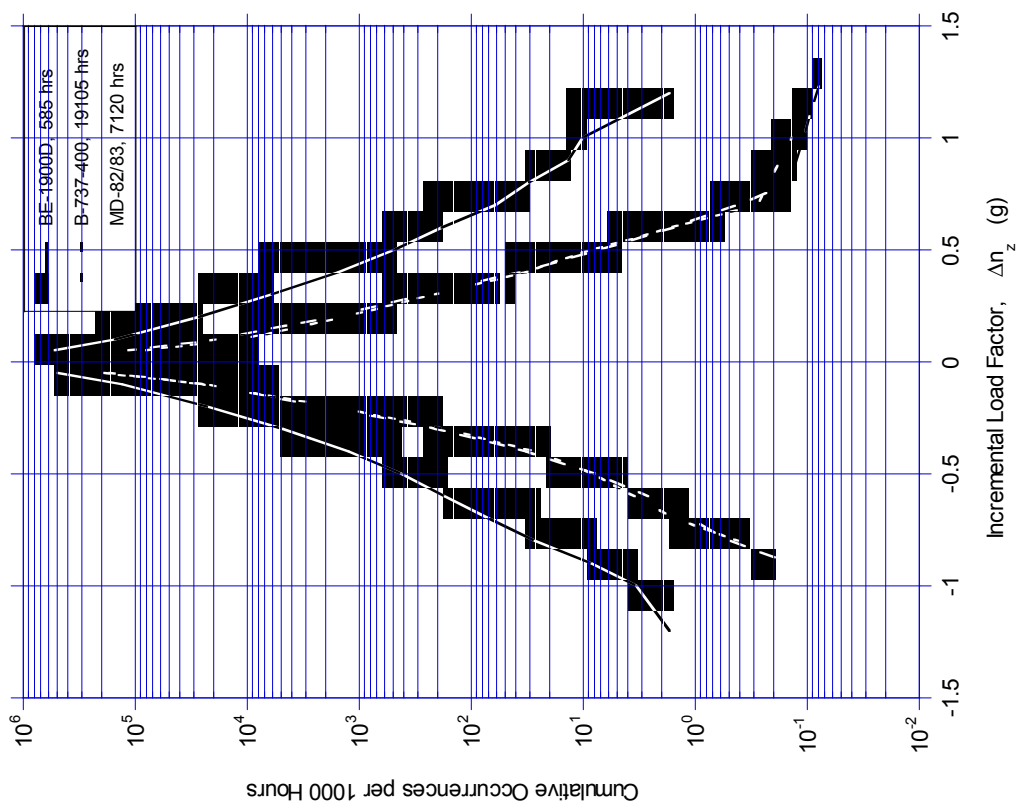


FIGURE A-25. COMPARISON OF CUMULATIVE OCCURRENCES OF INCREMENTAL GUST LOAD FACTOR PER 1000 HOURS FOR BE-1900D, B-737-400, AND MD-82/83, COMBINED FLIGHT PHASES

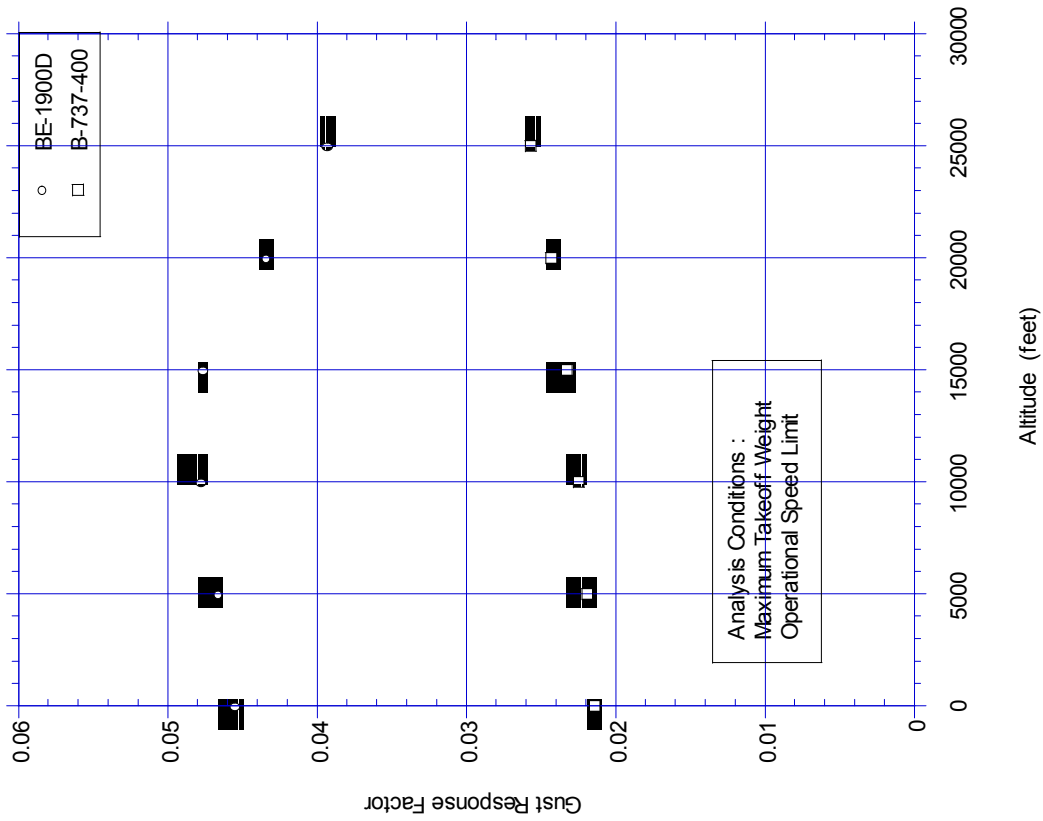


FIGURE A-26. COMPARISON OF BE-1900D AND B-737-400 GUST RESPONSE FACTORS

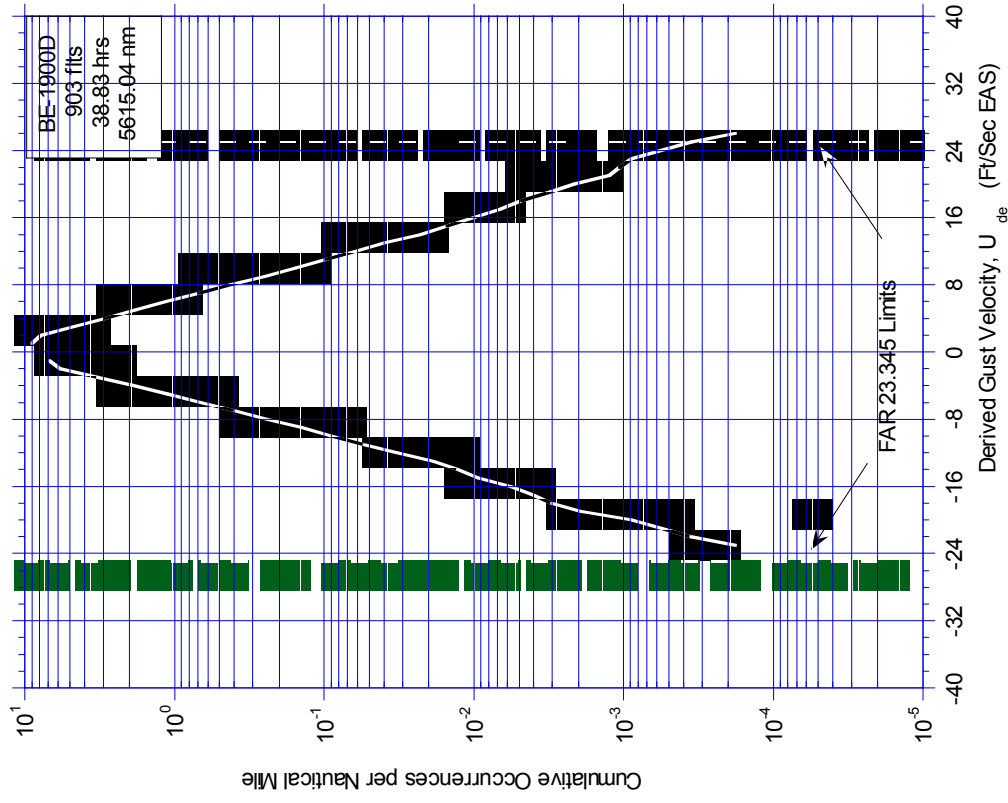


FIGURE A-28. CUMULATIVE OCCURRENCES OF DERIVED GUST VELOCITY PER NAUTICAL MILE FOR FLAP EXTENDED

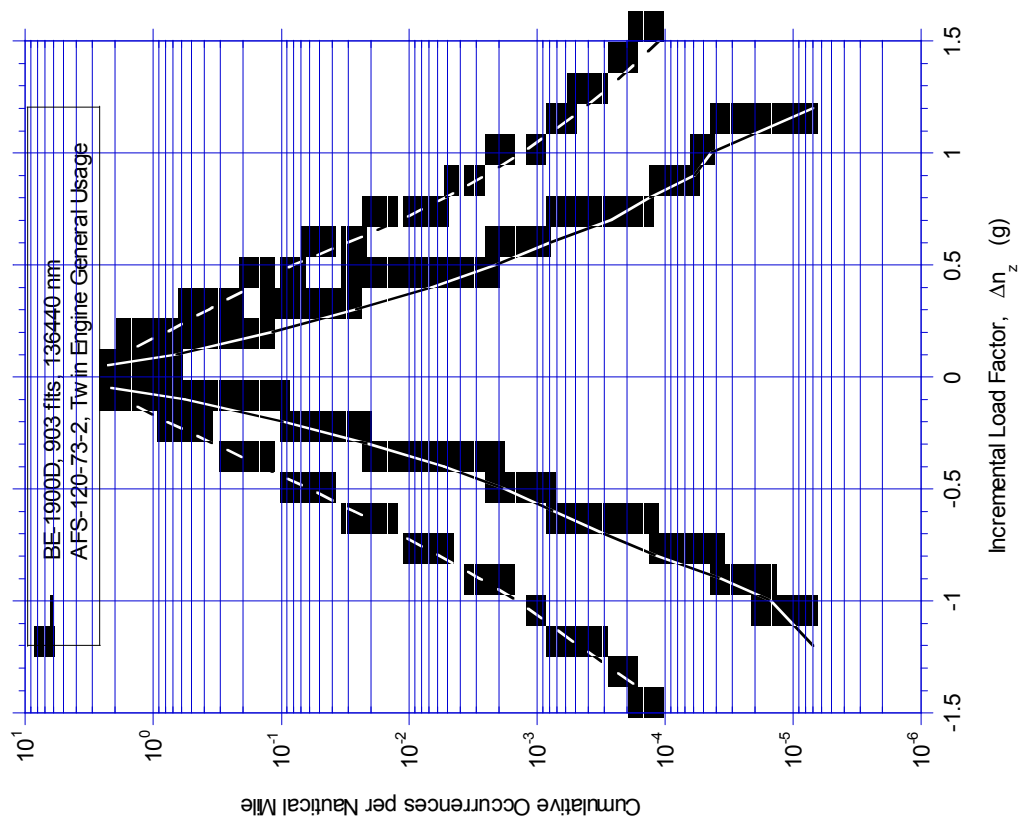


FIGURE A-27. COMPARISON OF CUMULATIVE OCCURRENCES OF INCREMENTAL GUST LOAD FACTOR PER NAUTICAL MILE, BE-1900D VS AFS-120-73-2

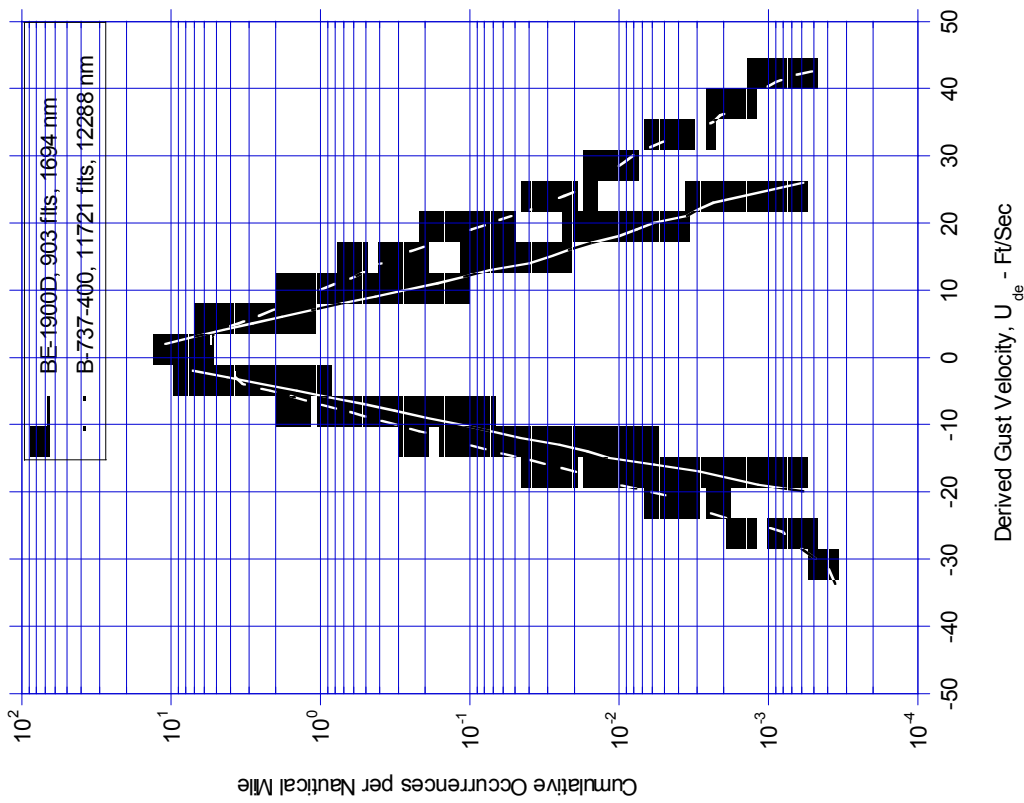


FIGURE A-29. CUMULATIVE OCCURRENCES OF DERIVED GUST VELOCITY PER NAUTICAL MILE FOR <math>< 500</math> FEET

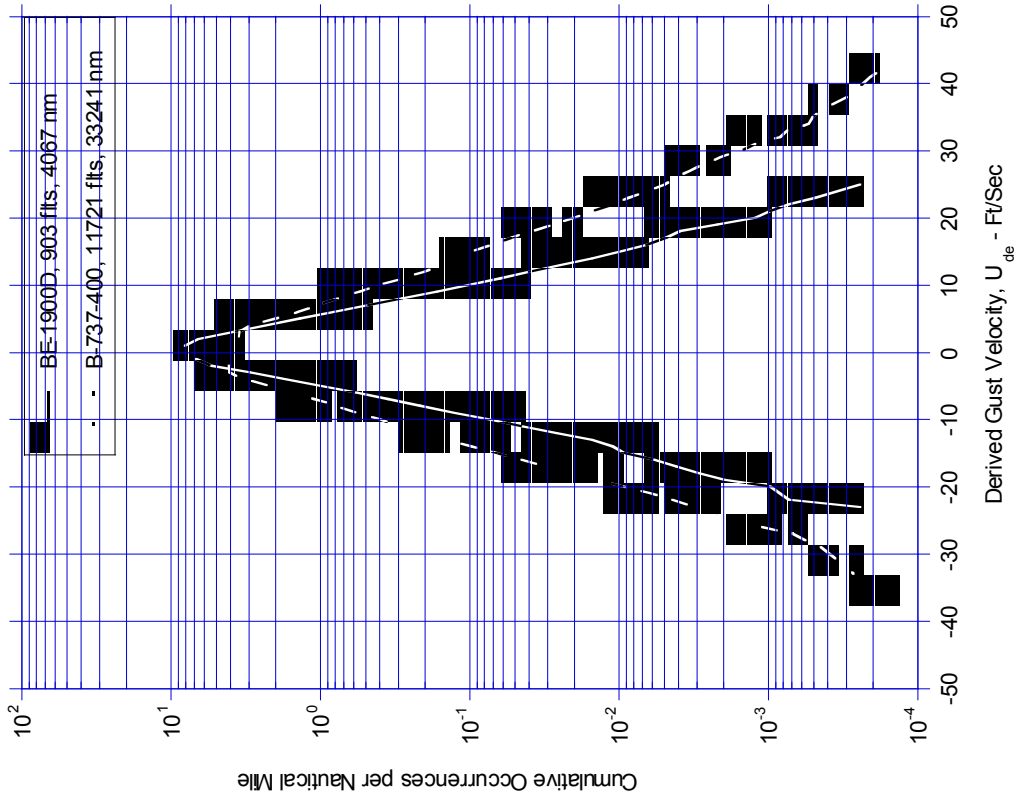


FIGURE A-30. CUMULATIVE OCCURRENCES OF DERIVED GUST VELOCITY PER NAUTICAL MILE FOR 500-1,500 FEET

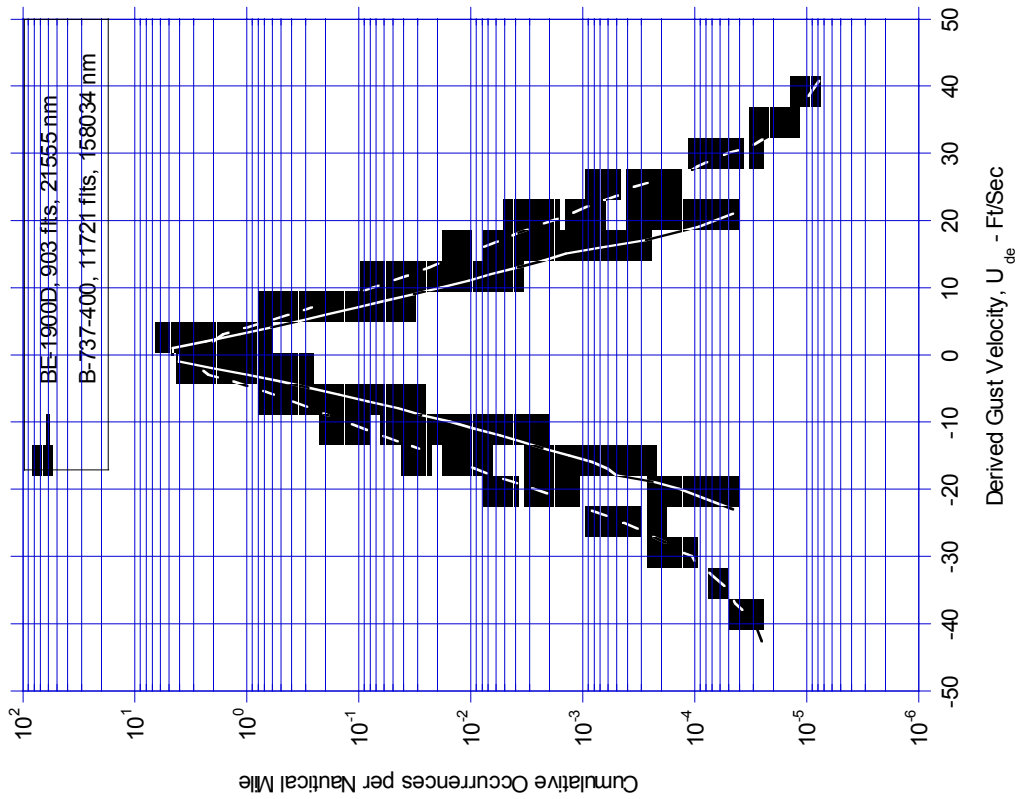


FIGURE A-31. CUMULATIVE OCCURRENCES OF DERIVED GUST VELOCITY PER NAUTICAL MILE FOR 1,500-4,500 FEET

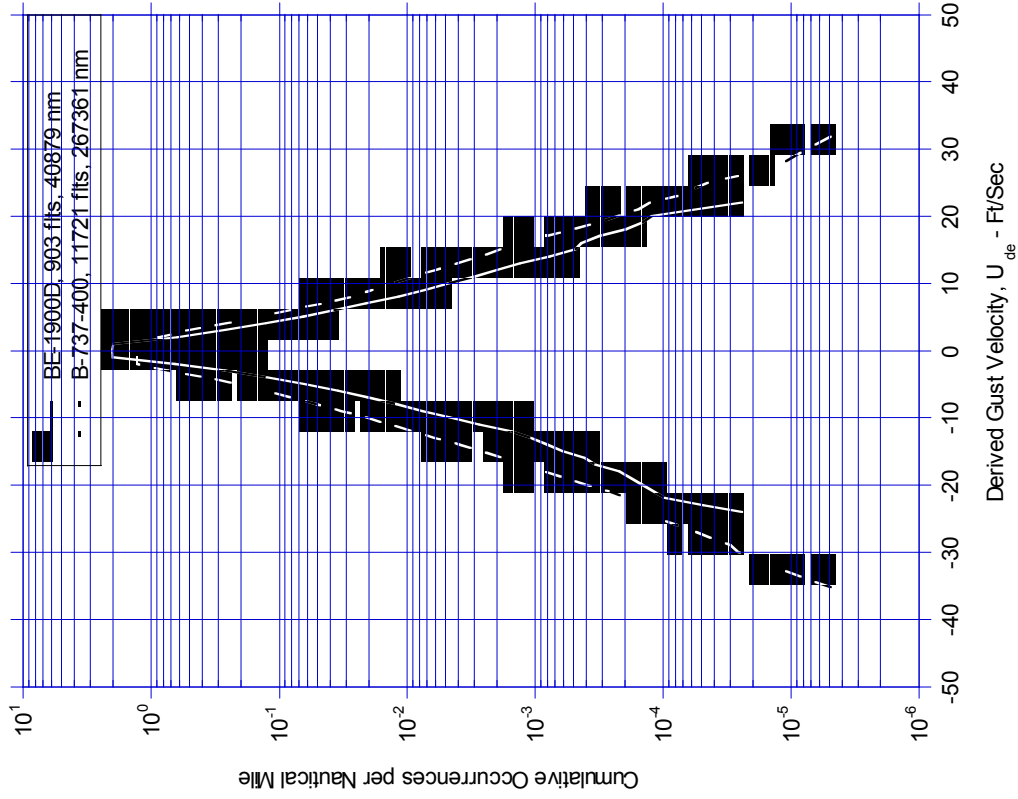


FIGURE A-32. CUMULATIVE OCCURRENCES OF DERIVED GUST VELOCITY PER NAUTICAL MILE FOR 4,500-9,500 FEET

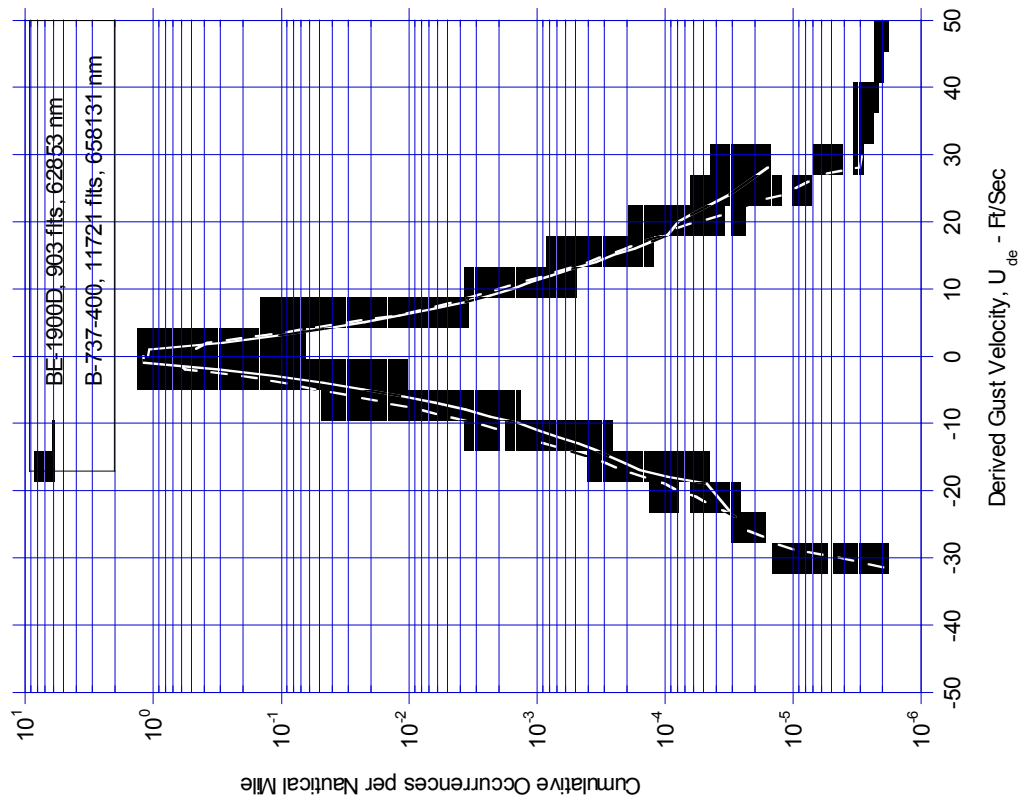


FIGURE A-33. CUMULATIVE OCCURRENCES OF DERIVED GUST VELOCITY PER NAUTICAL MILE FOR 9,500-19,500 FEET

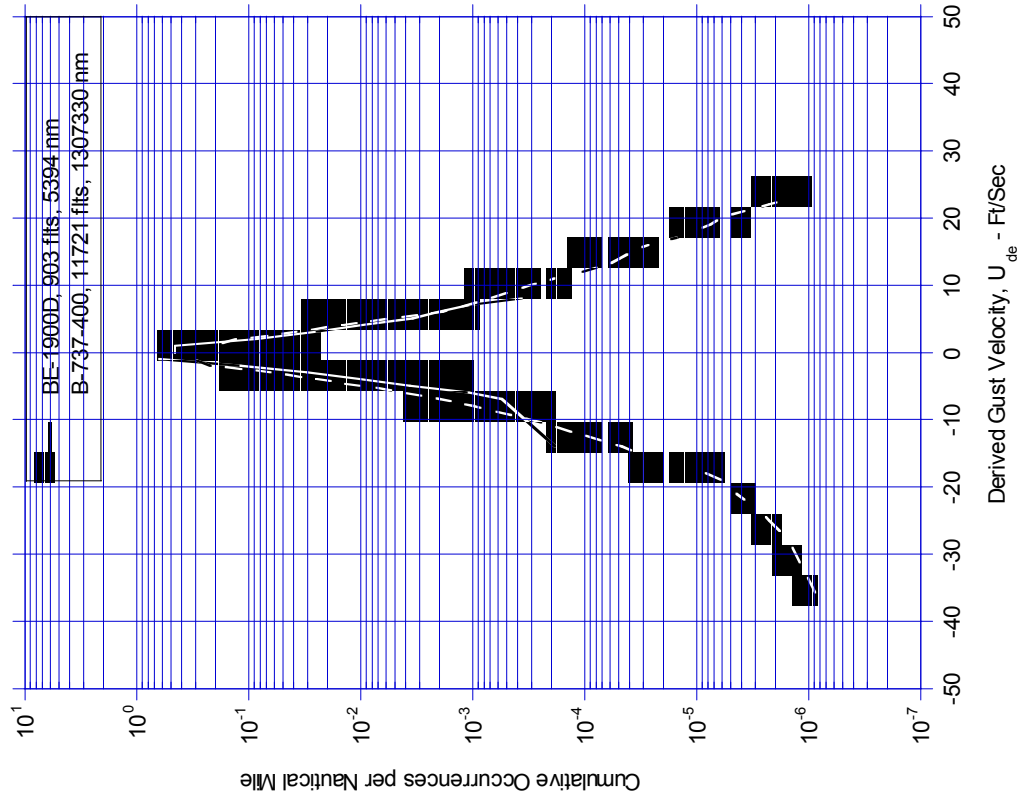


FIGURE A-34. CUMULATIVE OCCURRENCES OF DERIVED GUST VELOCITY PER NAUTICAL MILE FOR 19,500-29,500 FEET

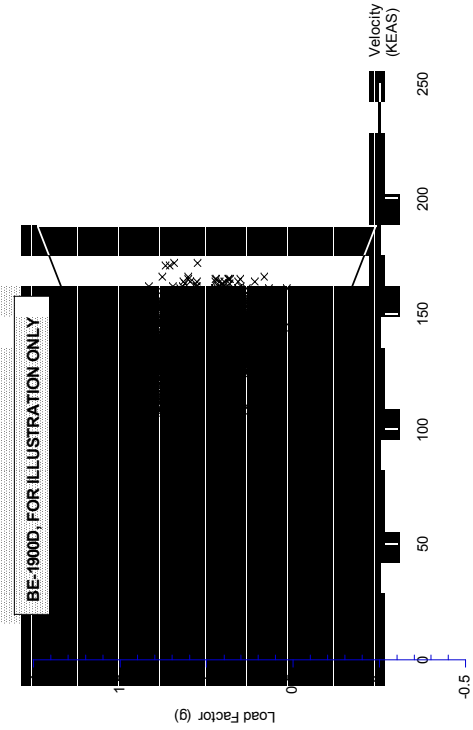


FIGURE A-35. COINCIDENT GUST LOAD FACTOR AND SPEED VS V-N DIAGRAM FOR HALF FLAPS DURING DEPARTURE

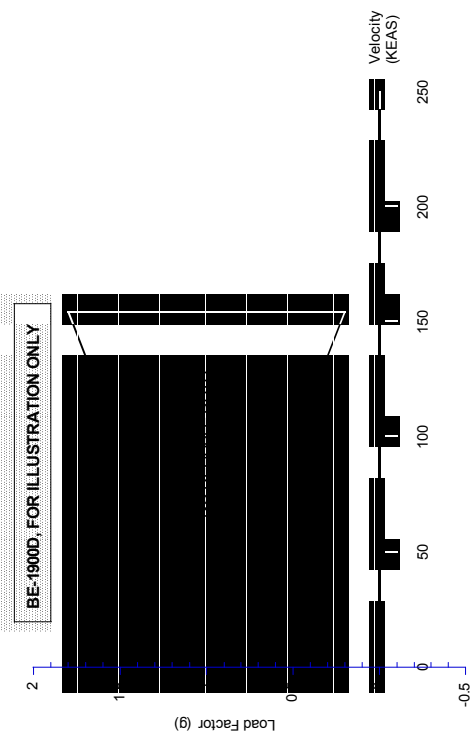


FIGURE A-36. COINCIDENT GUST LOAD FACTOR AND SPEED VS V-N DIAGRAM FOR FULL FLAPS DURING DEPARTURE

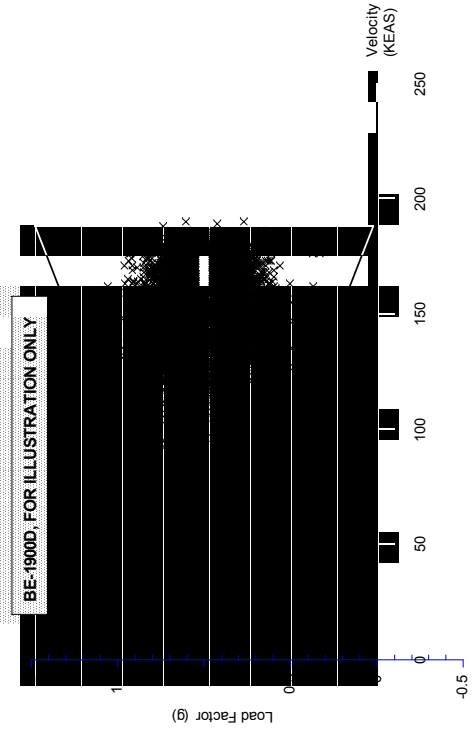


FIGURE A-37. COINCIDENT GUST LOAD FACTOR AND SPEED VS V-N DIAGRAM FOR HALF FLAPS DURING APPROACH

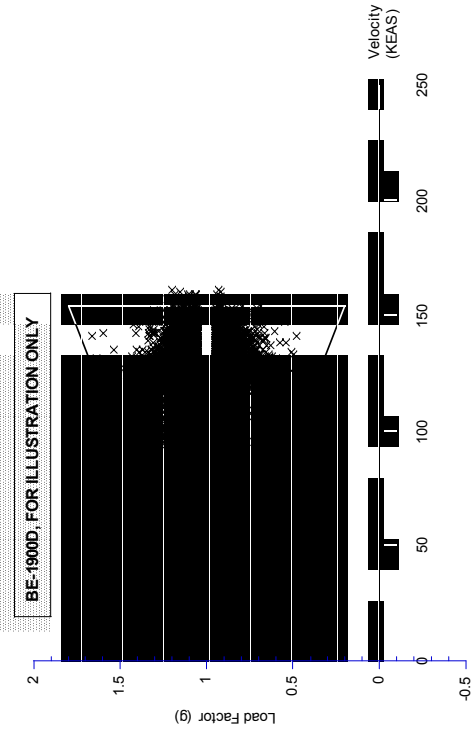


FIGURE A-38. COINCIDENT GUST LOAD FACTOR AND SPEED VS V-N DIAGRAM FOR FULL FLAPS DURING APPROACH

APPENDIX - A, STATISTICAL FORMATS,  
 FLIGHT LOADS DATA, MANEUVER LOADS DATA

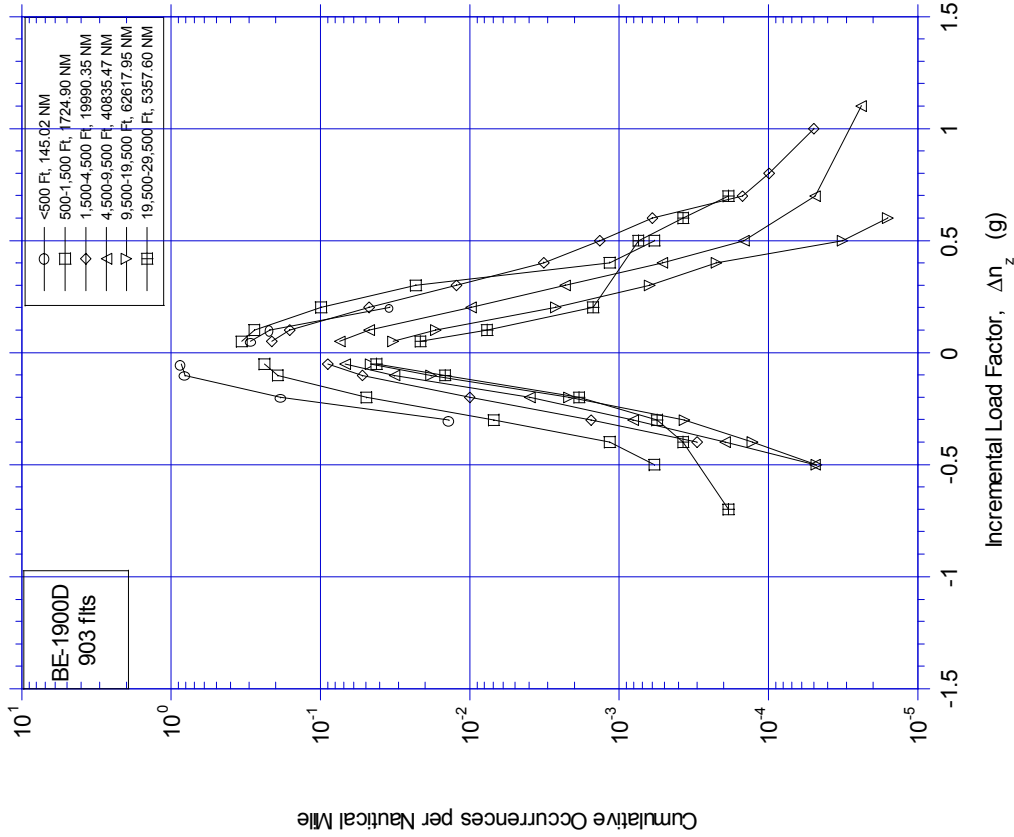


FIGURE A-39. CUMULATIVE OCCURRENCES OF INCREMENTAL MANEUVER LOAD FACTOR PER 1000 HOURS BY PRESSURE ALTITUDE FOR COMBINED CLIMB, CRUISE, AND DESCENT PHASES

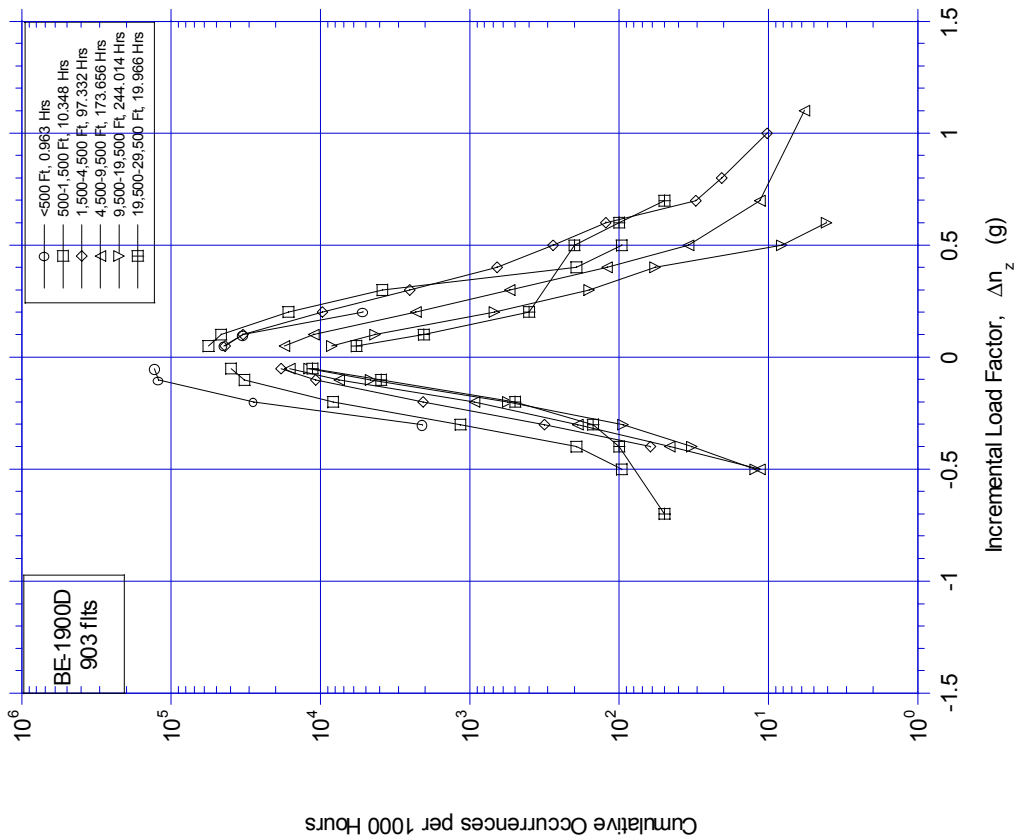


FIGURE A-40. CUMULATIVE OCCURRENCES OF INCREMENTAL MANEUVER LOAD FACTOR PER NAUTICAL MILE BY PRESSURE ALTITUDE FOR COMBINED CLIMB, CRUISE, AND DESCENT PHASES

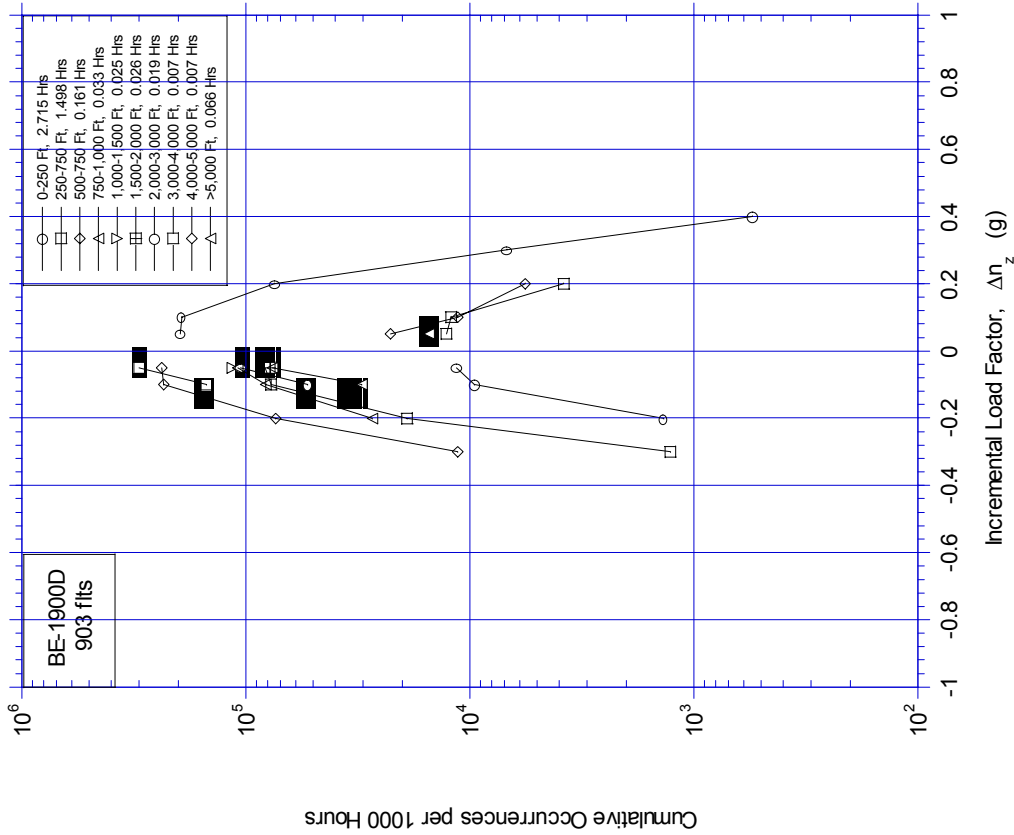


FIGURE A-41. CUMULATIVE OCCURRENCES OF INCREMENTAL MANEUVER LOAD FACTOR PER 1000 HOURS BY ALTITUDE ABOVE AIRPORT FOR DEPARTURE PHASE

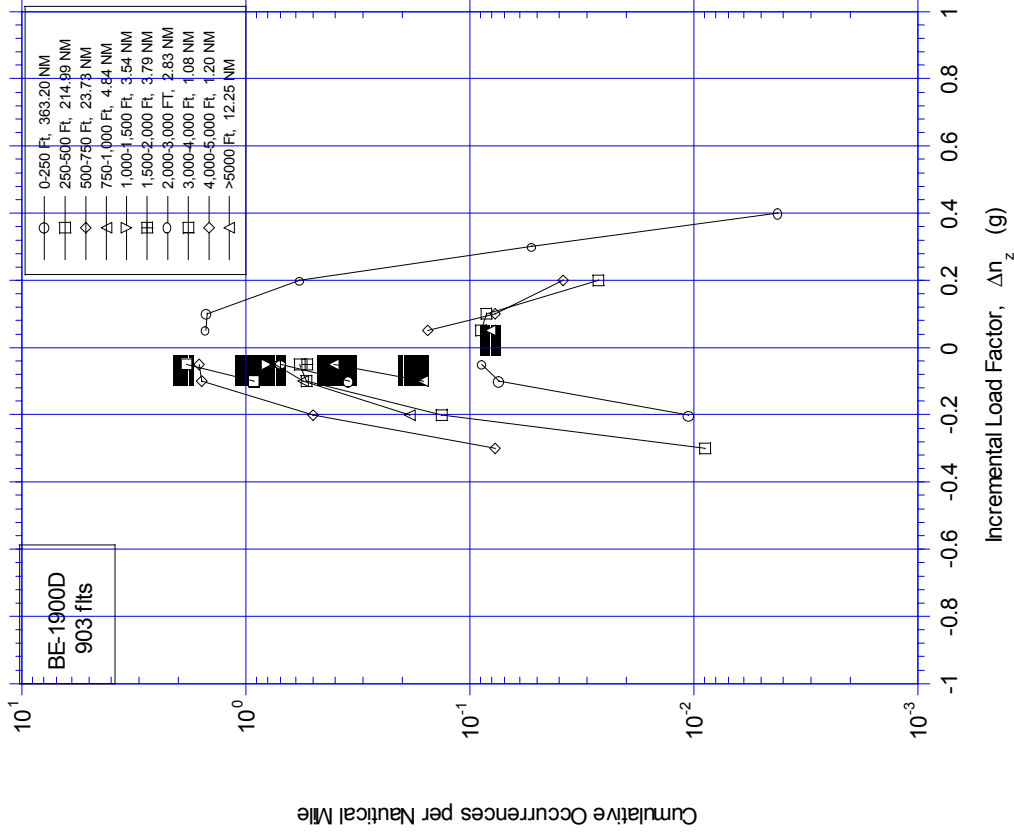


FIGURE A-42. CUMULATIVE OCCURRENCES OF INCREMENTAL MANEUVER LOAD FACTOR PER NAUTICAL MILE BY ALTITUDE ABOVE AIRPORT FOR DEPARTURE PHASE

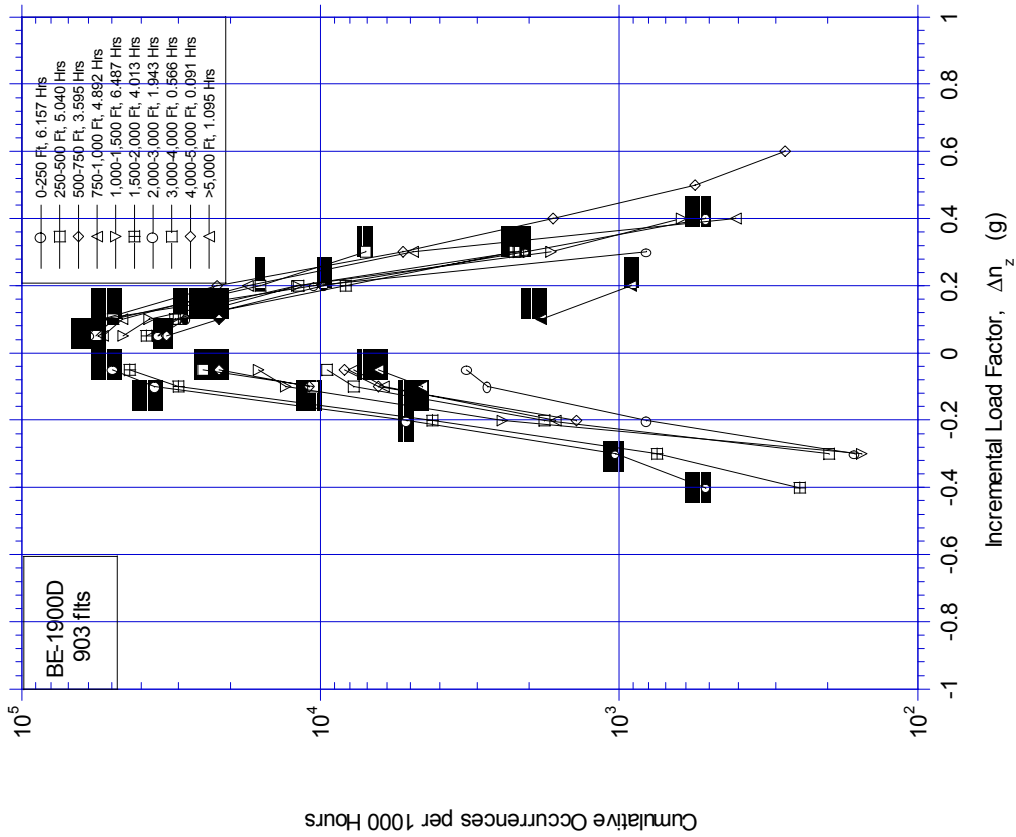


FIGURE A-43. CUMULATIVE OCCURRENCES OF INCREMENTAL MANEUVER LOAD FACTOR PER 1000 HOURS BY ALTITUDE ABOVE AIRPORT FOR APPROACH PHASE

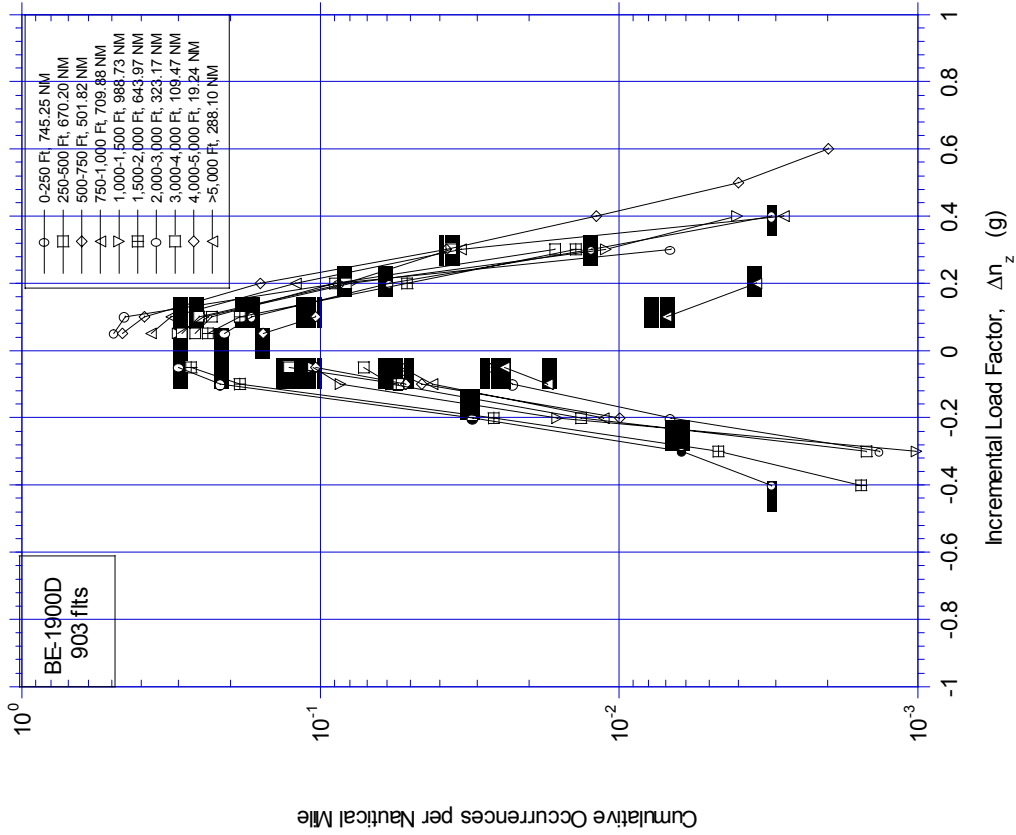


FIGURE A-44. CUMULATIVE OCCURRENCES OF INCREMENTAL MANEUVER LOAD FACTOR PER NAUTICAL MILE BY ALTITUDE ABOVE AIRPORT FOR APPROACH PHASE

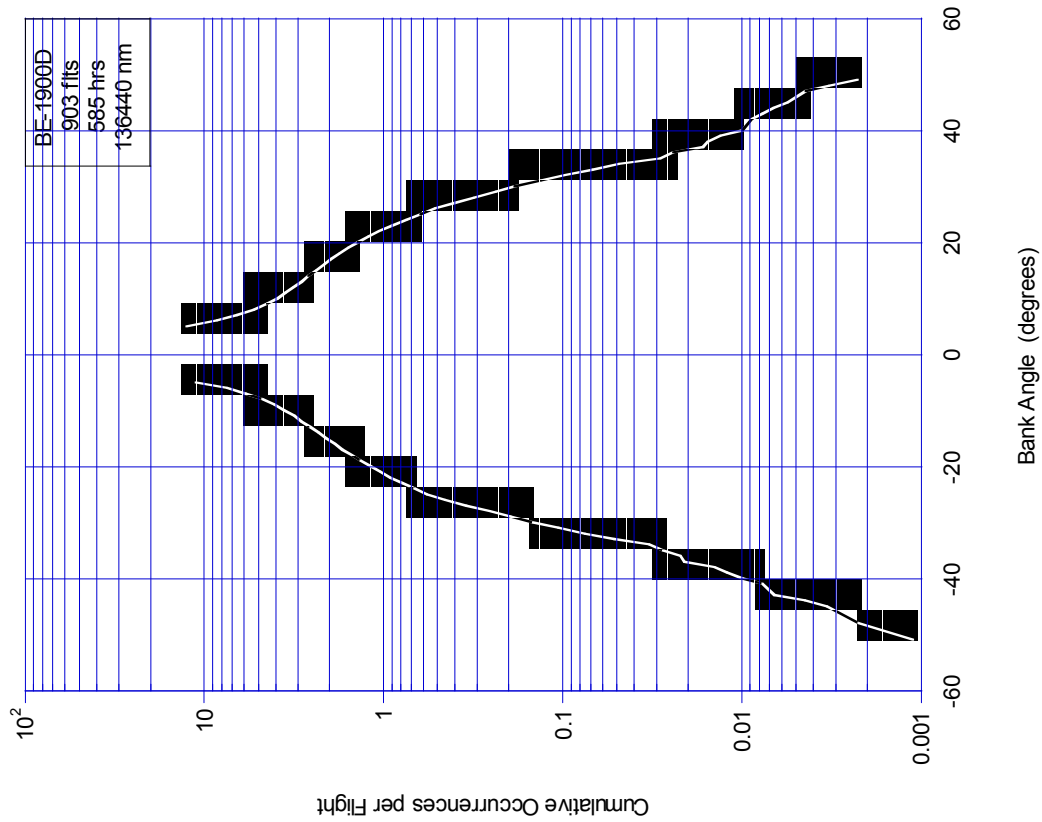


FIGURE A-46. CUMULATIVE OCCURRENCES PER FLIGHT OF PEAK BANK ANGLE

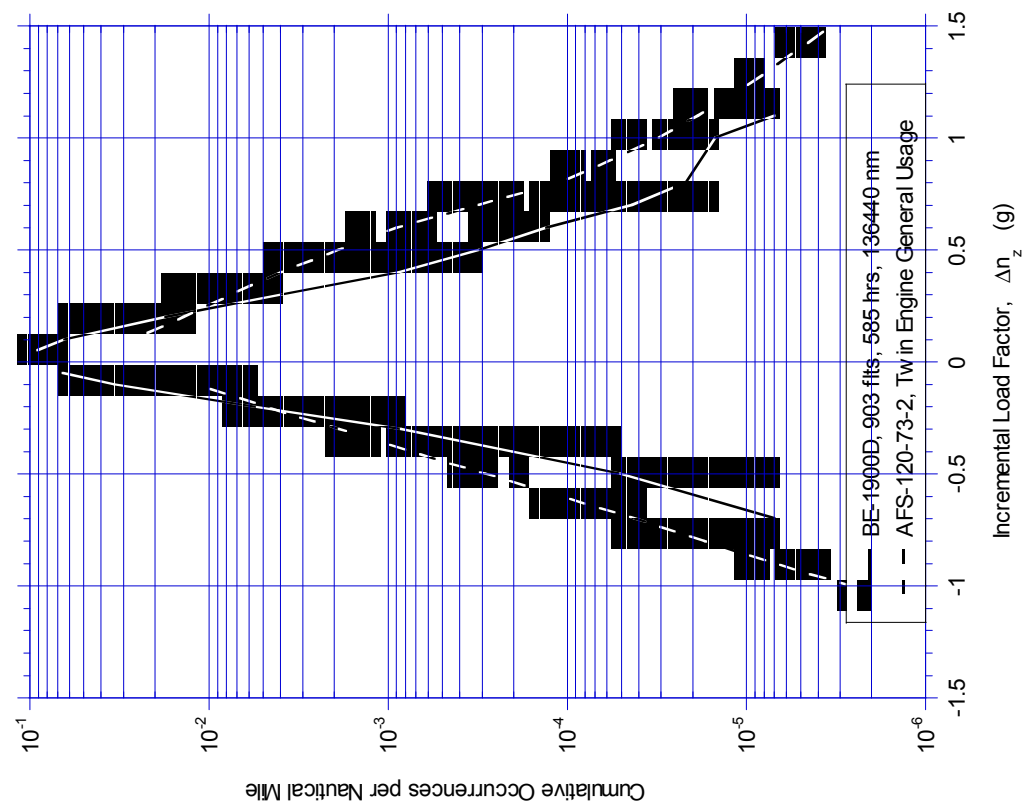


FIGURE A-45. COMPARISON OF CUMULATIVE OCCURRENCES OF INCREMENTAL MANEUVER LOAD FACTOR PER NAUTICAL MILE, BE-1900D VS AFS-120-73-2

APPENDIX A - STATITICAL FORMATS,  
 FLIGHT LOADS DATA, COMBINED MANEUVER AND GUST LOADS DATA

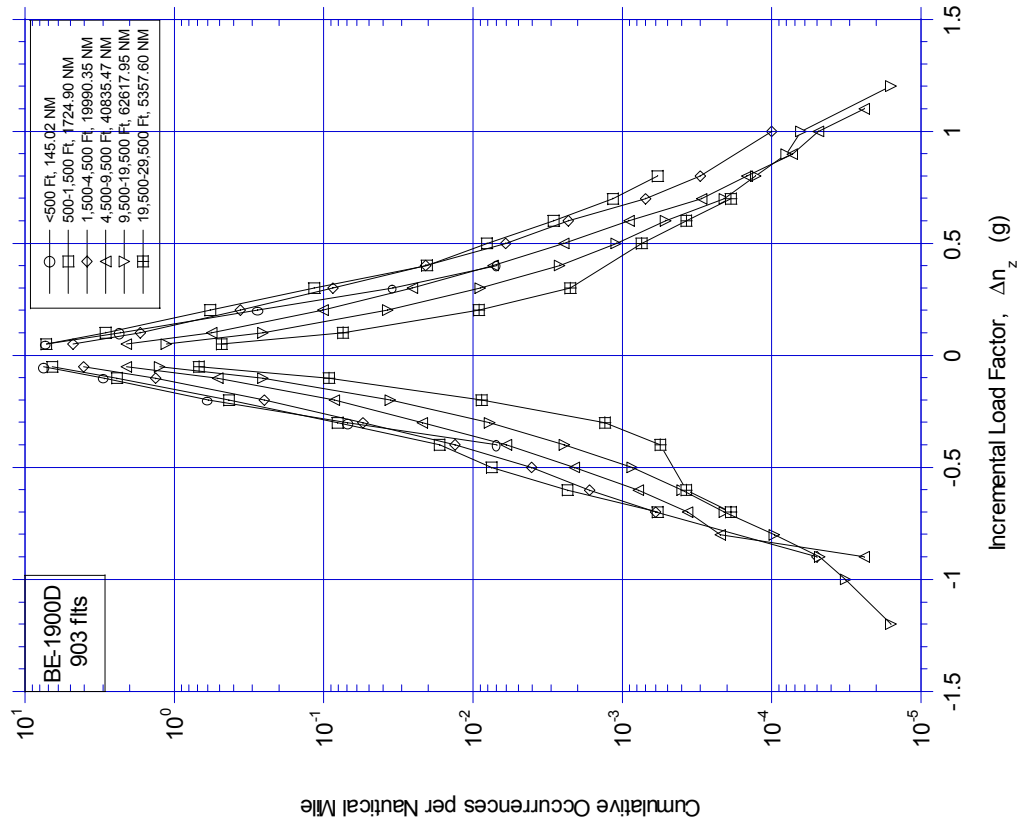


FIGURE A-47. CUMULATIVE OCCURRENCES OF INCREMENTAL LOAD FACTOR PER 1000 HOURS BY PRESSURE ALTITUDE FOR COMBINED CLIMB, CRUISE, AND DESCENT PHASES

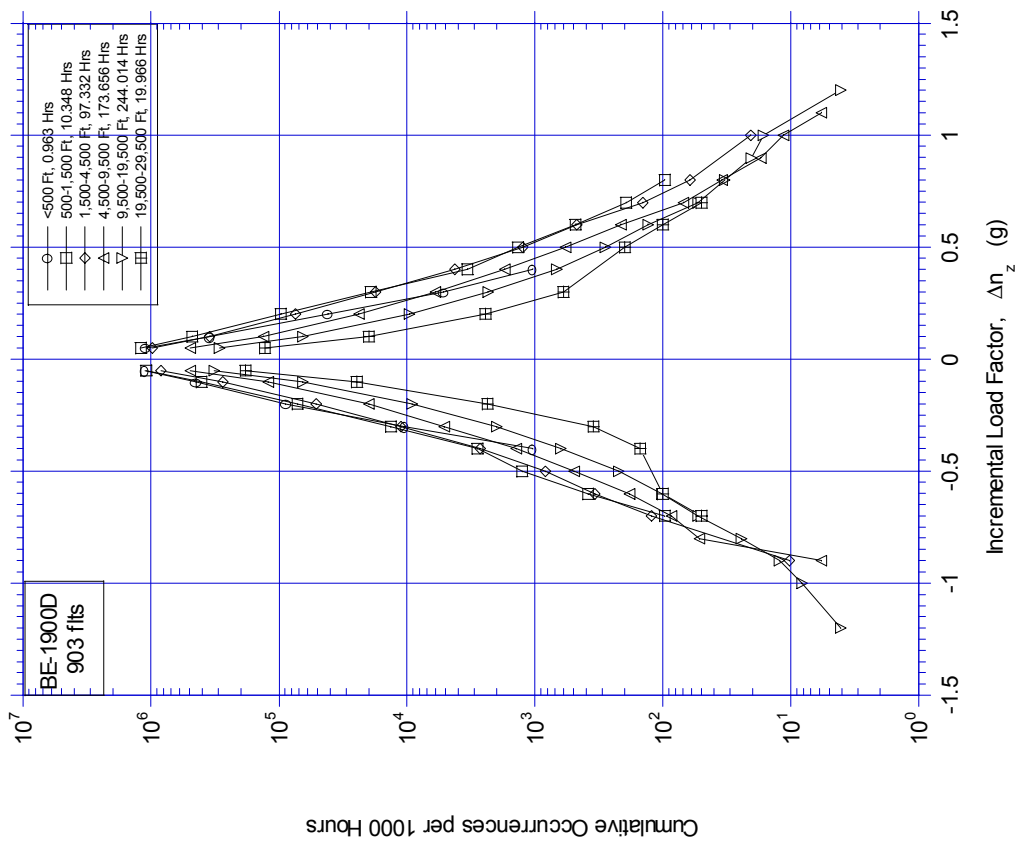


FIGURE A-48. CUMULATIVE OCCURRENCES OF INCREMENTAL LOAD FACTOR PER NAUTICAL MILE BY PRESSURE ALTITUDE FOR COMBINED CLIMB, CRUISE, AND DESCENT PHASES

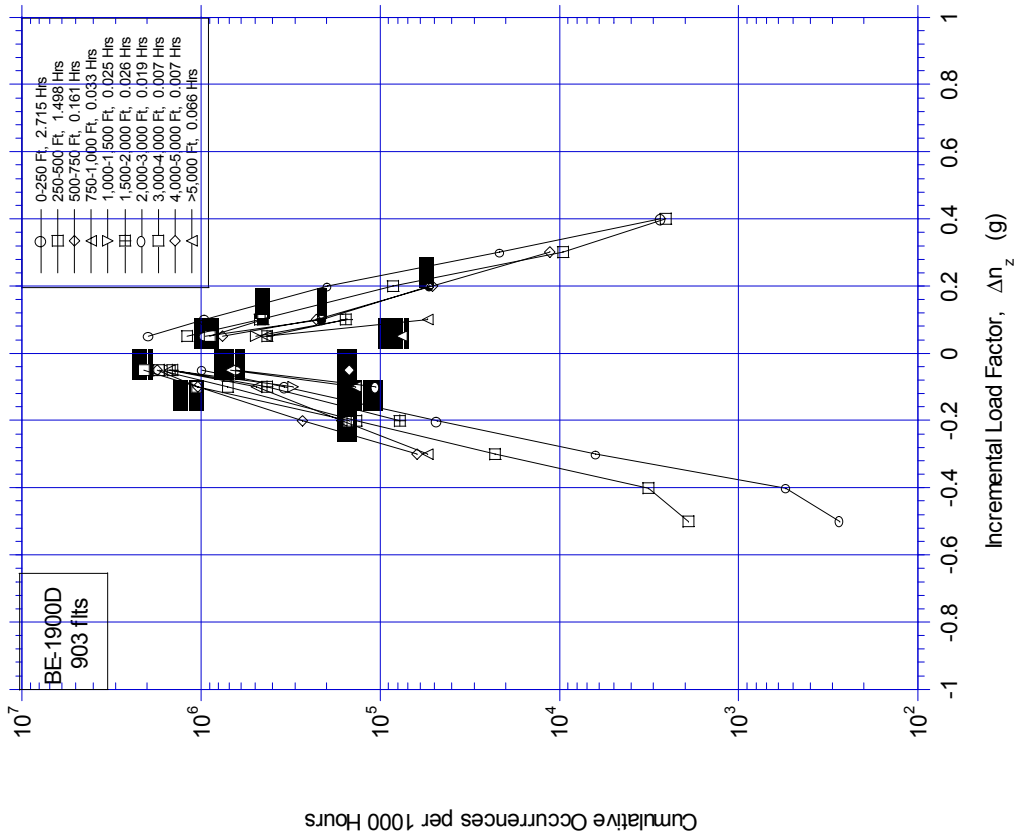


FIGURE A-49. CUMULATIVE OCCURRENCES OF INCREMENTAL LOAD FACTOR PER 1000 HOURS BY ALTITUDE ABOVE AIRPORT FOR DEPARTURE PHASE

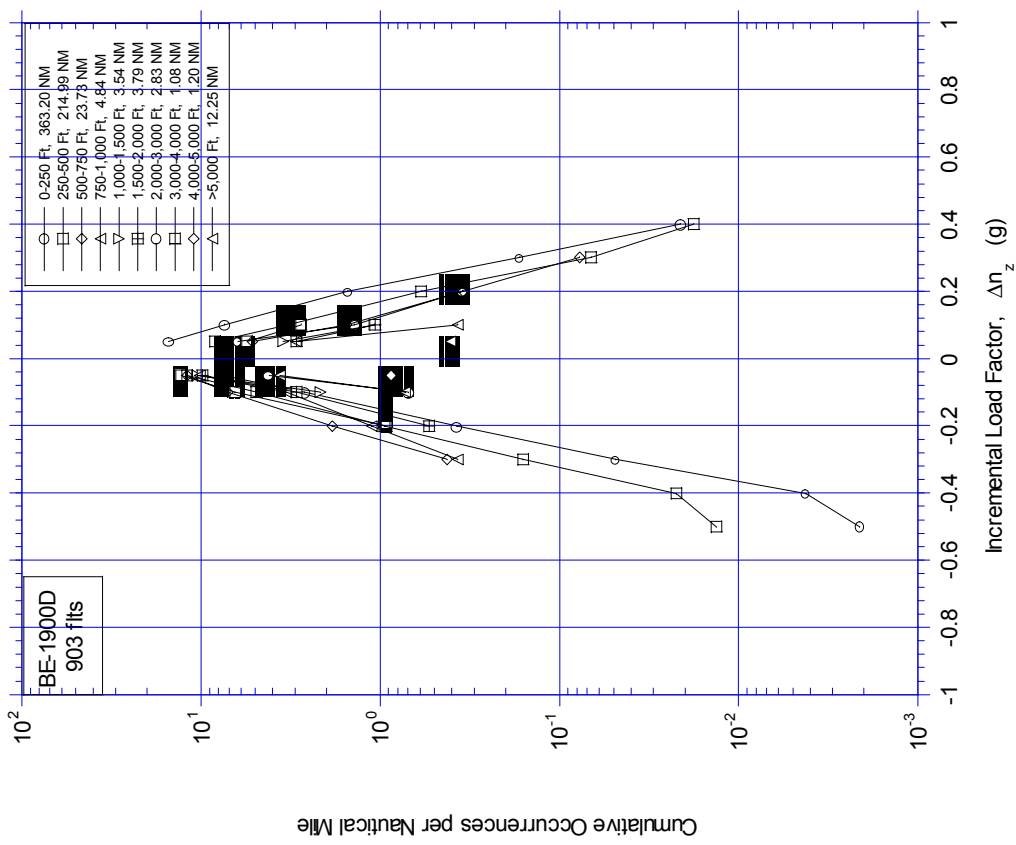


FIGURE A-50. CUMULATIVE OCCURRENCES OF INCREMENTAL LOAD FACTOR PER NAUTICAL MILE BY ALTITUDE ABOVE AIRPORT FOR DEPARTURE PHASE

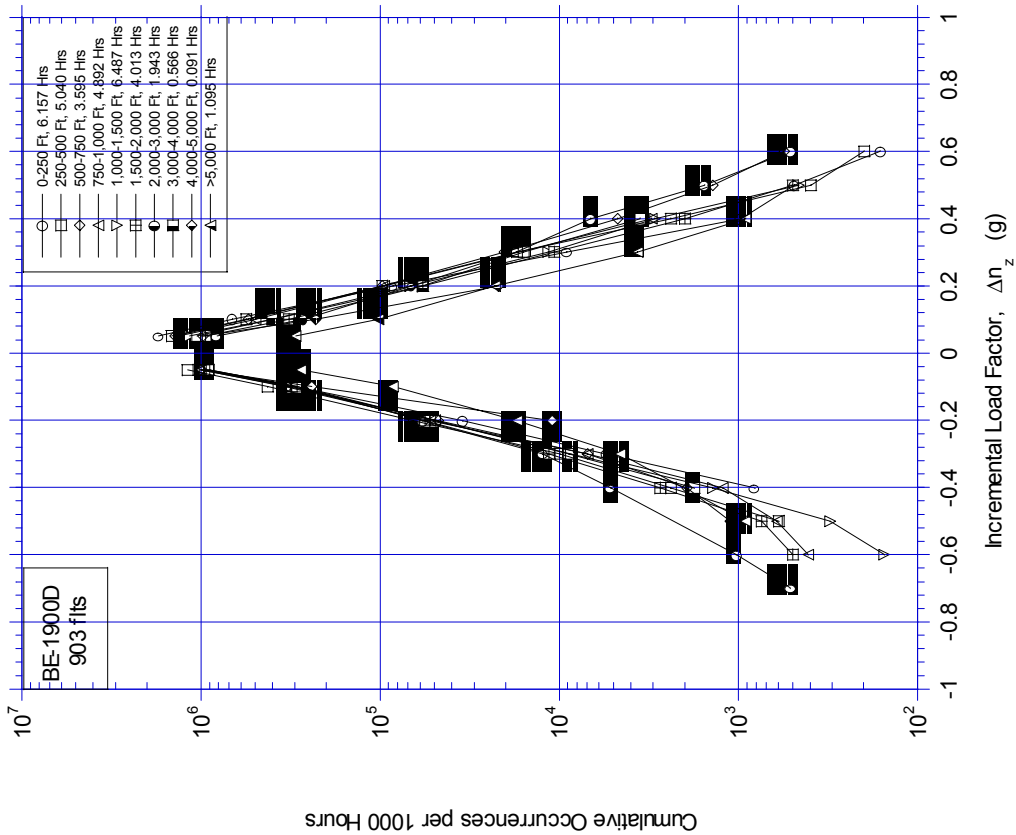


FIGURE A-51. CUMULATIVE OCCURRENCES OF INCREMENTAL LOAD FACTOR PER 1000 HOURS BY ALTITUDE ABOVE AIRPORT FOR APPROACH PHASE

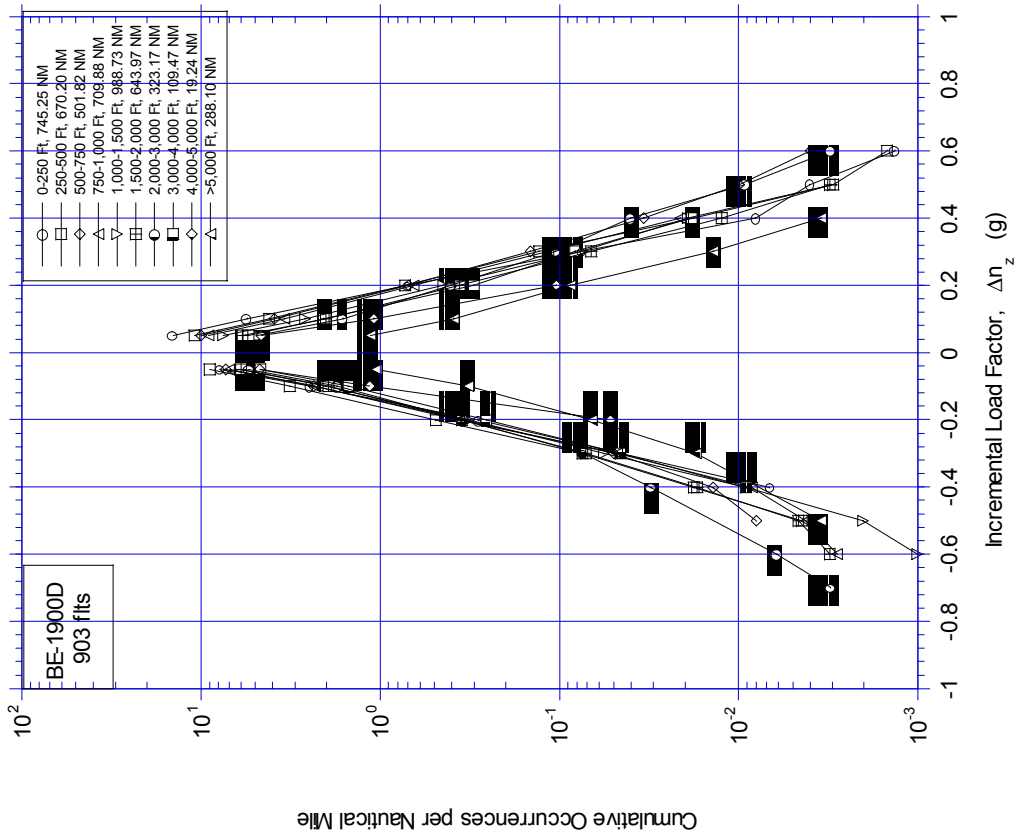


FIGURE A-52. CUMULATIVE OCCURRENCES OF INCREMENTAL LOAD FACTOR PER NAUTICAL MILE BY ALTITUDE ABOVE AIRPORT FOR APPROACH PHASE

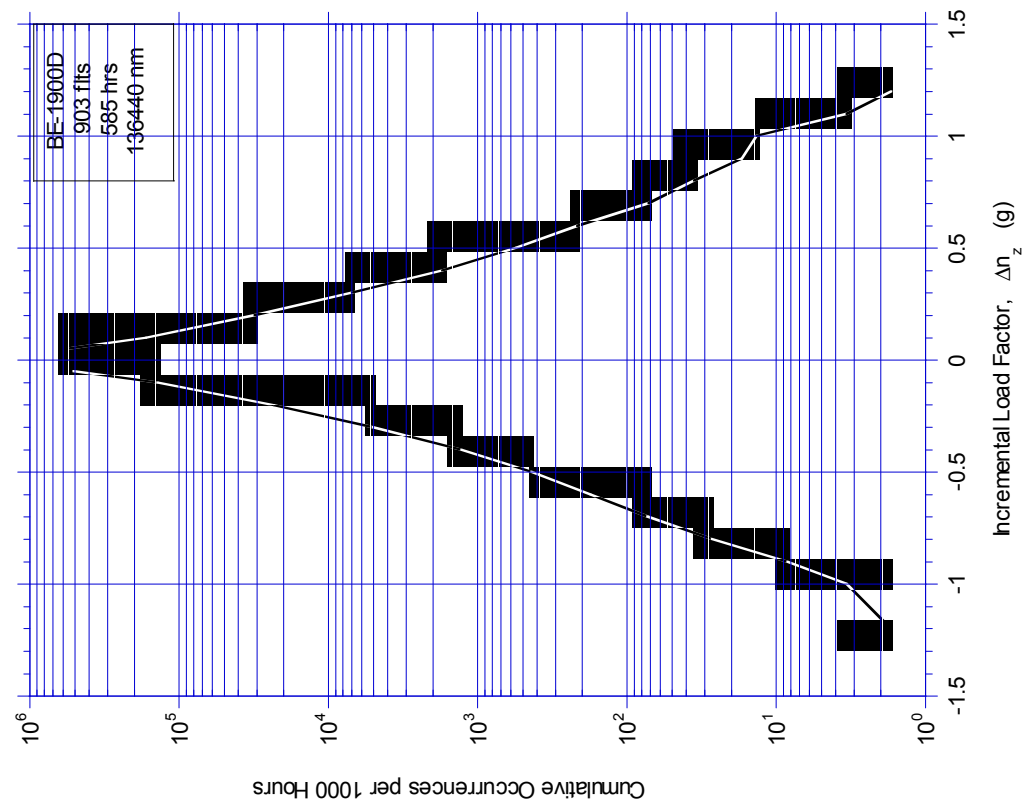


FIGURE A-53. CUMULATIVE OCCURRENCES OF INCREMENTAL LOAD FACTOR PER 1000 HOURS FOR COMBINED FLIGHT PHASES

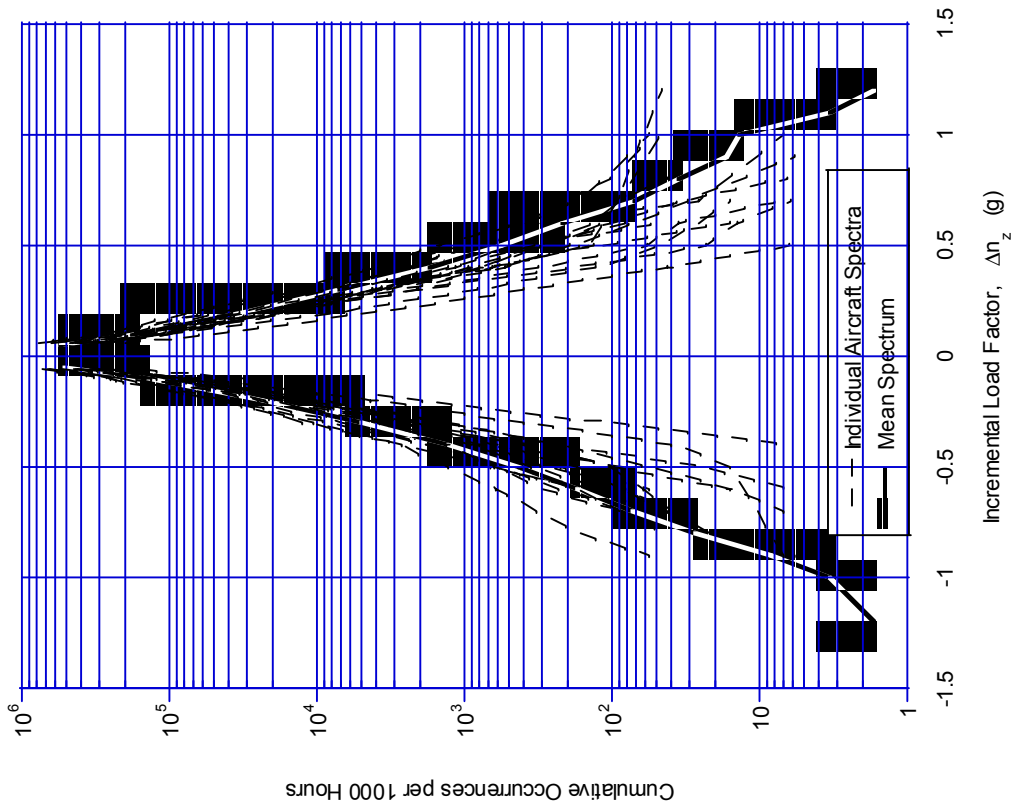


FIGURE A-54. CUMULATIVE OCCURRENCES OF INCREMENTAL LOAD FACTOR PER 1000 HOURS FOR INDIVIDUAL AIRCRAFT, COMBINED FLIGHT PHASES

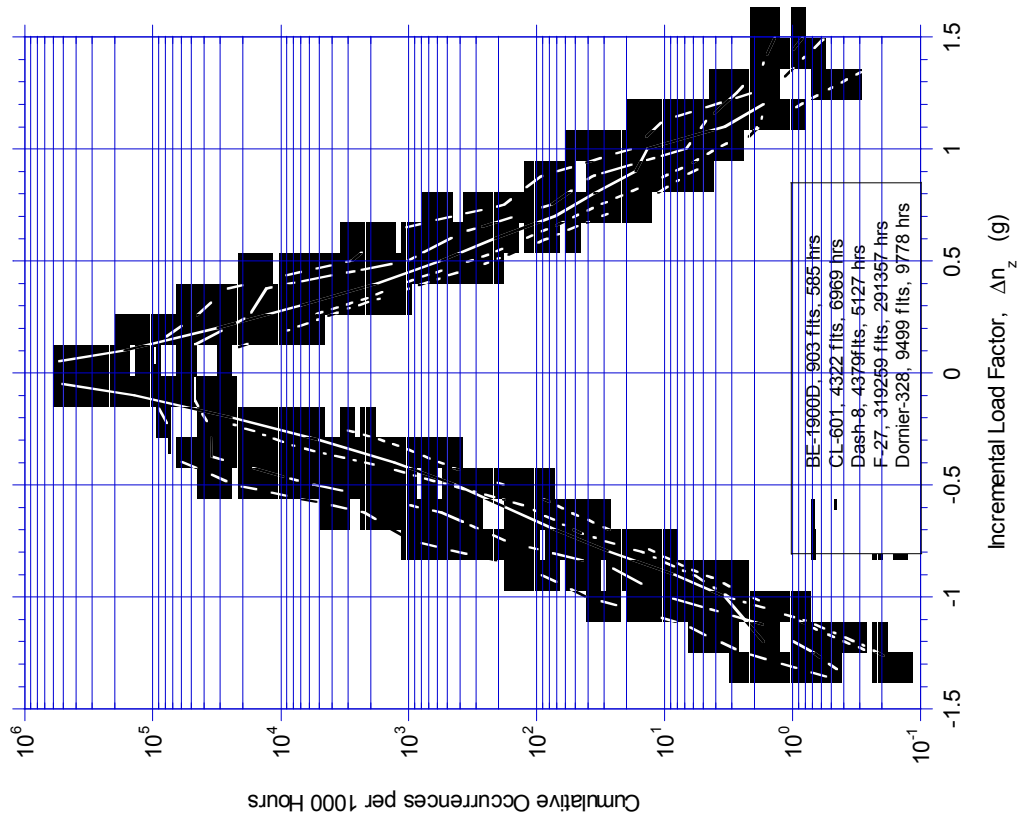


FIGURE A-55. COMPARISON OF CUMULATIVE OCCURRENCES OF INCREMENTAL LOAD FACTOR PER 1000 HOURS FOR BE-1900D, CL-601, AND DASH-8, F-27, AND DORNIER-328, COMBINED FLIGHT PHASES

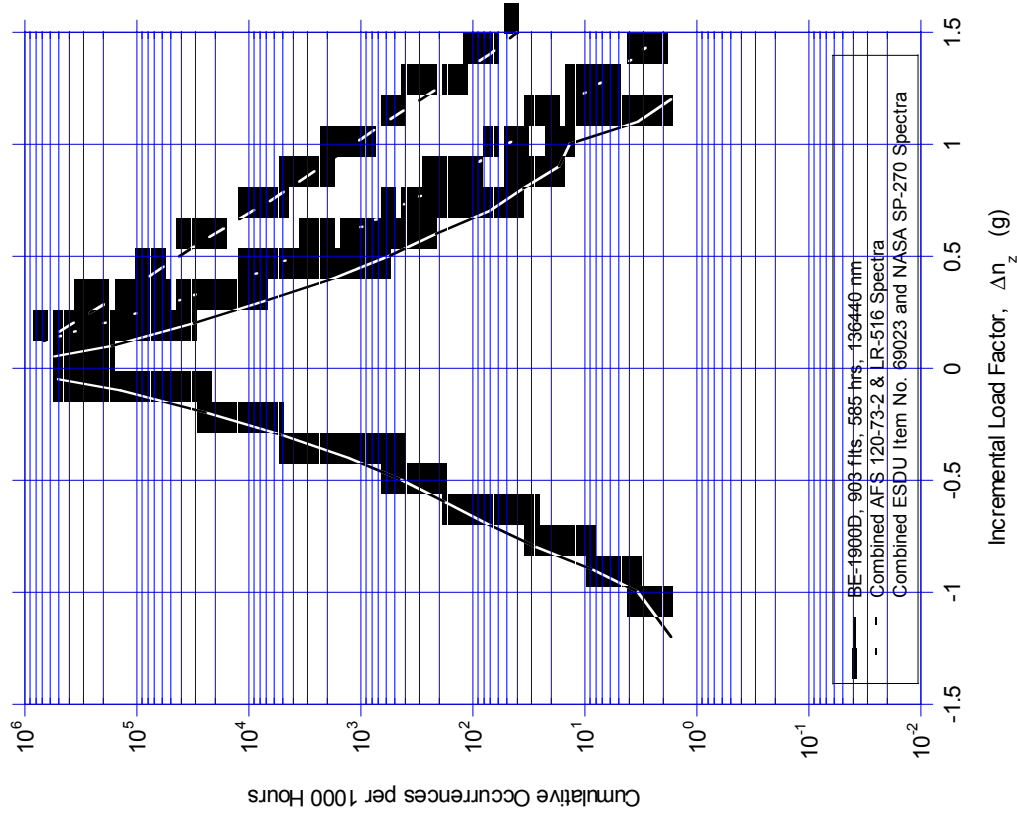


FIGURE A-56. COMPARISON OF CUMULATIVE OCCURRENCES OF INCREMENTAL LOAD FACTOR PER 1000 HOURS FOR BE-1900D AND SAE 931257, COMBINED FLIGHT PHASES

APPENDIX - A STATISTICAL FORMATS,  
SYSTEMS OPERATIONAL DATA, FLAP SYSTEM

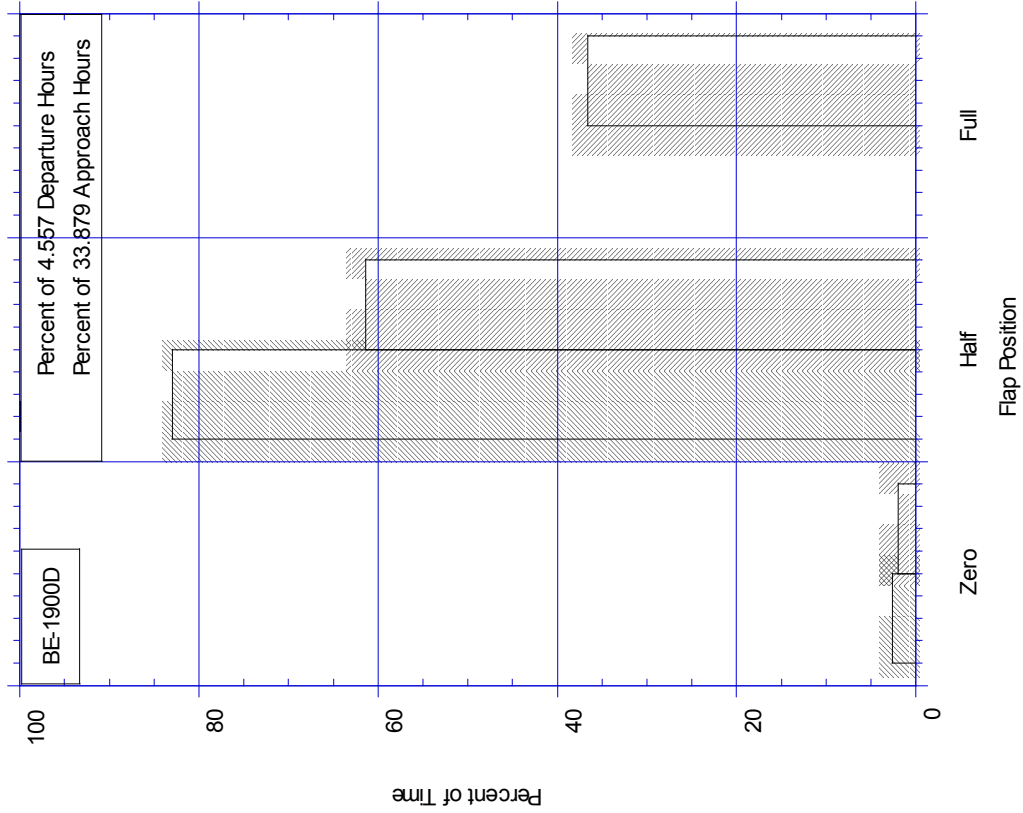


FIGURE A-58. PERCENT OF TIME IN FLAP DETENT DURING DEPARTURE AND APPROACH

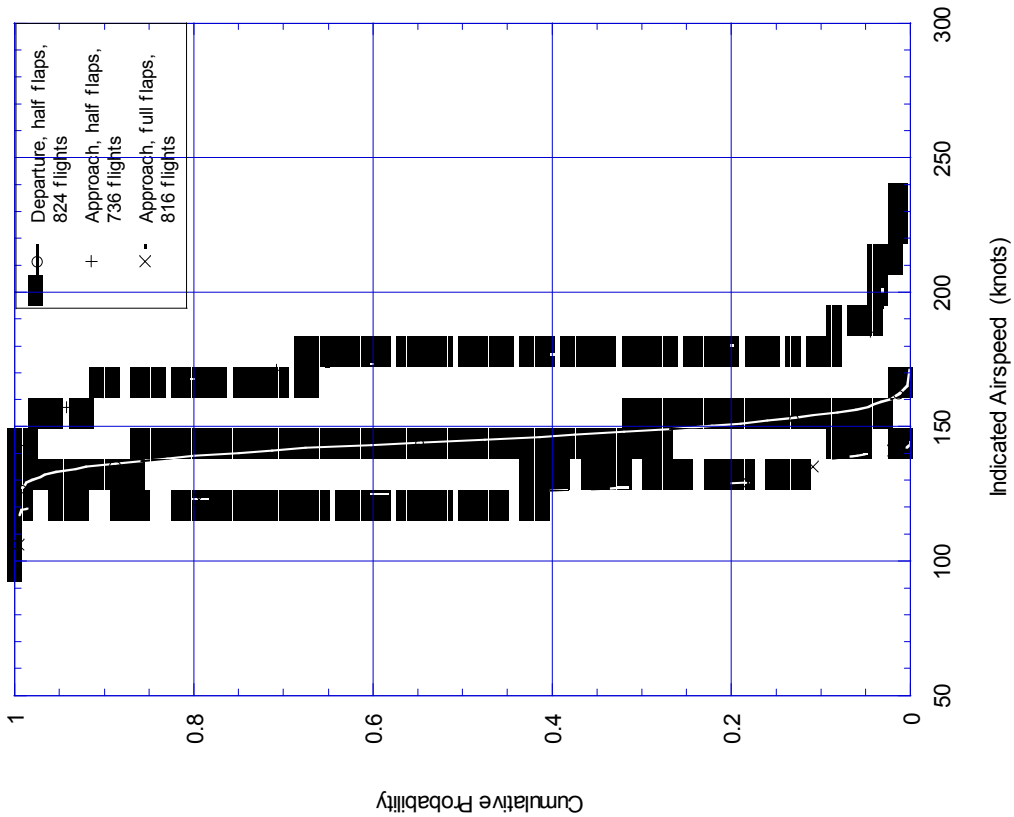


FIGURE A-57. CUMULATIVE PROBABILITY OF MAXIMUM AIRSPEED WITH FLAP EXTENDED

APPENDIX - A STATISTICAL FORMATS,  
SYSTEMS OPERATIONAL DATA, PROPULSION SYSTEM

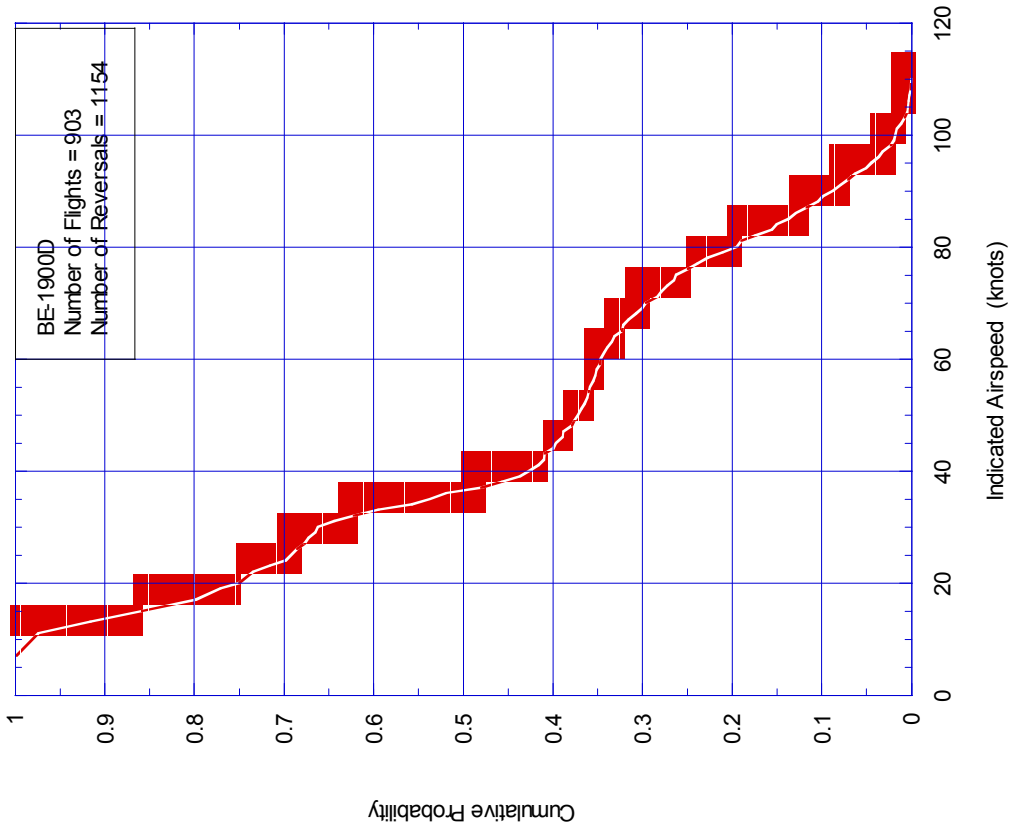


FIGURE A-59. CUMULATIVE PROBABILITY OF TIME IN REVERSED PROPELLER

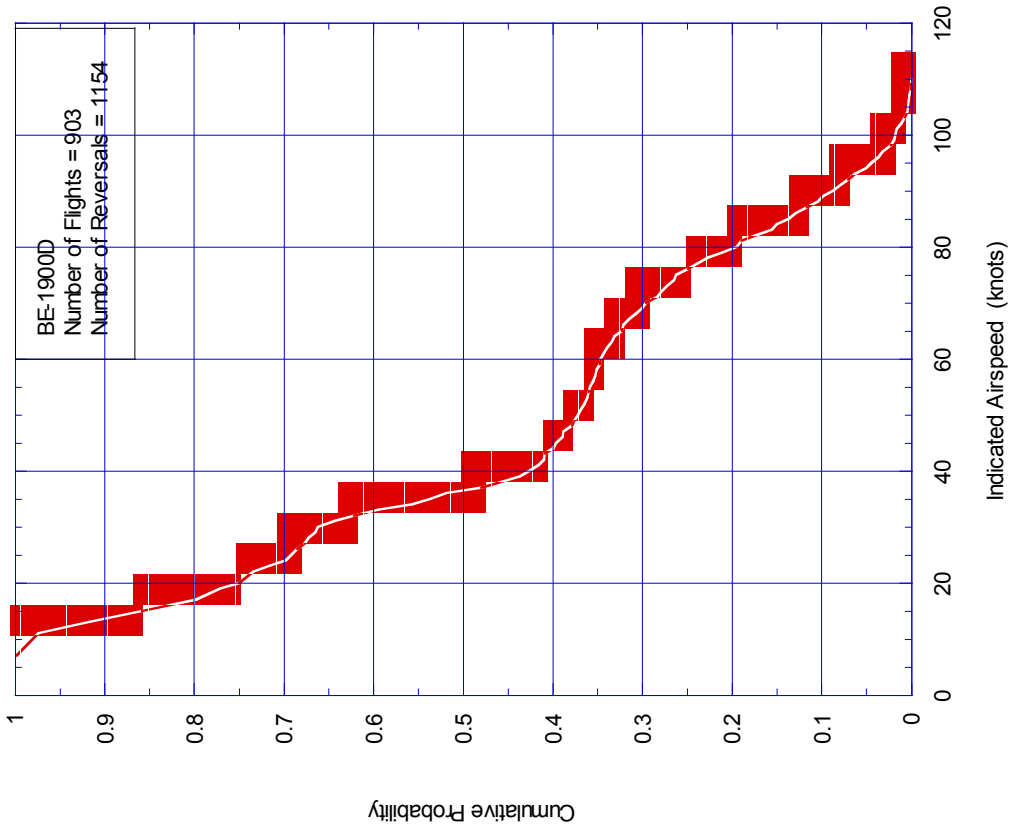


FIGURE A-60. CUMULATIVE PROBABILITY OF SPEED AT TIME OF PROPELLER REVERSAL, LEFT PROPELLER

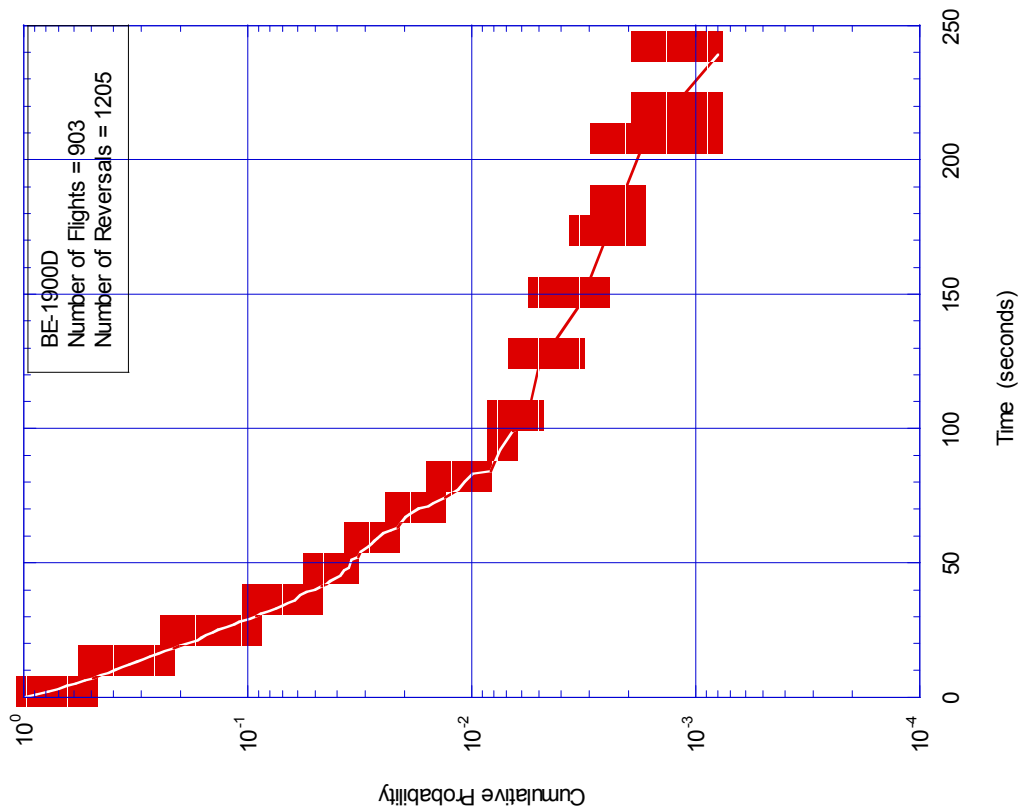


FIGURE A-61. CUMULATIVE PROBABILITY OF TIME WITH PROPELLER IN REVERSE, LEFT PROPELLER

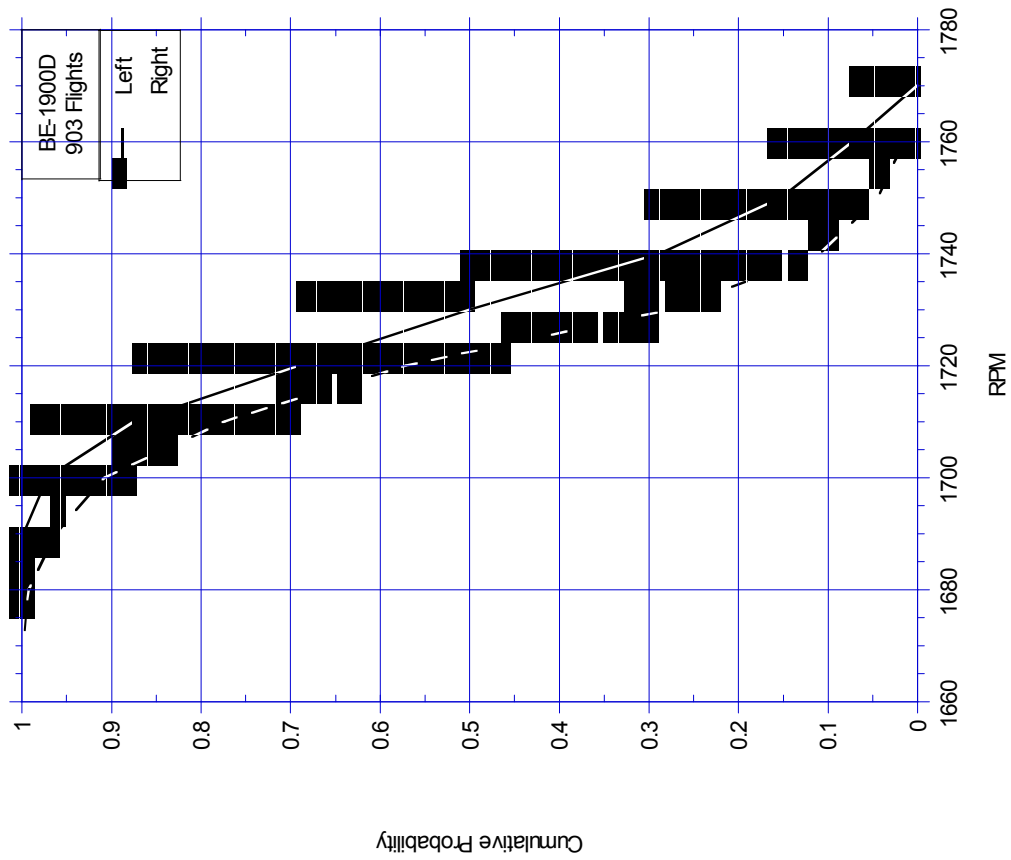


FIGURE A-62. CUMULATIVE PROBABILITY OF RPM AT LIFTOFF

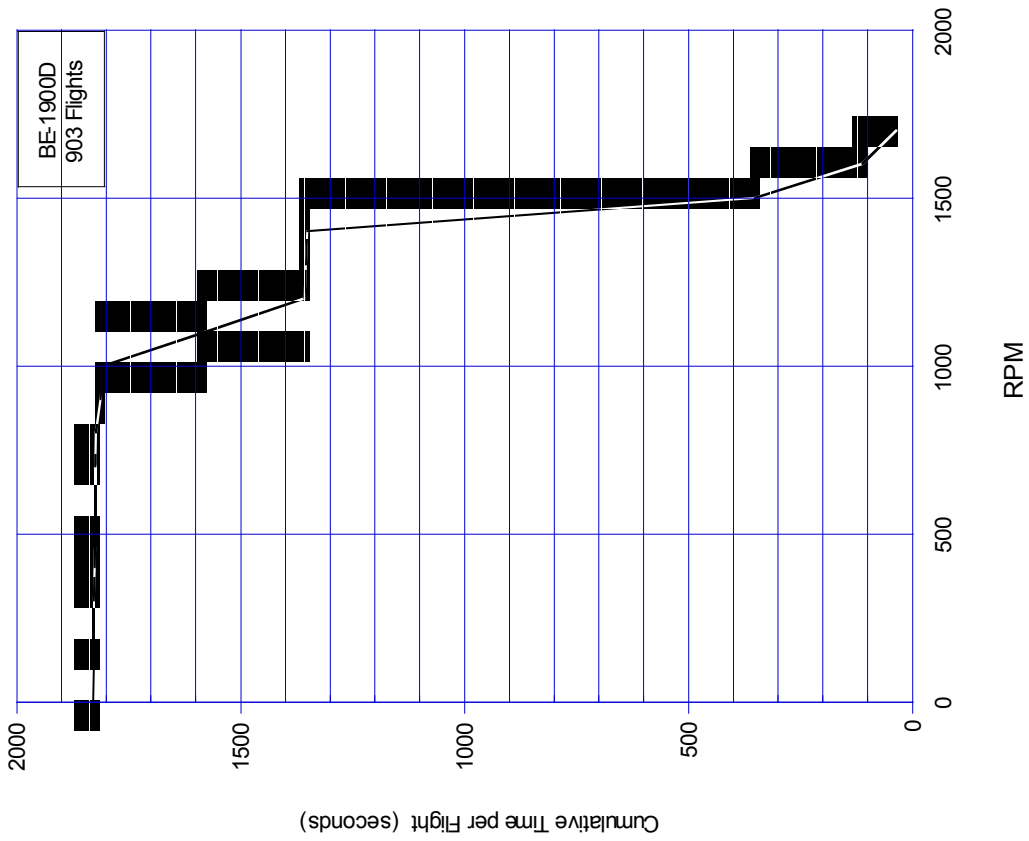


FIGURE A-63. CUMULATIVE TIME AT RPM LEVELS

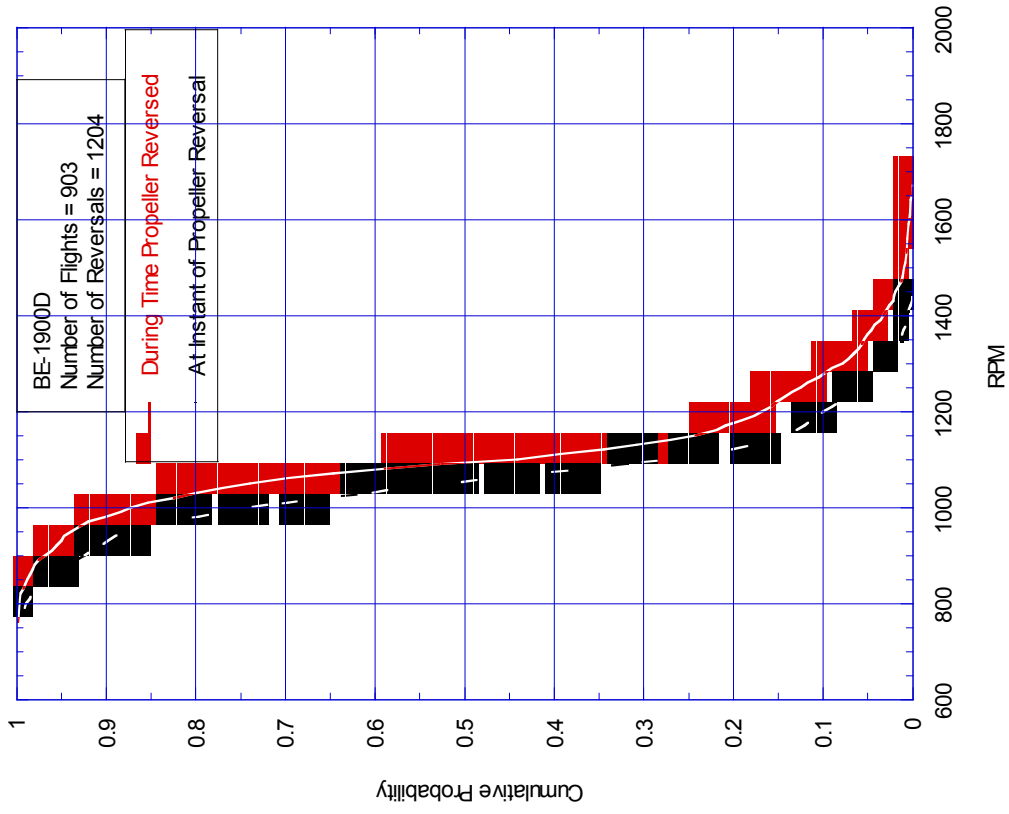


FIGURE A-64. CUMULATIVE PROBABILITY OF MAXIMUM RPM DURING REVERSE CYCLE, LEFT PROPELLER

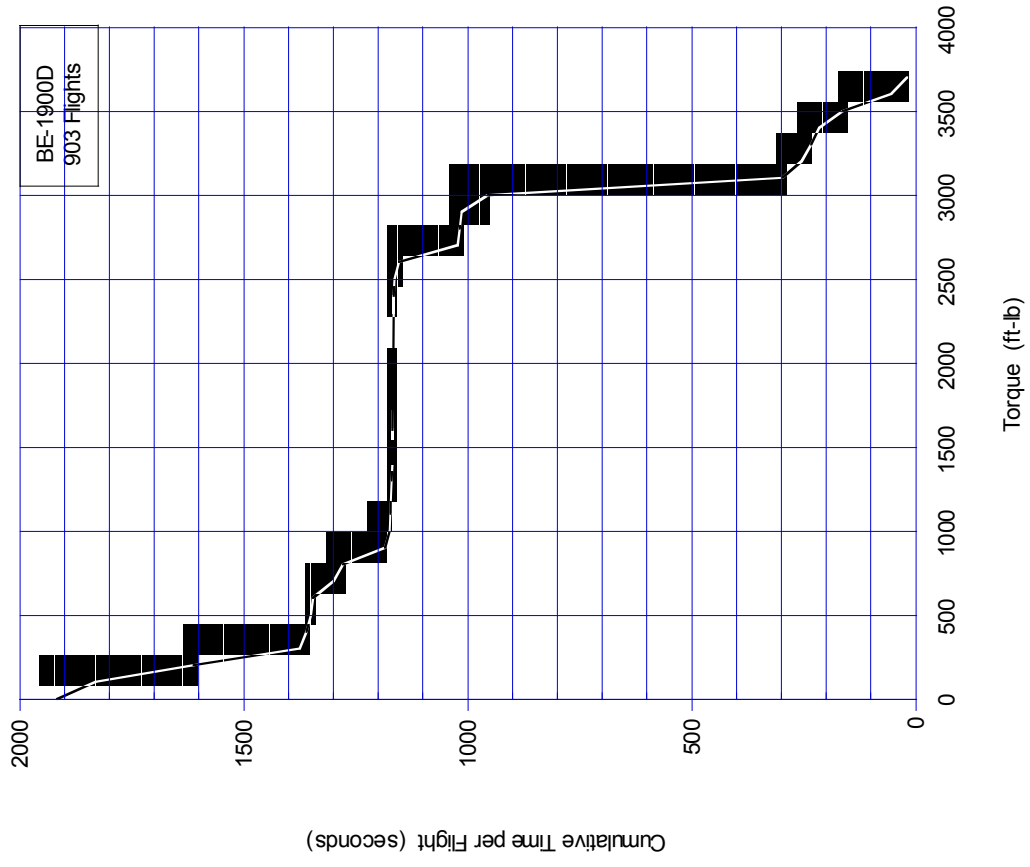


FIGURE A-65. CUMULATIVE PROBABILITY OF MAXIMUM TORQUE DURING TAKEOFF ROLL

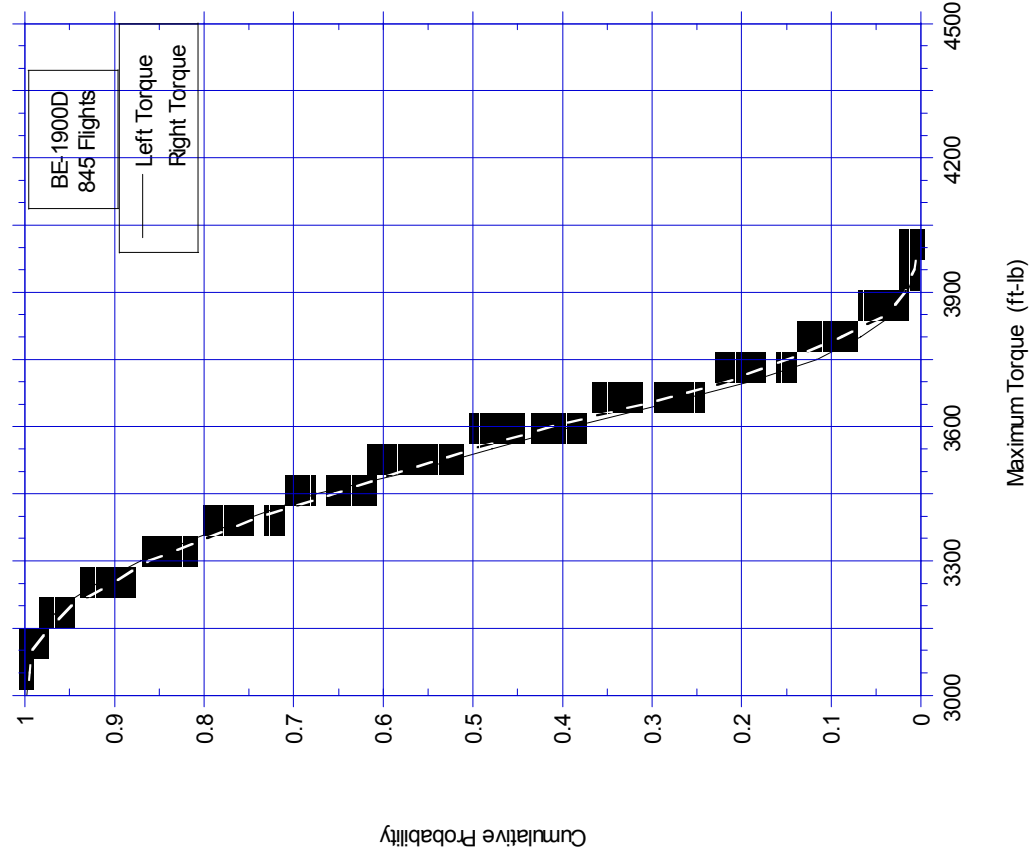


FIGURE A-66. CUMULATIVE TIME AT TORQUE LEVELS